UNIVERSIDADE DA BEIRA INTERIOR
Engenharia

Sizing Analysis of a Battery System for an Electrically-Propelled Airplane

Micael Valverde Teixeira

Dissertação para obtenção do Grau de Mestre em
Engenharia Aeronáutica
(ciclo de estudos integrado)
(versão revista após discussão)

Orientador: Prof. Doutor Francisco Miguel Ribeiro Proença Brojo

Covilhã, Julho de 2018

Acknowledgments

To my parents, which have always showed their unconditional support and love to me through all my life, inspiring me to be the man I am today and, for giving me every single opportunity to enrich my life with different experiences.

To my littles sister, that brought love to my life and, made me the happiest brother ever since.

To all my friends and colleagues, with which I shared these amazing six years in university and were always there side-by-side with me whenever I needed someone.

A special thanks to Daniela Ribeiro, the never-ending support and sacrifices made by her were much apreciated and will not soon be forgotten.

I would also like to extend my gratitude to my landlords, who took me in and offered me everything I needed throught my years in university.

Finally I would like to thank my thesis advisor, professor Francisco Brojo, for giving me the opportunity to realize this thesis and, giving me all assistance needed to accomplish it.

Resumo

O conceito de propulsão elétrica tem provado ao longo das últimas décadas que pode ser uma boa solução para substituir os motores de combustão interna em aviões, a fim de criar uma maneira mais eficiente, ambientalmente amigável e confiável de viajar através do ar. Mas ainda não foi capaz de atingir seu potencial devido a muitas limitações com as tecnologias ativas de hoje, principalmente as baterias. Várias empresas já começaram a equipar alguns modelos de aviões com motores elétricos e uma fonte de energia de bateria e usá-los como bancos de ensaio para futuras pesquisas e desenvolvimento de conceitos de propulsão elétrica. Como a maioria dessas empresas tende a tornar confidencial a informação sobre esse assunto devido à sua relevância na atualidade, foi desenvolvido um algoritmo capaz de usar os atuais métodos conceituais de projeto de avião e usar dados históricos para prever e avaliar o dimensionamento de um sistema de bateria para uma configuração de avião com propulsão elétrica. Como era de se esperar, o algoritmo mostrou que, com a atual tecnologia de baterias, os aviões movidos a eletricidade ainda estão longe de competir com seus equivalentes de motores de combustão interna. Ainda assim, as próximas décadas prometem ser instrumentais para o conceito de propulsão elétrica se afirmar no mercado de aviação.

Palavras-Chave

Propulsão elétrica, aviões com propulsão elétrica, tecnologia de baterias, propulsão distribuída, propulsão elétrica híbrida.

Abstract

The electric propulsion concept has proven over the past decades that it can be a good solution to substitute internal combustion engines in airplanes in order to create a more efficient, environmentally friendly and reliable way of travelling through air. Still it has not been able to reach its potential due to many limitations with today's active technologies, mainly the batteries. Several companies have already started to outfit some airplane models with electric motors and a battery power source and use them as test beds for future research and development of electric propulsion concepts. Since most of this companies tend to make information regarding this subject confidential due to its relevancy in today's age, an algorithm was developed, that is capable of using current conceptual airplane design methods and use historical data to predict and evaluate the sizing of a battery powered system for an electrically-propelled airplane configuration. As is was expected, the algorithm showed that with current battery technology, electrically-propelled airplanes are still far from being able to compete with their internal combustion engine counterparts. Still the next decades should prove to be instrumental for the electrical propulsion concept to assert itself in the aviation market.

Keywords

Electrical Propulsion, electrically-propelled airplanes, battery technology, distributed propulsion, hybrid-electric propulsion.

Index

Acknowledgments iii

Resumo v

Abstract vii

List of Figures xi

List of Acronyms xix

List of Chemical Elements xxi

1. Introduction 1

    1.1 Motivation 1

    1.2 Objectives of this Dissertation 3

    1.3 Organization of Thesis 4

2. State-of-Art 5

    2.1 Brief History of Electric Propulsion in Aviation 5

    2.2 Current Electrically-Propelled Airplane Landscape 8

    2.3 The Barriers to Electrical Propulsion 10

        2.3.1 Market Demand 11

        2.3.2 Battery Performance 11

        2.3.3 Fuel Cells Performance 16

        2.3.4 Solar Power Performance 18

        2.3.5 High Power Density Generators and Motors 20

        2.3.6 New Airplane Architecture 20

        2.3.7 Regulation 21

3. Case Study 23

    3.1 Selection of the Airplane 23

    3.2 Airplane's Specifications and Performance 23

    3.3 Numerical Model Thought Process 25

    3.4 Numerical Model Development 27

        3.4.1 Main Function 27

3.4.2 Motor and Battery Model Selection Function 30
3.4.3 Performance Estimation Function 33
3.4.4 Propeller Selection Function 35
3.4.5 Performance Function 44
3.4.6 Data Processing and Mission Profile Functions 46
4. Results 47
4.1 Results 47
5. Conclusions and Future Work 57
5.1 Conclusions 57
5.2 Future Work 57
References 59
Appendix A: Table of Results 65
Appendix B: Source Code 67

List of Figures

Figure 1.1: Total World CO_2 emissions from fuel combustion from 1971 to 2015 [1]. 1

Figure 1.2: Trend in emissions of air pollutants from transports [2]. 2

Figure 1.3: Contribution of the transport sector to total emissions of the main air pollutants, 2015 [2]. 2

Figure 2.1: Electric Propulsion parallel hybrid architecture schematic. 7

Figure 2.2: Electric Propulsion series hybrid architecture schematic. 7

Figure 2.3: Electric Propulsion turbo-electric architecture schematic. 7

Figure 2.4: Electric Propulsion all-electric architecture schematic. 7

Figure 2.5: Battery cell process of operation [28]. 12

Figure 2.6: Fuel cell process of operation [28]. 16

Figure 3.1: Numerical process design. 26

Figure 3.2: EMRAX 208 schematics and views [52]. 32

Figure 3.3: Blade division into subsections, taken from [54]. 35

Figure 3.4: Blade flow components, taken from [54]. 36

Figure 3.5: Side view of a typical stream tube of flow passing through a blade section, taken from [54]. 37

Figure 3.6: Front view of a typical streamtube of flow passing through a blade section, taken from [54]. 38

Figure 4.1: Thrust vs Airspeed graph. 49

Figure 4.2: Power vs Airspeed graph. 50

Figure 4.3: Thrust and Power Coefficients vs Advance Ratio graph. 51

Figure 4.4: Porpeller's Efficiency and Power Coefficient vs Advance Ratio graph. 51

Figure 4.5: Rate of Climb vs Airspeed graph. 52

Figure 4.6: Rate of Descent vs Airspeed graph. 53

Figure 4.7: Rate of Turn vs Airspeed graph. 53

Figure 4.8: ICE and EM Mass Distribution. 55

Figure 4.9: ICE and EM Total Mass. 55

Figure 4.10: Mission Profile graph. 56

List of Tables

Table 2.1: Primary lithium battery specifications [39]. 15

Table 2.2: Secondary lithium battery specifications [39]. 15

Table 3.1: Dynamic WT9 ICE configuration specifications..... 24

Table 3.2: Dynamic WT9 ICE configuration performances..... 24

Table 3.3: Terrain Friction Coefficients. 29

Table 3.4: $LiCoO_2$ battery specifications (model 18650)..... 30

Table 3.5: EMRAX 208 specifications [51]. 32

Table 4.1: Initial Battery System Sizing used for reference..... 48

Table 4.2: Chosen propeller properties..... 48

Table 4.3: Final Battery System Sizing..... 54

Nomenclature

a_1	Axial Inflow Factor
a_2	Angular Inflow Factor
AR	Wing Aspect Ratio
b	Wing span
B	Number of Blades of Propeller
c	Blades Chord
C_{batt}	Battery Capacity
C_D	Drag Coefficient
$C_{D,0}$	Drag coefficient at Zero Lift
C_L	Lift Coefficient
$C_{L,max}$	Maximum Lift Coefficient
$C_{p,prop}$	Propeller's Power Coefficient
$C_{q,prop}$	Propeller's Torque Coefficient
$C_{t,prop}$	Propeller's Thrust Coefficient
d	Blade's Diameter
D	Drag
e	Oswald Wing Efficiency Factor
E	Lift to Drag Ratio
E_{Climb}	Energy Needed During Climb
E_{cruise}	Energy Needed During Cruise
$E_{descent}$	Energy needed During Gliding
$Endurance$	Airplane's Achivable Endurance
E_{TO}	Energy Needed During Take-off
E / m_{batt}	Battery Specific Energy
g	Acceleration due to gravity
h_{max}	Absolute Ceiling
h_{OA}	Cruise Ceiling
h_{TO}	Take-off Altitude
H	Straight Line Ceiling
$I_{motor,max}$	Maximum Motor Current
$I0_{motor}$	Motor no-load Current
J	Advance Ratio
K	Drag-due-to-Lift Factor
K_A	Aerodynamic Term for take-off ground roll
Kt	Motor Torque Constant
K_T	Thrust Term for take-off ground roll

Kv_{fl}	Motor full-load Voltage Constant
Kv_{nl}	Motor no-load Voltage Constant
L	Lift
$m_{airftame}$	Airframe Mass
m_{batt}	Battery Mass
m_{empty}	Airplane's Empty Mass
m_{engine}	Engine Mass
m_{fuel}	Engine Fuel Mass
m_{motor}	Motor Mass
m_{TO}	Maximum Take-off Mass
M_{Tip}	Blade's Tip Mach Number
$MTOW$	Maximum Take-off Weight
n	Load Factor
n_{wing}	Wing Loading
n_{-}	Maximum Negative Load Factor
n_{+}	Maximum Positive Load Factor
N	Propeller Speed in Rotation Per Second
p	Blade Pitch
$Payload$	Avaiable mass of Airplane
P_{Cruise}	Power Availabe During Cruise
P_{excess}	Excess of Power
P_{Max}	Engine Maximum Mechanical Power
$P_{motor,max}$	Motor Maximum Mechanical Power
P_{prop}	Propeller's Power
P_{ROC}	Power Available at Climb
P_{ROD}	Power Consumed During Gliding
P_{TO}	Power Available at Take-off
PR	Power Required
PR_{cruise}	Power Required at Cruise
PR_{D}	Power Required at Descent
PR_{TO}	Power Required at Take-off
$P\ /\ m_{motor}$	Motor Power Density
Q	Torque
Q_{max}	Engine Maximum Torque
$Q_{motor,max}$	Maximum Motor Torque
r	Blade's Radius
$Range$	Airplane's Achivable Range
RPM_{max}	Engine Maximum Speed in rotation per minute
RPM_{climb}	Propeller's Speed At Climb in rotation per minute
RPM_{cruise}	Propeller's Speed At Cruise in rotation per minute

$RPM_{fl,motor}$	Motor full-load Speed in rotation per minute
$RPM_{nl,motor}$	Motor no-load Speed in rotation per minute
ROC	Rate of Climb
ROC_{OA}	Rate of Climb at Operating Altitude
ROC_{TO}	Rate of Climb at Take-off Altitude
ROC_0	Straight Line sea-level Rate of Climb
ROD	Rate of Descent
S	Wing Area
S_{TO}	Take-off Ground Roll
t_{climb}	Total Climbing Time
t_{cruise}	Total Cruising Time
$t_{descent}$	Total Gliding Time
t_{loiter}	Total Loiter Time
t_{TO}	Time to Take-off
T	Thrust
TR	Thrust Required
U_{batt}	Battery Voltage
$U_{motor,max}$	Maximum Motor Voltage
V_0	Axial Flow Velocity Vector
V_1	Local Flow Velovity Vector
V_2	Angular Flow Velocity Vector
V_{cruise}	Cruise Speed
V_{inf}	Airplane's Forward Velocity
V_{maneuv}	Maneuver Speed
$V_{max,turn}$	Maximum Rate of Turn Speed
V_{rot}	Rotation Speed
V_{sound}	Speed of Sound
V_{stall}	Stall Speed

Greek Symbols

a	Angle of Attack
Δq	Blade's Elemental Torque in a Slipstream
Δt	Blade's Elemental Thrust in a Slipstream
ΔQ	Blade's Elemental Torque
ΔT	Blade's Elemental Thrust
η_{motor}	Motor Efficiency
η_{prop}	Propeller Efficiency

θ	Geometric Pitch Angle
μ	Terrain Friction Coefficient
ρ_{OA}	Operating Altitude Air Density
ρ_{TO}	Take-off Altitude Air Density
Φ	Flow Angle
γ_{ROC}	Rate of Climb Angle
γ_{ROD}	Rate of Descent Angle
$\dot{\psi}$	Rate of Turn
$\dot{\psi}_{max,turn}$	Maximum Rate of Turn
ω	Angular Speed

Subscripts

Estimated	Values Obtained in the first validation of the code.

List of Acronyms

AFC	Alkaline Fuel Cells
BLDC	Brushless Direct Current
BPA	Battery Powered Airplane
BSFC	Brake Specific Fuel Consumption
DMFC	Direct Methanol Fuel Cells
EASA	European Aviation Safety Agency
EEA	European Environment Agency
EM	Electric Motor
EMF	Electro-Magnetic Force
EP	Electric Propulsion
EV	Electric Vehicle
FAA	Federal Aviation Administration
FBW	Fly by Wire
FCPA	Fuel Cell Powered Airplane
GA	General Aviation
GHG	Greenhouse gases
ICE	Internal Combustion Engine
LCA	Large Commercial Airplanes
MCFC	Molten Carbonate Fuel Cells
MEA	More Electric Airplane
OCV	Open Voltage
OEM	Original Equipment Manufacturers
PAFC	Phosphoric Acid Fuel Cells
PEM	Proton Exchange Membrane
PMSM	Permanent Magnet Sinusoidal Motor
PWM	Pulse Width Modulation
RA	Regional Airplanes
RFC	Regenerative Fuel Cells
SOFC	Solid-Oxide Fuel-Cell
UAT	Urban Air Taxis
VTOL	Vertical Take-off and Landing

List of Chemical Elements

CO_2	Carbon Dioxide
H_2O	Water
Li	Lithium
$LiAgV_4O_{11}$	Lithium hexafluorophosphate
$LiCoO_2$	Lithium Cobalt Oxide
$Li(CF)_n$	Lithium Tetrafluoroborate
$LiFePO_4$	Litihum Iron Phosphate
$LiFeS_2$	Lithium Iron Disulfide
LiI_2	Lithium Iodide
$LiMnO_2$	Lithium Manganese Dioxide
$LiMn_2O_4$	Lithium Manganese Oxide
LiO_2	Lithium Superoxide
Li_2O_2	Lithium Peroxide
$LiOH\cdot H_2O$	Lithium Hydroxide
$LiSOCl_2$	Lithium Thionyl Chloride
$LiSO_2$	Lithium Sulfur Dioxide
$LiSO_2Cl_2$	Lithium Sulfuryl Choride
NCA	Nickel Cobalt Aluminum
NCM	Nickel Manganese Cobalt
NOx	Nitrogen Oxides
O_2	Oxygen

Chapter 1

Introduction

Electric Propulsion (EP) has been at the fore front for research and development of newer and better technologies for many space oriented projects and missions for the past decades. Yet it as only seen some relative breakthroughs in aviation for the past years, due to current technologies related with supplying electric motors (EM), not being able to supply enough energy to compete with today's market of internal combustion engines (ICE). This is expected to change in the next decades, as many industrial giants in this market work hard every year, to make EP in aeronautics a more viable, cleaner and efficient option as opposed to the current trends of ICE.

1.1 Motivation

EP driven airplanes have been introducing themselves slowly but steadily in the aviation market for the past years. This is due to a rising concern of the public, aviation companies and civil aviation organizations of the problem concerning the steady rise of fossil fuels demand over the past decades, which directly impacts the environment in the form of CO_2, among others [1], emissions released from the fossil fuels combustion, that contribute to an increase of the greenhouse gases (GHG), which has been blamed as the main cause for global warming. Figure 1.1 gives an indicative of this trend.

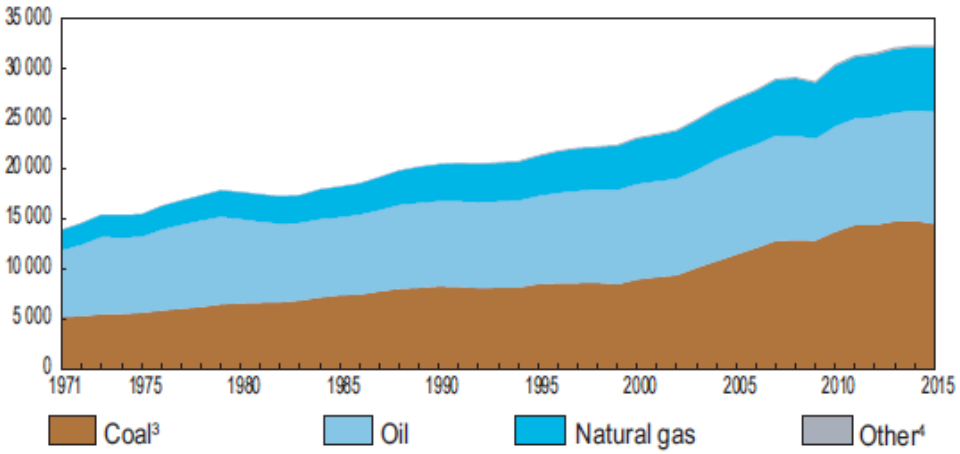

Figure 1.1: Total World CO_2 emissions from fuel combustion from 1971 to 2015 [1].

Still, the European Environment Agency (EEA) states that progress has been made since 1990 in reducing the emissions of many air pollutants from the transport sector, despite the general increase in activity within the sector [2]. Figure 1.2 illustrates this.

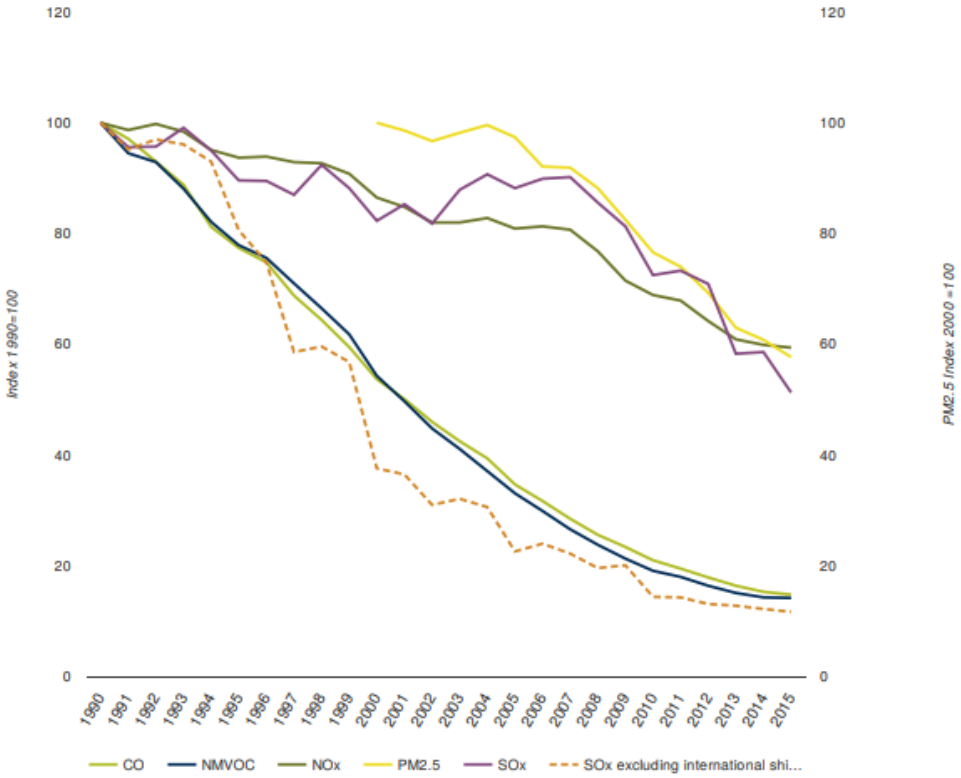

Figure 1.2: Trend in emissions of air pollutants from transports [2].

Figure 1.3 divides the many emissions of air pollutants by the existing transport sectors, in order to give a better assessment of the current situation regarding emissions.

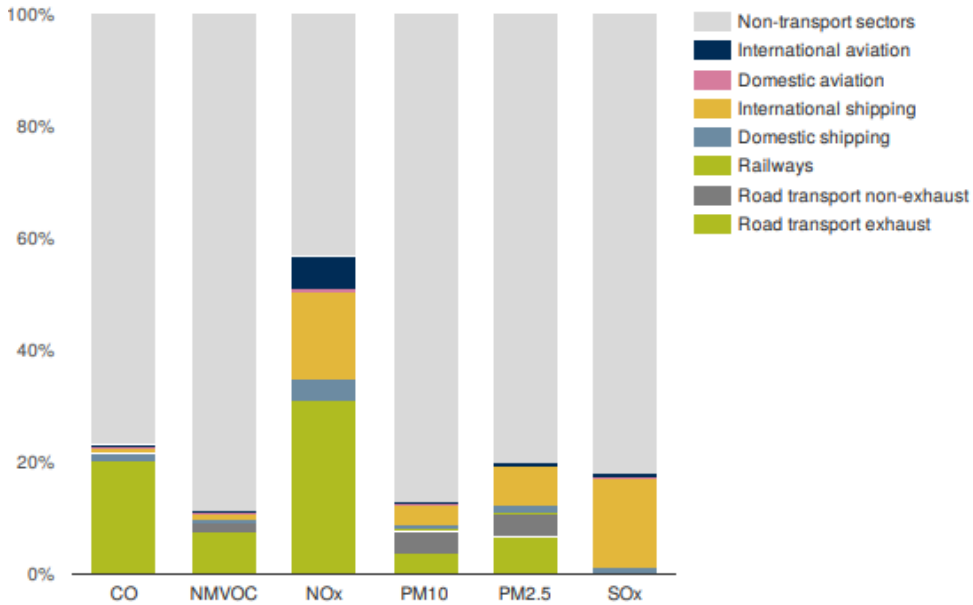

Figure 1.3: Contribution of the transport sector to total emissions of the main air pollutants, 2015 [2].

As can be seen in figure 1.3, the aviation sector contributes to a significant amount of NOx gases or pollutants, about 7.3% [2]. These gases are usually produced from reactions among

nitrogen and oxygen during combustion of fuels and, contribute to the formation of smog, acid rains, as well as depletion of tropospheric ozone.

It is imperative to try to minimize these emissions as much as possible. Just like it was done with the discovery and integration of renewable energy into a country's power supply for high demand of energy and, at the same time being environmentally friendly, there needs to be a change in mentality for the aviation and manufacturing companies. Even though, at the moment, the transition of ICE into EM, appears to be considerably costly and lengthy, it brings more benefits and profits to the table in a near future, as EM present a significantly lower operating cost compared to ICE and are much more efficient at converting energy into useful shaft power, approximately 95% as opposed to an average of 30%-40% for ICE. Until a few years back this feat was not so easily though, as battery technology development was lagging at the time, compared with the rest of the contributors to EP, but nowadays this is certainly not true anymore. Battery technology advancements have occurred and the aviation companies have been taking notice of this and are cautiously adapting to this transition, these companies include Boeing, Airbus, Rolls-Royce, Siemens, as well as research organizations such as NASA. It is expected that for the next decades there will be a big technological revolution and this will permit these companies to finally achieve the concept of an all-electric, environmentally friendly, airplane capable of competing with current big commercial ICE airplanes.

Still, before companies can make this giant leap, it is necessary to focus firstly, on the small-scale aviation, the general aviation sector. As of today, there are multiple examples of small airplanes outfitted with EM that have demonstrated a capacity to accomplish flight at reduced range and endurance performances. The purpose of this dissertation, is to evaluate one example and see how well it fares in performance, when compared with its ICE counterpart.

1.2 Objectives of this Dissertation

The objectives of this dissertation are as follows:

- Do a description of current state-of-art of EP, how it stands today and a brief summary of its evolution.
- Evaluate de advantages and disadvantages of EP.
- Review how battery technology has been progressing over the years.
- Evaluate other types of power supply system being developed for EP.
- Select a prominent airplane to be studied with an EM.
- Select a combination of EM and battery system to be studied.
- Conceptualize an algorithm capable of analyzing the performance of the EM airplane and compare it with its ICE counterpart.
- Report any conclusions taken from this work.

1.3 Organization of Thesis

Following this introduction, chapter 2 summarizes fundamentals of EP system components and its current state, referring to current battery technology and other types of power supply systems, such as fuel cells and solar power integration. EM technology will also be briefly discussed but not delved into. An overview of the advantages and disadvantages of EP will also be given. EP evolution history will also be, briefly covered.

In chapter 3 an overview of the thought process behind the algorithm development will be given and, a detailed step by step explanation of each process will be presented.

Chapter 4, will contain the selection of the airplane model to be studied, as well as the EP systems to be used. This includes EM selection as well as a battery type cell to be used as base to size the battery system needed. It will also feature the results obtained from the developed algorithm. An analysis of these results will be made as well as a comparison with the ICE values given.

In Chapter 5 the necessary conclusions and observations will be unveiled and, finally some future work will be presented.

Chapter 2

State-of-Art

There has been a consistent increase in the electrification of airplanes systems, research into EP, and fundamentally, a greater investment of money and business effort into electrically-propelled airplanes for the past years.

Electrification not only offers the capability to reduce emissions, but could also unlock the potential for more energy-efficient airplanes and brand-new architecture types. Still, to this day there are many technological and regulatory barriers that need to be overcome before any significant change can occur. A brief discussion of the history of electrically-propelled airplanes and the two concurrent technological trends of the More Electrical Airplane (MEA) and EP will be made, as well as the barriers that need to be overcome in order to pave the way to a more electric and environment friendly future.

2.1 Brief History of Electric Propulsion in Aviation

Contrary to what might be believed, EP was one of the first types of propulsion to be used to power a propeller. The first electrically powered airship was prototyped by the French chemist and aviator Tissandier, who attached a Siemens EM to a dirigible to power its propeller, achieving the first flight in 1883 [3], 20 years before the first powered flight realized by Wright Brother's Wright Flyer I, with a gasoline engine. Due to the rise of ICE in the following years and subsequent development of the gas turbine, the aviation sector quickly moved to these sources of power, fueled by oil-derivative compounds, and abandoned for some time, the EP concept as battery technology started to fall short in comparison with the energy these fuels could deliver.

However, during and after WW2 mankind experienced a scale up in electrification in all its activities, and this prompted a new combined effort in researching and developing newer and more capable and efficient battery technologies, which in parallel permitted the rise of EP in the aviation and aerospace sectors in the late 20^{th} century. Since then, the electrification in the aviation industry as manifested itself in two ways. The MEA, an evolutionary trend in which each successive generation of airplanes show an intent to employ more electrical equipment in place of systems that would previously have been of mechanical, hydraulic or pneumatic origin. The EP, a potentially revolutionary new approach that, if adopted widely, would transform large segments of the aerospace industry, affecting not only the area of propulsion, but also airplane's systems and possibly leading to radically new airplane's architecture.

Since the dawn of the aviation era, non-propulsive airplanes systems such as actuation, de-icing and, air-conditioning, have been dependent on mechanical, hydraulic and pneumatic sources of power. These systems were traditionally powered by the airplanes engines, with power extracted via a variety of mechanisms. As modern airplanes evolved, achieving tremendous increases in range, speed and capacity, the complexity of their systems increased parallel. While hydraulics were more robust and could generate large forces, these systems often suffered from a lack of reliability and high maintenance costs. Pneumatic systems, also expressed drawbacks of low efficiency and, similar to hydraulics systems, presented a very complex structure. Leaks in both systems were often difficult to locate, hard to trace and, time consuming to repair which would result in inconvenience for operators and passengers alike making it very costly.

Alternatively, electrically powered systems did not suffer from many of the shortcomings inherent in hydraulic, pneumatic and mechanical systems. These systems were flexible, light and exhibited high efficiency values. With the introduction of electrical cabin equipment and avionics and Fly by Wire (FBW) systems MEA become more and more popular. Despite these advances, electrical systems did come with drawbacks related to the need to advance in power electronics, in order to handle the ever-increasing loads. However, as a result of the advantages of increasing electrification in terms of reduced weight, greater reliability, lower maintenance costs and increased efficiency, it is expected to see a continuation or even acceleration of the MEA trend, as long as the current higher costs of some electrical systems can be restrained.

Compared to the evolutionary MEA trend, EP represents a radical change from today's propulsion technologies, although EP is not without historical precedent. After the first EP flight by Tissandier's experimental Airship in 1884, the world would only see the next major milestone achieved in 1973, when NiCad-battery powered HB ME-1 [4], the first fixed wing manned electrically-propelled airplane, made its first flight. The next remarkable step was achieved in 1979, when Mauro Solar Riser [5], the first manned solar-powered airplane, took to the air for the first time. In the same year, Bryan Allan successfully crossed the Channel between England and France with the solar-powered Gossamer Albatross [3][5].

Since then, many electrically powered airplanes have been built, including NASA's solar driven UAVs, the battery powered Alisport Silent Club and Lange Antares gliders and, development programs like the Airbus/Siemens E-Fan X [6-7]. Within the area of EP, there are three broad airplane architectures choices designers can make.

Hybrid-electric architectures either augment a traditional turbo-fan with an electric motor in parallel hybrid configuration, or use a turbo-shaft and generators bolstered by a battery to feed a set of EM-driven fans in a series configuration [8-9]. Both types continue to employ a turbo-fan for large parts of the flight envelope due to the current shortcomings of battery capacity and, draw on electrical power either in high thrust parts of the flight envelope such as take-off

and climb, or switch entirely to battery power during cruise, when thrust requirements are low. Figure 2.1 and 2.2, show a schematic of this architecture type, for parallel hybrid and series hybrid, respectively.

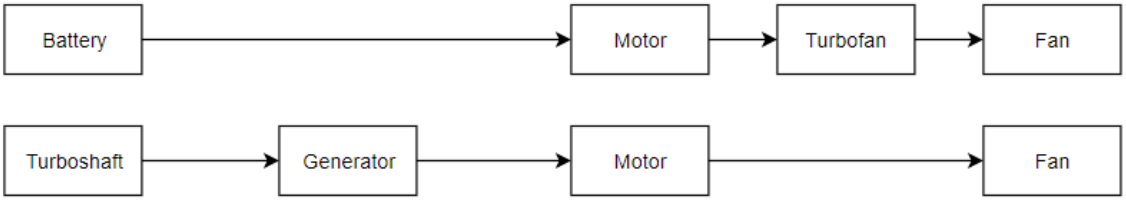

Figure 2.1: Electric Propulsion parallel hybrid architecture schematic.

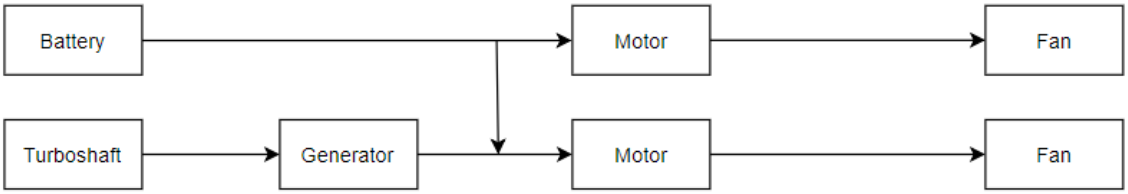

Figure 2.2: Electric Propulsion series hybrid architecture schematic.

A second configuration is a turbo-electric architecture, where kinetic energy from a turbo-shaft is transformed via a generator into electrical energy to drive one or multiple distributed electric motor driven fans. This configuration gives the airplane designer complete freedom over the number and location of the propulsive fans, potentially leading to more efficient designs with higher propulsive efficiency [10-13]. A schematic of this type of architecture is presented in figure 2.3.

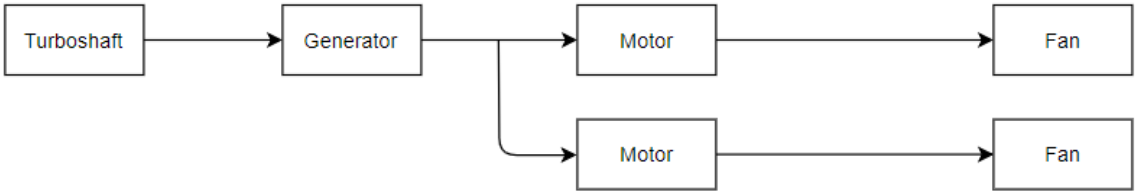

Figure 2.3: Electric Propulsion turbo-electric architecture schematic.

The third and final option is all-electric propulsion, where the sole source of supply is a battery and the gas turbine and associated fuel system present in the hybrid-electric architecture type and turbo-electric configurations are completely eliminated. As it has been emphasized, the range of an airplane with an all-electric propulsion system will heavily depend on the battery storage capacity and weight [14-16]. As before, next follows a representation of the all-electric architecture type schematic, figure 2.4.

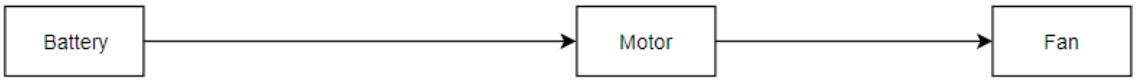

Figure 2.4: Electric Propulsion all-electric architecture schematic.

2.2 Current Electrically-Propelled Airplane Landscape

It has been clear that, for the past decades, investors and engineers are aligned in the potential of EP and teams around the world are already making strides towards further electrification. There has been a significant increase in development of EP driven airplane programs, ranging from incumbent aerospace giants to new start-ups, which are making the industry bustling with activity.

These new programs can be categorized into 4 main focus points: General Aviation (GA), Urban Air Taxis (UAT), Regional Airplanes (RA) and Large Commercial Airplanes (LCA). Around half of all new programs have been launched by start-ups and, 5% of these are being backed by major non- aerospace companies. Only 20% of these programs are being launched by major airframe Original Equipment Manufacturers (OEM), such as Boeing [17], Cessna and Agusta Westland. Most of the developments in this category are being conducted by Airbus in conjunction with Rolls-Royce and NASA [6-7].

Most of these developments are split roughly equally between North America and Europe, reflecting the location of current production of most of the world's airplanes. A considerable amount of these projects, almost half of them, are only focusing on single fan designs, with a third aiming to capture the propulsive efficiency benefits of EP through distributed fans [18-21]. It should be pointed out that much of these programs being developed are only expected to have major breakthroughs in the upcoming decades, as other systems technologies also need to progress much further.

The segment of GA has been a hotbed of development activity. The uptake in this segment has been enabled by existing airplane architectures already using propellers for propulsion either allowing a simple substitution of the powerplant or allowing designers of new platforms to draw on a plethora of relevant past data. GA incumbents have been releasing retrofitted versions of already existing airplanes, such as the electric Cessna 172 and Pipistrel's Taurus Electro or WATTsUP electric trainer. Small start-ups have also jumped in and proven their value with the development of programs such as the DigiSky with the SkySpark demonstrator. This class of airplane has proven to be an effective segment as a test bed for further development of EP airplanes and, as a result will be the main focal point of this dissertation.

There has been clear acceleration in the launch of development projects for 1-4 passenger UAT. Typical developments in this area are currently targeting a limited range of up to 50 km, with vertical take-off and landing (VTOL) and all-electrical propulsion to give the benefits of low noise pollution and zero emissions.

Many of these developments have advanced and made ground-breaking progress. In Germany, the VoloCopter VC-200 flew as early as 2013 [22]. Since the fourth quarter of 2017, VoloCopter has been authorized as an Autonomous Air Taxi in Dubai, having received clearance from the

United Arab Emirates' Roads and Transport Authority. Lilium Aviation also performed its maiden flight in 2016 and plans a 5-seater taxi for urban mobility, and the Chinese drone company Ehang has also been cleared as of last year to start testing its Ehang 184 in Nevada [23], beginning its FAA regulatory approval process.

A number of other organizations and companies are operating in stealth mode without much press release, but have also made noteworthy progress. Zee Aero's full-scale prototype was recently spotted in flight, while Joby Aviation's S2 was expected to start full-scale prototype testing earlier this year. Other projects like the DeLorean Aerospace's DR-7 continue to make progress with a VTOL flying car, due for its first flight in late 2018.

A further development in these urban mobility concepts actually came from automotive companies like Geely and mobility providers like Uber. The former has entered the aerospace industry by acquiring US-based Terrafugia, with its TF-X flying car concept. The latter provided a detailed business case in its "Elevate" white paper published in October 2016 [24], which in turn motivated additional organizations like Bell Helicopter, Mooney Aircraft and Pipistrel to partner with Uber to work on an undisclosed project. While this may just be an early spike of activity before the pace of development settles down, there certainly seems to be a willingness from corporates and investors alike to enter this field.

Aerospace incumbents, not to be undone, are also investing considerable resources into the trend. However, industry giants Airbus and Boeing are taking different approaches. Airbus has taken an holistic approach with an Urban Air Mobility portfolio, not only initiating projects within existing divisions such as Airbus Helicopter and the CityAirbus [25], a four-seater all-electric multi-rotor VTOL airplane for urban environments, but also identifying a need for increase in development with the creation of a dedicated new organization named A^3, a Silicon Valley-based outpost tasked with overseeing the development of Vahana, a single-seat autonomous electrically-propelled airplane which was expected to carry out its first full-scale demonstration flight by the end of 2017 [26]. Concurrently, Airbus remains on the lookout for potential investments in start-ups through Airbus Ventures. Boeing, on the other hand, has chosen a largely opportunistic approach by dedicating its venture capital arm HorizonX to finding promising start-ups to invest in, often along with partners, including the Zunum RA program.

In the next size category are the RA with ranges between 500-1,000 km that are targeting both commercial inter-city transport and GA use by corporations and high net worth individuals. Developers in this segment are evaluating both hybrid and all-electrical propulsion and have a business case related not only to the replacement of current non-electric airplanes, but also to competing with road or rail-based transportation, drawing on the benefits of EP in terms of reduced noise and zero emissions.

New ventures launched in this segment include Eviation's Alice project, a nine passenger all-electric commuter and business airplane planned to first fly in late 2018, whilst others appear a little further behind in development such as XTI Aviation's TriFan 600, a six-seat hybrid-electric VTOL business airplane and an initial product from Zunum Aero, which is developing commercial aviation platforms of three different sizes, with the smallest and first-to-market variant being a 10-seater RA.

RA are also being considered by some companies as test beds, subsequently to be scaled up to larger platforms. Existing aerospace and aviation companies are thus also active in this segment. Boeing, for example, has recently partnered with JetBlue to co-invest in the aforementioned Zunum Aero, which plans to eventually scale up its regional development to a 50-seater platform.

The well-documented barriers to entry in the LCA segment mean that most of the development activity in electrically-propelled LCA has been focused on by the incumbents, mainly Airbus and Boeing.

Airbus has already gone so far as to release a roadmap to the first electric LCA, though without a predicted entry into service date, in pursuit of the company's long-term goal of developing a single aisle airplane with a hybrid-electric configuration. The size of the, airplane would require around 40 MW of power for take-off and 20 MW for cruise, in support of which Airbus is developing a demonstrator airplane called the E-Fan X in the 2 MW class that is scheduled to fly within the next 2 years [6-7]. In parallel, Boeing has also released a roadmap to an electrically-propelled airplane for around 2030, building on the achievements of the more Electric 787 and demonstrating the way in which the more electric airplane technology described earlier is complementary to and paving the way towards EP.

In a challenge to the incumbents, Wright Electric, a new start-up staffed by a team previously funded by NASA, has established a goal that all short-haul flights should be electrically-powered within the next 20 years. In support of this goal, Wright Electric has announced its intention to build a 150-seat electrically-propelled airplane within a decade to compete with the smaller members of the A320 Airbus and 737 Boeing families [27]. The company is taking an opportunistic approach to exactly which technologies should be implemented, indicating that if, should battery technology advance with sufficient speed then the airplane will feature an all-electric concept, while if progress on batteries becomes stale, then a hybrid-electric approach will be adopted instead. These technical barriers to EP will be explored with more detail in the next section.

2.3 The Barriers to Electrical Propulsion

Despite the clear enthusiasm that electrically-propelled airplanes have demonstrated by the plethora of new development programs launched, a significant number of barriers remain,

spanning market demand, technology, and regulation. In this section some of the barriers that EP will need to overcome, are described.

2.3.1 Market Demand

The first and foremost barrier for applications such as UAT is that of demonstrating whether there is market demand at a price that generates an acceptable return on investment to cover development and operating costs. In many ways the arguments in favor of UAT are reminiscent of those put forward in favor of air taxi companies operating Very Light Jets. Furthermore, UAT programs will need to break the traditional aerospace cycle of development cost over-runs and schedule delays, but perhaps this is just where the injection of outside experience and flexibility will overcome the traditional aerospace operating method.

Similar challenges will also exist in the RA segment. Although the 40-50 seat RA market was holding in the late 1990s and early 2000s, recently airlines have switched to buying larger RA in the 70-90 seat category owing to the high per-seat cost of smaller airplanes. As many of the initial sets of electrically-propelled RA appear to be targeting the declining smaller end of the RA market, the manufacturers will have to convince the airlines of the valuable proposition these new products will offer. Furthermore, regional jets typically fly 6-8 sectors per day, so any all-electric RA will need to either have a very rapid re-charging capability, or the ability to exchange depleted batteries for freshly-charged batteries within the time of the airplane's turnaround at the gate. This leads to the second barrier to EP, the current battery technology employed.

2.3.2 Battery Performance

A battery is an electrochemical device that converts stored chemical energy into electrical power. In half of the cell, positively charged ions, called cations, migrate to a cathode electrode through an electrolyte. In the other half of the cell, negatively charged ions, called anions, migrate to the anode electrode through an electrolyte, as shown in figure 2.5. An electrical load can be placed between the battery leads. Batteries operate with a closed thermodynamic cycle.

High battery storage capacity and low weight are clearly crucial to all-electric and hybrid-electric architectures and, in order to allow the creation of products with commercially viable payload-range characteristics. It is generally acknowledged that electrical storage systems used for all-electric airplanes, need high specific energy values, to become cost-effective and efficient, considering a bare minimum of 500 Wh/kg as a good starting value.

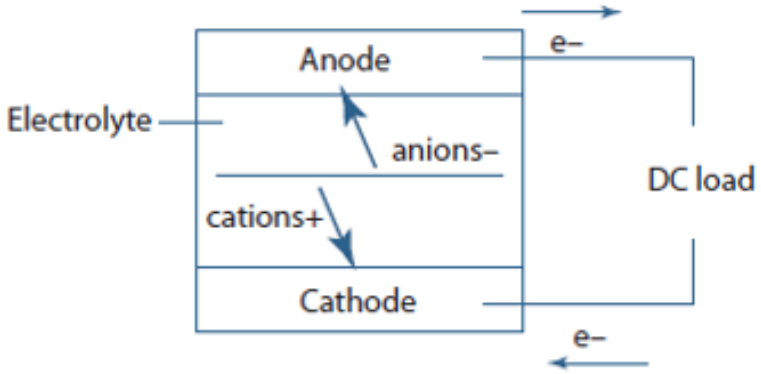

Figure 2.5: Battery cell process of operation [28].

The problem is, in the current spectrum of today's battery technology, commercial batteries offer a range of values from 150-250 Wh/kg. This does not mean that, there are no batteries currently that can provide higher values of specific energy than the ones mentioned before. As a matter of fact, currently the highest demonstrated value of specific energy reported till this day ranges from 500-700 Wh/kg. The problem is that, these batteries employ technologies, more specifically electro-chemistries, that have been reported as possibly very toxic and corrosive and, even susceptible to detonation if not handled properly, such is the case of Boeing 787 Dreamliner lithium ion battery incidents of 2013. Due to this, most of the batteries have seen very small utilization, currently in private and military sectors and almost none for the commercial sector, due to its safety risks [29].

There is one promising technology in development, that if it were to prove to be successful, it could revolutionize the EP industry, and enable a giant leap in its development. This is referring to the Lithium-air batteries. At present, two types of reversible lithium-air batteries have been proposed [30], namely non-aqueous and aqueous systems. The former, reports to be able to produce up to 3.460 kWh/kg from the reaction:

$$2Li + O_2 = Li_2O_2 \quad (2.1)$$

And an open cell voltage (OCV) of 2.96V demonstrated in for the discharge state. For the charged state, oxygen is excluded and the specific energy density is reported to be able to reach values of approximately 11.7 kWh/kg, which comes just short of the energy density provided by gasoline of around 13 kWh/kg at its purest form. The latter calculates its specific energy density from the reaction:

$$4Li + 6H_2O + O_2 = 4(LiOH{\cdot}H_2O) \quad (2.2)$$

But due to its active electro-chemistry reactions and, formation of unwanted concentrations and saturation of some of its products, the specific energy density resultant from the reaction, for the discharged state with and OCV of 3.0V, is about 2.004 kWh/kg, and 1.910 kWh/kg for

the charged state. Until recently, no technical basis existed, to support these estimated values obtained by their reaction's calculation. This was due to the challenges found in developing cathode materials and electrolyte systems for these batteries. References [31-34] give an insight to what these challenges are.

However, with the advancements of nanotechnology for the past years, this has enabled some progresses in achieving a possible solution for its current challenges. Several authors [35-36] have proposed one of the possible solutions, by developing a high density, graphene-based porous structure used as the cathode for LiO_2 batteries. This solution has proved to be a major breakthrough in the development of these batteries and possibly serving as a test bed for future developments. The following years will prove to be instrumental for the maturation of this technology and development of the first possible battery capable of standing toe-to-toe with fossil fuels.

Focusing now on more immediate and existing battery technology, a brief description will be made on the current lithium-ion batteries, which have proven to be the current leading battery technology for most applications in day-to-day life.

Lithium-based battery systems are characterized by high energy density levels, relatively high voltages, and low weight-to-volume ratio but, in general, tend to be more expensive than equivalent battery technologies with aqueous electrolytes, such as alkali disposable batteries and zinc/air batteries in the primary battery sector, and nickel metal hydride, nickel cadmium and lead batteries in the secondary battery sector [37].

Primary lithium batteries have existed since the 1970s, are easy to use and provide convenient sources of energy for portable applications. The batteries usually require no or very little maintenance and have a long shelf life; modern lithium batteries can usually be stored for up to 10 years, and there are special batteries with solid state electrolyte that can be stored for more than 20 years. The storage tolerance at elevated temperatures is generally good, in some cases up to 70°C. There are 3 classes of primary lithium batteries, firstly solid-state batteries, which are characterized by low power but superior shelf live. The term solid-state is used because the electrolyte is solid and the ion transmission between the electrodes takes place in a solid, non-electrically conductive material, usually a polymer. Secondly, batteries with a solid cathode are usually found in coin cells or small cylindrical batteries. Thirdly, batteries with soluble cathodes, which are usually found in industrial and military applications, manufactured in large cell sizes, up to 35-40 Ah, but also available in smaller sizes. All of these batteries have lithium anodes. The cathode material determines the battery system.

Over the last few years the market has seen the introduction of battery types in which the cathode consists of a mixture of different electrode materials. The purpose of these batteries is to provide a system that can accommodate both high and low loads.

There are two main groups of rechargeable lithium batteries, one of which uses lithium metal as the negative electrode. These are called lithium metal batteries. Lithium metal batteries were launched on a limited scale for consumer electronic products in the 1980s, but were withdrawn quickly because of safety problems with the lithium electrode. Lithium reacts with the electrolyte, forming dendrites on the surface of the electrode. Under repeated charging, the surface of the anode increases, with a corresponding increase in its reactivity and thermal sensitivity. More recently, however, the lithium metal anodes have once again found practical application in research, although they have not yet been marketed on a large scale. One way of reducing the fire risk in lithium metal batteries is to replace the electrolyte with a solid-state polymer electrolyte, that does not react with lithium.

The second type of rechargeable lithium battery is called a lithium ion battery, which has a negative terminal that consists of a carbon-based material, usually graphite, or another type of alloy or material that permits storage, of lithium in the structure. This category includes lithium polymer batteries, which differ from traditional lithium ion batteries in that they have an electrolyte that is bound within a nonconducting polymer matrix. Lithium ion batteries were introduced by SONY in 1991. This type of battery is constantly gaining new ground, and the areas of use are constantly expanding, and lithium ion batteries are currently used in all sorts of portable applications within consumer electronics, medical technology and military systems. The general properties that contribute to this are the high energy density of the lithium ion battery and its specific energy, compared with other rechargeable types of battery. Its other properties include low self-discharge and, relatively long recharge lifetimes. High costs and the safety aspects are its main barriers, as well as the fact that access to large cell types, battery cells with a capacity exceeding 5 Ah, is limited. Existing lithium ion batteries also suffer from functional limitations at low temperatures. Tables 2.1 and 2.2 give an overview of the main primary and secondary lithium battery types and its main properties, respectively.

Further analysis suggests that the current trajectory of Lithium-ion battery development will bring gravimetric density to about 400-450 Wh/kg by the mid-2020s [38]. However, further development or new battery chemistries will need to reach the 500 Wh/kg mark, and even if batteries were to reach this level, the energy storage density will still be a factor of 25 lower than the approximately 12 kWh/kg delivered by jet fuel. In addition to high energy density, high re-charging speeds and long battery life-cycles will be crucial to underpinning the economics of battery-powered airplanes. Therefore lithium-air batteries are seen as the ultimate goal for research and development for all-electric flight, as they are currently the only type of batteries that theoretically can go toe-to-toe with its fossil fuel counterpart.

Table 2.1: Primary lithium battery specifications [39].

System	Rated Voltage [V]	Specific Energy [Wh/kg]	Energy Density [Wh/l]
Class 1: Solid-State System			
LiI_2	2.8	220 - 280	820 - 1030
Class 2: Batteries with Solid Cathodes			
$Li(CF)_n$	3.0	220 - 590	550 - 1050
$LiFeS_2$	1.5	260	500
$LiMnO_2$	3.0	230 - 270	535 - 620
$LiAgV_4O_{11}$	3.2	270	780
Class 3: Batteries with Soluble Cathodes			
$LiSO_2$	3.0	260	415
$LiSOCl_2$	3.6	275 - 590	630 - 1100
$LiSO_2Cl_2$	3.95	450	900

Table 2.2: Secondary lithium battery specifications [39].

Cathode Material	Rated Voltage [V]	Specific Energy [Wh/kg]
$LiCoO_2$	3.6	110 - 190
$LiMn_2O_4$	3.7 – 3.8	110 - 120
NCM	3.7	95 - 130
NCA	3.7	--
$LiFePO_4$	3.2 – 3.3	95 - 140

Still, as mentioned before, currently these batteries present even more barriers and constraints to its development, one of which is its relative lower energy density capabilities compared with the other existing lithium batteries, as well as being very unstable due to excessive expansions of the battery derived by its electro-chemical reactions. This leads to one of the other main barriers to EP which is, battery safety/hazard containment. With many past events of lithium ion battery incidents that can be read from [29] in mind, electrically-propelled airplane developers will need to develop effective hazard containment systems for batteries, not only to meet airworthiness requirements, but also to satisfy public safety concerns. Whilst hazard containment systems for batteries are arguably less challenging than for volatile aviation fuel, the need for such systems are often overlooked in the race for higher energy densities.

Batteries are not the only method of storing energy through electrical means, fuel cells also deserve its recognition as a possible storage device for an all-electrical airplane. The next section is devoted to this system, a brief explanation of its process will be given, as well as, the advantages and disadvantages when compared with batteries.

2.3.3 Fuel Cells Performance

Fuel cells are electrochemical devices that use chemical reactions of a fuel source and oxidizer to generate electrical power. The fuel and oxidizer are consumed in the conversion process and, the byproducts are either exhausted from the fuel cell or stored onboard the airplane. The reaction between the fuel and oxidizer occurs in the presence of an electrolyte which is not consumed. Fuel cells have an open thermodynamic cycle.

Hydrogen-powered fuel cells operate in a similar manner regardless of type, figure 2.6 exemplifies this. A catalyst converts hydrogen into a positively charged hydrogen ion and a negatively charged electron at the anode. The hydrogen ions freely pass through the electrolyte, but the electrons are blocked.

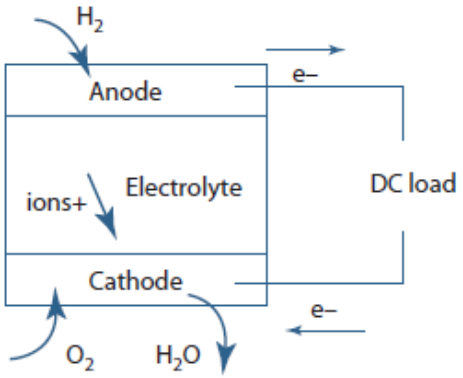

Figure 2.6: Fuel cell process of operation [28].

This creates a voltage potential difference between the anode and cathode. The electrons are directed via porous gas electrodes embedded in the cathode and anode. The hydrogen ions combine with oxygen, and the electrons returning from the electrical load to form water, which can be either liquid water or water vapor.

Because water vapor is the only emission, fuel cells are widely considered to be a clean power source. Multiple individual fuel cells can be combined in a fuel-cell stack. Like batteries, the fuel cells can be arranged in series or parallel to produce the desired voltage or peak current. The voltage per cell is defined by the fuel cell type, and the peak current is a function of the active surface area. The two most common types of fuel cell are proton exchange membrane (PEM) and solid-oxide fuel-cell (SOFC) types.

PEM and some SOFCs react with hydrogen and oxygen to generate electricity and water. The equivalent Brake Specific Fuel Consumption (BSFC) for a PEM fuel cell can be approximately 91.24–152.07 g/kWh, where the reference fuel is hydrogen. The temperature of the PEM fuel cell must be controlled to prevent thermal loading failure. The chemical reaction is exothermic, so that the heat generated must be rejected to keep the system within the operating limits.

The electrolyte membrane must generally be kept low to prevent damage, which requires rejection of low-grade heat.

The membrane must be properly hydrated to ensure that water is created and evaporated at the same rate. If the required hydration is not maintained, the membrane will dry and crack, allowing the hydrogen and oxygen to react directly and generate destructive heating. On the other hydration extreme, excessive water will flood the electrodes and block the reaction. PEM fuel cell systems involve numerous support systems to ensure effective operations. Actively controlled pumps must properly hydrate the membrane. Thermal management might require heat exchangers. The incoming air might require conditioning, including dehumidification and pressurization.

SOFC are high-temperature fuel cells that have the potential to run on numerous fuel types in addition to hydrogen. SOFC are not as mature as PEM because of challenges with high-temperature materials. However, SOFC offer the potential for greater efficiency. An airbreathing fuel-cell system must intake air for the oxygen required for operation. High altitude operation might require one or more turbos to provide air at the appropriate pressure, much like a reciprocating engine. A combustor separate from the fuel cell burns hydrogen gas and conditioned oxygen to drive the turbo expander, which, in turn, drives the compressor.

Fuel-cell systems can operate in a regenerative fashion. The byproduct of hydrogen-oxygen fuel cell operation is water, which can be captured and stored. Power is provided to an electrolyzer by a separate power source, such as solar arrays, to separate water into hydrogen and oxygen in a reverse osmosis process. The hydrogen and oxygen are generally stored in gaseous form to avoid the losses associated with cryogenic storage. Fuel cells that perform the function of an electrolyzer when operating in reverse are known as regenerative fuel cells (RFC). RFC are generally not as efficient as optimized electrolyzer systems, but they can provide weight savings and complexity reductions by combining both functions into a single element.

One of the biggest advantages of fuel cells relative to batteries is the hydrogen's very high specific energy value of 33.3 kWh/kg, which even stands out from the gasoline's value of approximately 13.0 kWh/kg. However, hydrogen is notorious for being explosive. Public perceptions are driven to a large extent by the famous Hindenburg airship accident, which was primarily caused by the flammable skins rather than the hydrogen lifting gas. Still, many of these concerns might be unfounded. Hydrogen is the lightest gas and tends to diffuse quickly upon interaction with the atmosphere. Hydrogen can be stored and handled safely with proper equipment and procedures. The main methods of hydrogen storage are pressurized hydrogen gas, cryogenically cooled liquid hydrogen, and chemical storage.

Unlike conventional batteries, the reactants are external, meaning that as long as the reactants continue to be fed to the fuel cell, electricity can be produced. Moreover, refueling an empty reactant tank is also much faster than recharging a battery.

There are other types of fuel cells currently in existence, including alkaline fuel cells (AFC), direct methanol fuel cells (DMFC), phosphoric acid fuel cells (PAFC) and molten carbonate fuel cells (MCFC). However, PEM fuel cells are seen as the most viable for vehicular applications due to many of its characteristics such as the electrolyte being solid, and so leaking of corrosive fluids is not an issue and the fuel cell can operate in any orientation, the operating temperature being relatively low (80-100°C) meaning start-up times are short, the relatively high power density compared to the other fuel cell types and, finally the possibility of using air to supply the required oxygen through an airbreathing system.

One of the main drawbacks of a battery powered airplane (BPA) is that the limited energy capacity of batteries means that the airplane range is significantly less than that of a conventional airplane. With the ability to carry more energy on-board the airplane, the advantages of a fuel cell powered airplane (FCPA) start to become apparent. The FCPA can achieve a much longer range with an on-board hydrogen gas tank, making the FCPA range competitive with conventional and hybrid airplanes. Although at a first glance, fuel cells look like a more prominent solution for future electrification of airplanes, the reality is that batteries continue to be perceived by most as the prominent solution for the realization of the all-electric airplane dilemma [40].

The efficiency of a BPA is unsurpassed and it will always take more energy to get from point A to point B in an FCPA. The higher efficiency is due to the electrochemical reaction in batteries being more efficient than the reaction in a PEM fuel cell but also because the latter requires a balance of plant system that delivers the external reactants to the reaction sites. The efficiency of the PEM fuel cells is increased dramatically with higher reactant pressure, and the air compressor consumes the most energy of the balance of plant components, thereby reducing the efficiency the most. The BPA also relies on simpler technology that does not cost as much to build. While BPA have range and recharging limitations, FCPA boast an efficiency that is higher than ICE airplanes but do not offer a large enough gain to overcome the higher purchase price and lack of hydrogen refueling infrastructure that currently exists [40].

2.3.4 Solar Power Performance

Solar powered airplanes have also been at the forefront of EP research and development and, to this day have already accomplished considerable milestones in this area, such as the Solar Impulse II, which completed the first flight around the world, taking over 505 days to fly 42000 km at an average speed of 72.4 km/h, being only powered by solar energy through more than 17000 solar cells [41].

Solar cells use the photovoltaic effect to convert the sun's radiated power into electrical power. This power does not require onboard energy storage for peak daylight operations. However, multiday flights require that excess energy be stored to power the airplane through the night. An airplane that solves this energy balance can operate almost indefinitely, bounded only by reliability and component life, as was shown with the Solar Impulse II program.

Individual solar cells are combined in solar arrays. Much like a battery and fuel cells, the solar cells can be arranged in combinations of series and parallel to yield the appropriate voltage. Integrating solar arrays on an airplane involves compromises across a number of disciplines.

A flat array panel can be mounted on the aft upper surface of the wing, perhaps between the maximum thickness point and the trailing edge. This is the region of the airfoil with the least curvature on the upper surface. An externally mounted array requires a large flat section over this region, which increases the airfoil drag and can reduce the maximum lift coefficient. Even arrays made of brittle crystalline cells can accommodate some curvature, and so very large solar-powered airplanes can have externally mounted arrays on relatively conventional airfoils [28].

Alternatively, the array can be mounted inside a wing, though this requires a covering material that does not absorb light in the critical wavelength range for the solar cell. Also, any structure required to maintain the wing aerodynamic geometry, such as ribs and spars, can cast a shadow on the array. Solar arrays cause structural challenges. Solar-powered airplanes usually have gossamer structures, and the solar arrays comprise a large portion of the wing weight. Most of the solar-array weight is aft of the wing torsional axis, which can require additional structure or active aeroelastic control along the wing to prevent flutter. The weight of the arrays can create static sink on the wings both along the span and torsionally [28].

Solar arrays drive wing sizing. Many solar-powered airplane design efforts find that the wing area required to generate propulsion power is greater than the optimum wing area for minimum power flight. The wing must grow to accommodate the additional solar collection area. However, the increased area results in higher airplane weight, more drag, and hence more required power. The wing sizing is often solved through optimization. Other surfaces such as horizontal tails may grow in size to increase the collection area. Solar arrays perform best when oriented normal to the sun vector. Aerodynamic surfaces such as wings and horizontal stabilizers perform best when nearly horizontal. The stressing conditions for solar-powered flight involve low sun angles, which coincide with early morning, late afternoon, winter, and extreme latitude flight. To collect at these low sun angles, the aerodynamic surfaces must be made more vertical to increase the normal component of the sun vector [28].

Some approaches include the Aurora Flight Sciences Vulture Z-wing, vertically folding wing tips, and rolling vertical tails. All of these configurations increase the power required for flight, but

more than compensate for this by increasing the power generated by the arrays. These configurations convert to a minimum drag state to reduce the power required to fly at night. As can be observed solar power yields feasible results but at the cost of restrains that make this kind of technology impossible to be implemented for the all-electric airplane capable of standing its ground to ICE models performances. This type of technology would be more suitable for long sustained missions such as unmanned reconnaissance airplanes and, aerospace programs such as satellites.

2.3.5 High Power Density Generators and Motors

Hybrid-electric, turbo-electric and all-electric airplanes will all require light, efficient and high-power density motors to fit in with the weight and size constraints of an airplane, particularly for configurations that employ multiple distributed fans to achieve high propulsive efficiency. Hybrid-electric and turbo-electric architectures will also require light, efficient and high-power density generators to convert shaft power to electricity, along with an intermediate, lightweight gearbox to reduce the turbine's high rotational speed to a slower rate suitable for a generator.

Fortunately motor and generator development has been far more successful in the immediate time compared with battery technology and, as of today there is a plethora of light, efficient high-powered EM, capable of providing up to 300 kW, with power-densities of about 9.0 kW/kg and efficiencies of 95%.

In addition to generating quantities of power an order of magnitude larger than current airplane, electrically-propelled airplanes will need the power electronics to convert, switch and condition this power. As well as performing these functions with minimum electrical loss, the requisite power electronics will also need to operate with the minimum associated heat generation. This factor is particularly important given the multi-MW electrical power systems that will be required for RA and LCA and the resulting need to dump any surplus of heat generated. Conventional airplanes can currently use fuel as a reservoir to dump surplus heat, but this option will not be available in electrically-propelled airplanes.

Also, transmitting large quantities of electrical power around an airplane should ideally be done at high voltages in order to minimize resistive losses, however transmitting high power at high voltage will inevitably lead to the risk of insulation breakdown and arcing given the limitations imposed by Paschen’s Law. At the same time, long cable runs in configurations employing multiple propulsive fans distributed around the airplane will add further weight, compounding the additional weight already required for on-board batteries.

2.3.6 New Airplane Architecture

As was mentioned before, the conventional structural configuration, is not the best suitable design type to model electrically-propelled airplanes, as these can benefit greatly from certain

aspects that conventional airplane designs just cannot offer, such as more aerodynamic configurations.

One of the potential improvements offered by EP is the benefit of boundary layer ingestion [42]. Many of the RA and LCA electric architectures propose the use of aft-mounted propulsion systems, positioned such that air coming off the airplane fuselage is ingested into the propulsion system. Despite the relatively slower speed of the ingested air, electric fans would suffer from less efficiency loss in the more disturbed air compared to the fan of a conventional turbofan, whilst also benefitting from fewer installation constraints.

Designers have also been pushing for a more distributed propulsion system configuration, as it offers a wide array of benefits to electrically-propelled airplanes, but at the moment, also offer a significant amount of challenges that need to be resolved in order to make this idea a key feature of future EP concepts. Del Rosario et al offer some clarity and insight on this subject.

2.3.7 Regulation

To enable the potential of EP aviation, there will need to be effective new regulations for new technologies, new platforms and new aviation systems.

First, as new technologies are developed in the field of electric aviation, each technology will need to have regulatory backing to be applied. For example, regulation will play a part in verifying and certifying the use of MEA systems, and any progression with EP will require airworthiness certification, as well as broad regulatory acceptance for enabling technologies such as high-powered batteries, high voltage distribution, and boundary layer ingestion.

Second, regulation will be critical to enable new platforms. Regulation and certification procedures for new architectures such as distributed fans will be required to allow the full potential of EP to be achieved.

Third, if and when technologies and platforms progress to enable UAT, far-reaching regulatory changes would be required to enable entirely new aviation systems, such as for the regulation and control of urban commuter air transportation systems, as well as integration with other urban infrastructure and corresponding regulatory regimes.

At the heart of regulation are the issues of safety and reliability. In an age of increasingly significant cyber-security concerns, the introduction of autonomous flight systems and the potential of urban commuter air transport become even more challenging with the possibility of vulnerable software and systems. Engineers, investors and regulators alike must address two main safety issues. First, air traffic control infrastructure and airspace management will become of paramount importance, necessitating the management of an increasing number of UAVs and the management of potential urban commuter air transports, requiring control of an

entirely new airspace, coupled with integration into existing air traffic control systems. Second, governments, regulators and private companies alike will have to invest in measures to prevent cyber-security breaches in increasingly software-driven airplane, for all platform types. In recent months, both the FAA and EASA have taken meaningful steps to open the doors to EP. A key change is in FAA Part 23 and EASA CS23. Since 2017, larger classes of GA airplanes are able to fly non-traditional engine types legally, including EM. This not only opens revenue potential for developers in general aviation, but this category of platform is a key stepping stone to even larger architectures. There is, however, a long journey ahead and regulation must keep pace with technological evolution for electrically-propelled airplanes to achieve their potential.

Chapter 3

Case Study

In this chapter, a prominent general aviation airplane will be selected and an overview of its specifications will be made regarding performance, aerodynamics, weights and propulsion system. A structural analysis won't be performed as the objective of this dissertation is to analyze the impact of substituting an ICE with an EM and consequent storage device in an airplane and verify the changes in performance, using an algorithm written in the program MATLAB.

3.1 Selection of the Airplane

Starting with the selection of the airplane, the general aviation market in today's age offers a vast range of selection for both commercial and non-commercial activities with many types of needs and services This includes flying clubs, flight training schools, agricultural aviation, flight competitions and transportation of light cargo or a small number of passengers, normally between 1 to 5 depending on the configuration of the airplane.

Flight training schools offer a vast selection of airplanes that are normally confined to a small area where they operate removing the need for high endurance, high range performance operations which is a mandatory requisite for airplanes with EM propulsion system installed due to current battery technologies as was be shown in Chapter 2 referring to the batteries performance barriers. Moreover, the fact that, today's charging capabilities of the batteries are very time consuming, presents yet another barrier for implementation of this technology in today's flight market.

For the reasons listed above it was decided by the author, that his efforts would be focused on selecting an airplane in the flight training schools sector. The author, having the pleasure to have already experienced flight in the Aerospool Dynamic WT9 ultralight airplane from hangar 5 flight academy, situated in Cascais, Lisbon and, after doing some research about the airplane's background decided that it would be a good test bed for this study.

3.2 Airplane's Specifications and Performance

The Aerospool Dynamic WT9 ultralight airplane as the name suggests is an ultralight designed and produced by Aerospool manufacturing company native to Slovakia. It features cantilever low-wing, a two-seats-side-by-side configuration enclosed cockpit, a fixed or retractable tricycle landing gear, a single engine in tractor configuration, being by standard the Rotax 912USL, capable of providing up to 73.5kW of maximum power and, a EVRA PerformanceLine propeller of 3 blades, 1.750m of diameter and a fixed pitch, ground adjustable with pitch

setting of 23º measured 200mm from blade tip (75% of radius) which corresponds approximately to 1.750m of fixed pitch.

The following table 3.1, contains the airplane's aerodynamics, weight/masses and propulsion system specifications, taken from [44-46].

Table 3.1: Dynamic WT9 ICE configuration specifications.

Airplane's Specifications			
Aerodynamic	S	[m^2]	10.5
	B	[m]	8.926
	AR	--	7.588
	e	--	0.8
	K	--	0.052437
	$C_{L,max}$	--	1.95
	$C_{D,0}$	--	0.006
Weigh/Masses	m_{TO}	[kg]	600.0
	MTOW	[N]	5883.99
	n_{wing}	[N/m^2]	560.38
	$m_{airframe}$	[kg]	293.4
	payload	[kg]	164.8
Engine	m_{engine}	[kg]	56.6
	P_{max}	[kW]	73.5
	Q_{max}	[Nm]	128
	RPM_{max}	[rev/min]	5800
Propeller	B	--	3
	d	[m]	1.750
	p	[m]	1.750

The next table 3.2, presents the airplane's performance parameters, taken from [43-44].

Table 3.2: Dynamic WT9 ICE configuration performances.

Airplane's Performances		
n_+	--	4
n_-	--	-2
V_{stall}	[m/s]	23.9127
V_{rot}	[m/s]	28.6952
V_{maneuv}	[m/s]	47.8254
V_{cruise}	[m/s]	60.20
S_{TO}	[m]	160

ROC	[m/min]	330
ROD	[m/min]	180
h_{max}	[m]	5500
h_{OA}	[m]	4500
m_{fuel}	[kg]	85.2
Endurance	[h]	8.2
Range	[km]	1411

3.3 Numerical Model Thought Process

In order to achieve the objective of this dissertation, which was to create an algorithm capable of delivering to the user, with inputs related to the airplane's specifications and performances, an EM propulsion system suitable for substitution of the ICE propulsion system currently in use, several constraints were needed to be implemented, in order for the outcomes to not exceed realistic values.

Another objective that was established by the author, further into the realization of this dissertation, was the necessity to remove the need to rely on other external programs to obtain important data relevant to this study, in order to save time and remove inconvenience of having losses of precision in the results, when transferring data from one program to another, thus a function was added to the algorithm that included the selection of a propeller and its performance calculation.

The numerical process featured in figure 3.1 demonstrates how the code will iterate until a converged solution yields a feasible result.

Since the algorithm will not include any physical changes to the airplane body or wing structure, the variables related to aerodynamics and most masses can be considered fixed variables, so the algorithm will use the current wing measurements and configuration as the first constraints related to the airplane, as well as its masses. The maximum take-off mass and a minimum recommended payload will be used as constraints in order to define the array of values that the EM and battery system masses can take without infringing the constraints established by the total mass of the airplane and the minimum acceptable payload. Finally, it was decided to add one final constraint, which referred to the main performance requirement of the flight mission, whether it will be range or endurance.

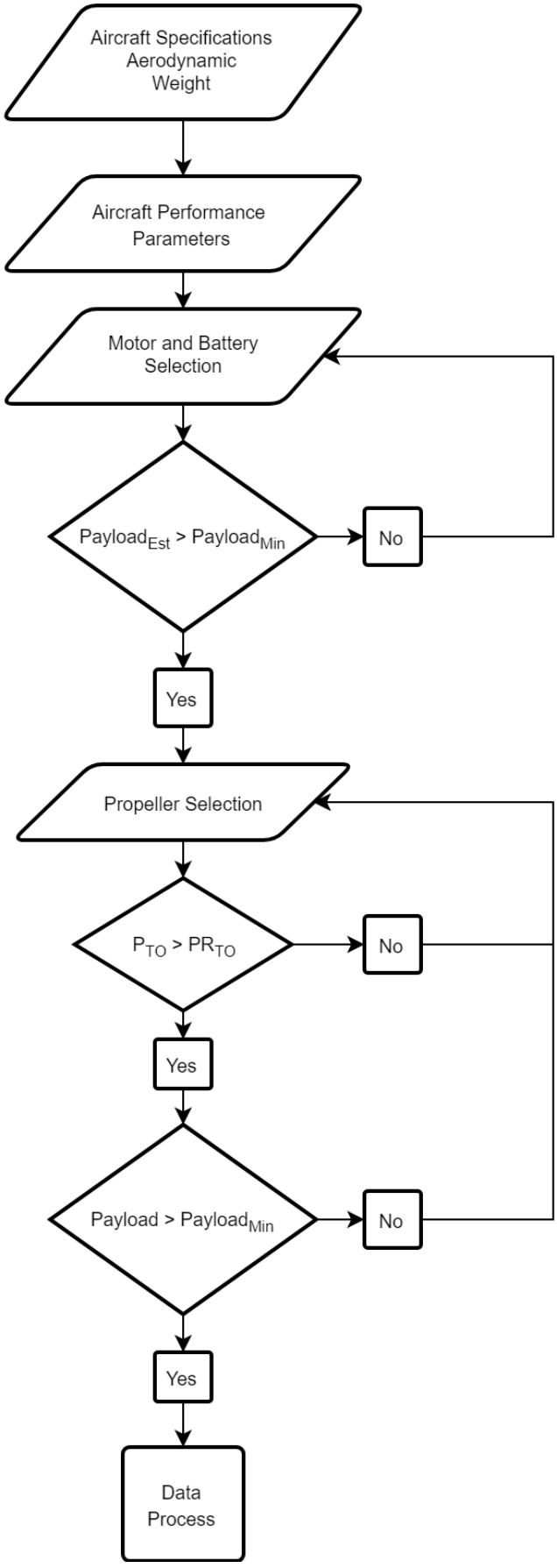

Figure 3.1: Numerical process design.

Having set these constraints, the code was divided into two main phases, the first one would focus on performing an early estimation of the necessary energy to achieve the established flight mission, using variables such as power required at each flight segment, calculated with the values given by the ICE configuration, predominantly the cruise speed, rate of climb and rate of descent and verify if both the EM and battery systems chosen by the user as inputs, respect the constraints established by the airplane's specifications. If the verification fails, the code will request the user a new EM and battery systems, in order to restart the verification process, if the verification succeeds, the code will continue into the second phase.

In the second phase, the code will initiate with the selection of a propeller and its properties and, will start a series of iterative processes, in order to verify if the chosen propeller, can meet the necessary requirements and, at the same time guarantee that the array of results do not exceed the boundaries established. If this does not verify, the code will ask the user a new set of properties for the propeller selection and, will start with a new set of iterations for a new verification. By contrast, if the verification does succeed the code will return the final solution with every single relevant result and the corresponding graphs, accordingly.

3.4 Numerical Model Development

In this chapter, the numerical model will be implemented and, explained step by step, presenting every equation accordingly. It is important to mention that the code was divided into 7 distinct functions: main function, motor and Battery selection function, performance estimation function, propeller selection function, performance function, data processing function and, finally, mission profile function. The code was structured this way in order to facilitate implementation of every segment of it, into the main function without having the extra work to write constantly the same lines of code and make the code too long and hard to read, as it uses a vast number of iterations that repeat the same processes, in case these are not validated by the inputs of the user with the established constraints.

3.4.1 Main Function

The code starts with requesting both relevant mission altitudes, take-off altitude and cruising altitude, which will be named has operating altitude and, delivers through the MATLAB function "atmosisa" the values of temperature, speed of sound, air pressure and air density which correspond to the ISA values for both chosen altitudes, accordingly. After this, the user is requested to input the values of the aerodynamic and weight variables from the airplane.

Having both the wingspan "b" and wing area "S" the code calculates the wing aspect ratio through:

$$AR = \frac{b^2}{S} \qquad (3.1)$$

Now the Oswald span efficiency factor "e" needs to be defined and, [47] established that this value could range from 0.7 to 0.85 in subsonic speed for conventional fixed-wing airplanes with a moderate aspect ratio and sweep with wing flaps retracted, so in this case study the value was defined as 0.8. After this, the drag-due-to-lift factor "K" can be calculated accordingly:

$$K = \frac{1}{\pi e AR} \quad (3.2)$$

The only variables left in this section are the maximum lift coefficient "$C_{L,max}$" and drag at zero lift "$C_{D,0}$", which will have to be obtained through an external 3D aerodynamic analysis program called XFLR5, in which the user introduces an airfoil representative of the airplane's wing airfoil and analyses its aerodynamic properties. In this case study, after some extensive research, it was found that the Nasa/Langley MS(1)-0313 airfoil was a good fit for this airplane.

Moving on, the next set of data requested are the weight specifications of the airplane, these include the maximum take-off mass "m_{TO}", the airframe mass of the airplane "$m_{Airframe}$" and the minimum acceptable payload "payload" which are taken from the ICE system configuration and, the maximum take-off weight "MTOW" which is calculated as such:

$$MTOW = gm_{to} \quad (3.3)$$

And, the wing loading "n_{wing}" applied to the aircraft which is also calculated as follows:

$$n_{wing} = \frac{MTOW}{S} \quad (3.4)$$

Having introduced the airplane's specifications, the next step will be to give the airplane's performance parameters. These parameters will be based on the values taken from the ICE system, as our objective is to remove and substitute this system in favor for one eco-friendlier and, also more efficient, as EM systems do not suffer from some of the disadvantages that ICE systems suffer, since the internal mechanisms differ substantially from one another.

Still, in terms of power production, both propulsion systems are capable of offering, nowadays with the advances in EM technology, similar performance results. The biggest difference expected from both systems is the power supply system, which will, as a result, demonstrate a contrast in the performance parameters related with maximum range and endurance outputs.

For these reasons, it is acceptable to use the established performance parameters of the ICE, in order to obtain a preliminary estimation of the battery mass necessary to perform the flight mission requested, with the type of battery and EM introduced by the user.

First the maximum positive and negative load factors, "n_+" and "n_-", need to be defined, as this will allow determining the flight envelope and, consequently the different speeds, that are

required to be calculated with the proper equations. Having the maximum positive load factor defined, the stall speed "V_{stall}" can be calculated firstly:

$$V_{Stall} = \sqrt{\frac{2MTOW}{\rho_{TO} S Cl_{max}}} \quad (3.5)$$

After calculating the stall speed, the maneuvering speed "V_{maneuv}" and the rotation speed "V_{rot}" can be obtained by performing the next set of calculations, accordingly. The constant value of 1.2 in equation 3.7 is referred as a standard value for the rotation speed, reported by SKYbrabry.

$$V_{maneuv} = \sqrt{n_+} V_{stall} \quad (3.6)$$

$$V_{rot} = 1.2 V_{stall} \quad (3.7)$$

Finally, the cruise speed is defined, by the value taken from the ICE system. Then the user is asked to give information about the terrain in which the airplane will be taking-off, choosing from 5 different options, taking the form of the variable "μ".

Table 3.3: Terrain Friction Coefficients.

Terrain Type	**μ**
Asphalt	0.020
Concrete	0.030
Dirt	0.050
Low Grass	0.050
High Grass	0.100

Next, the rate of climb "ROC", the rate of descent "ROD" and the take-off ground roll "S_{TO}" need to be given, to enable the estimation of time for each flight segment, to calculate the total energy needed for the established flight mission. The values given by the ICE will be used here as well. It is also worth to consider the efficiency at which the propeller normally performs, in order to avoid losses in precision from the results obtained in the estimation phase process, for this reason, an average propeller efficiency of 0.8 will be adopted.

Finally, before moving to the motor and battery selection, a final performance requirement is needed to be established, to finalize all of the constraints. The code gives the option to choose between a maximum range or endurance requirement to the user. Depending on the option chosen by the user, some equations will differ further ahead.

3.4.2 Motor and Battery Model Selection Function

In this next section, the code requests the user a battery cell, in order to model and size a battery system capable of supplying the necessary energy for the whole flight mission, as well as an EM capable of producing enough power for each flight segment.

For the selection of the battery cell, in today's market, there is a vast selection of different types of batteries which differ from each other in voltage, amperage, capacity, mass and most importantly electrochemical reactions which result in different types of applications. Nowadays, the lithium batteries prove to be one of the most versatile types of batteries coming to the market offering a wide range of applications. The different lithium-cathode-electrolyte chemistry type batteries offer a more robust and ideal type configuration in flying applications.

One of the most important, if not the single most important factor, to account for EM and battery powered airplanes is the battery cell energy to mass ratio, given in Wh/kg. The more energy J = Ws can be fitted per kilogram, the more energy is available for less mass, this results directly in higher performances, such as higher range and higher endurance with a lesser battery pack mass, which is crucial for flying more economically and efficiently.

Having this in mind and, observing table 2.1 from chapter 2, it can be seen that the lithium cobalt oxide ($LiCoO_2$) batteries offer a good value of energy to mass ratio for the secondary battery type class. The next table shows a lithium cobalt oxide based cell specifications, that will be used for this case study [48]. It needs to be noted that for the purpose of this analysis, parameters such as commercial availability, safety risks, and efficiencies losses regarding the battery electro-chemical reactions among others will not be considered. This analysis should be considered as a hypothetical case.

Table 3.4: $LiCoO_2$ battery specifications (model 18650).

Battery cell		
U_{batt}	[V]	3.7
C_{batt}	[Ah]	2.4
m_{batt}	[kg]	0.045
E/m_{batt}	[Wh/kg]	197.3

After introducing the three main battery specifications, the code calculates the battery cell energy to mass ratio through the following equation:

$$E/m_{batt} = \frac{C_{batt} U_{batt}}{m_{batt}} \quad (3.8)$$

With the battery selection done, the code moves on to the EM selection. Nowadays, similarly to the batteries, there is a vast selection of EM in the market that differ from each other, in

the type of configuration, mechanisms involved and use in applications. Brushless EM are being predominant in the Electric Vehicle (EV) sector these days. They provide many advantages when compared with other types of EM in EV applications, such as the brushed EM.

Considering all the information obtained about EM, the author chose the EMRAX as the best option for this case study. The EMRAX 208 is an axial flux permanent magnet motor with sinusoidal thee phase current, which is more commonly known as a PMSM (Permanent Magnet Sinusoidal Motor) [49-50]. PMSM mostly behaves as BLDC EM. Both are powered by DC power source, but PMSM possesses an inverter which transforms the DC into AC, one of the bigger differences between these two is that PMSM exhibits a sinusoidal back EMF, sinusoidal current and distributed windings, as for BLDC, it possesses a trapezoidal back EMF, square wave current and, concentrated windings.

The EMRAX was developed mostly for airplane industry since 2008 by EMRAX Innovative E-Motors company, native to Slovenia. Their motors possess high fault tolerant characteristics, also high reliability and one of the great advantages is that they currently feature one of the best-in-class power densities, up to 9 kW per kg making them very suitable for electrically-powered airplanes.

These motors are already used in several aerospace applications, such as the EMRAX d.o.o Apis EA2 electric glider plane, Pipistrel d.o.o Electric Taurus glider plane, the Alexander Schleicher GmbH glider plane, the Axter Aerospace airplane, the Eurosportaircraft airplane and even the SunSeeker Duo solar-powered flight Airplane, among others. EMRAX currently supports 5 motors that differ from each other mainly in the amount of mechanical power each can deliver. In the end, the author decided to go with the EMRAX 208 module, as it demonstrated similar performance capabilities as the ICE Rotax 912USL.

The EM specifications will be presented in the next table (table 3.4). Unfortunately, this motor works in a constant torque regime, due to the nature of its configuration, as it possesses a current controller that uses a technique called PWM (Pulse-Width Modulation) which allows the variation of voltage applied by the power source through a variation in frequency. This allows for an increase in speed of the motor regime while maintaining a constant torque regime until the rated speed of the motor, after which, the magnetic flux created in the motor starts to suffer an effect called magnetic field weakening, which lowers the overall torque produced by the motor as the velocity increases.

In reality the torque is never actually constant, but close to, because of losses associated with the mechanisms of the motor [49-50]. Due to this, the code will not feature the motor's performance calculations, as it is impossible to predict real results, without fieldwork testing of the motor. Thankfully the manufacturer already provides these results in graphs, which will be the focus point, to validate future results provided by the code.

Table 3.5: EMRAX 208 specifications [51].

EM specifications		
$U_{motor,max}$	[V]	320
$I_{motor,max}$	[A]	320
$I0_{motor}$	[A]	8
$Q_{motor,max}$	[Nm]	150
$RPM_{nl,motor}$	[rev/min]	7040
$RPM_{fl,motor}$	[rev/min]	5760
Kv_{nl}	[rev/minV]	22
Kv_{fl}	[rev/minV]	18
Kt	[Nm/A]	0.469
$P_{motor,max}$	[kW]	80
m_{motor}	[kg]	9.1
P/m_{motor}	[W/kg]	8791.21
η_{motor}	--	0.96

Figure 3.2, shows a schematic and front, back and side views of the EMRAX 208.

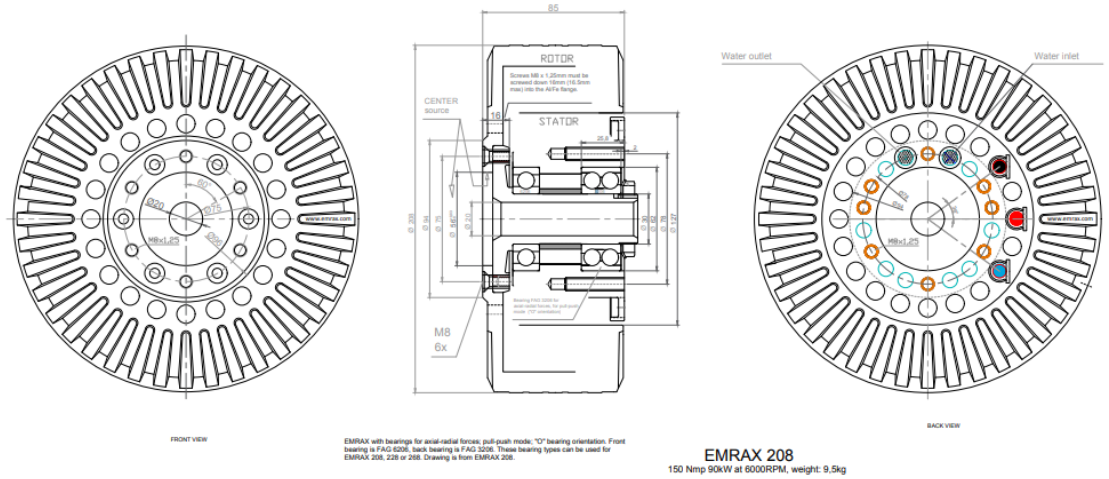

Figure 3.2: EMRAX 208 schematics and views [52].

In the motor specifications, only the speed constant at full-load and no-load "Kv_{fl}" and "Kv_{nl}", the torque constant "Kt" and, power density "P/m_{motor}" are calculated by the code, all the other variables are introduced directly by the user, taken from the manufacturer table specs.

$$Kv_{nl} = \frac{RPM_{motor,nl}}{U_{motor}} \quad (3.9)$$

$$Kv_{fl} = \frac{RPM_{motor,fl}}{U_{motor}} \quad (3.10)$$

$$P/m_{motor} = \frac{P_{mech,motor}}{m_{motor}} \quad (3.11)$$

3.4.3 Performance Estimation Function

Immediately after introducing the motor specs variables, the code runs a first verification process. It will verify if the motor is capable of supplying enough electrical power to overcome the power necessary to take-off. If the verification succeeds, the code will move on, if not, the code will give a warning and ask the user to introduce another motor with new specs.

$$PR_{TO,estimated} = \frac{1}{\eta_{prop}\eta_{motor}} * \frac{V_{rot}1.44MTOW^2}{g\rho_{TO}SCl_{max}S_{TO,desired}} \quad (3.12)$$

Having obtained an estimation of the required electrical power to take-off, the estimated required electrical powers at cruise and descending flight need to be calculated, in order to be able to do a preliminary estimation of the total energy needed to accomplish the established flight mission.

$$PR_{cruise,estimated} = \frac{1}{\eta_{prop}\eta_{motor}} * \left[\frac{1}{2}\rho_{OA}V_{cruise,desired}{}^3SCd_0 + \left[\frac{MTOW}{S}\right] * \left[\frac{K*MTOW}{\frac{1}{2}\rho_{OA}V_{cruise,desired}}\right]\right] \quad (3.13)$$

$$PR_{D,estimated} = I0_{motor} * \frac{RPM_{motor,nl}}{Kv_{nl}} \quad (3.14)$$

For the descending flight, there are two different types, denominated powered descending flight and, gliding flight. Most ICE airplanes prefer to use a powered descending flight, as most ICE suffer from poor reliable transition from gliding to powered flight because of the longer time it takes to charge the engines from idle stance to a cruise condition. EM do not suffer from this and, can instantly go from a no-load stance to a cruise condition, making gliding descending a very interesting choice for pilots in EP airplanes. This allows for a minimum consumption of energy derived from the no-load current caused by heat losses.

After calculating all the required powers, an estimation of the total energy needed to accomplish the established mission flight can be done by multiplying each required power with its corresponding flight time. The code also adds 15 minutes of cruise flight time in order to include a loiter phase if necessary. It is also important to mention that, depending on the performance requirement chosen by the user, either range or endurance, the total energy needed for the battery pack equation will vary slightly as can be seen in equations 3.15 and 3.16, respectively.

$$E_{battpack,estimated} = PR_{TO,estimated}\left[\frac{h_{OA}}{\frac{ROC_{desired}}{60}}\right] + PR_{cruise,estimated}\left[\frac{RNG_{required}}{V_{cruise,desired}} - \frac{h_{OA}}{\frac{ROC_{desired}}{60}} - \frac{h_{OA}}{\frac{ROD_{desired}}{60}}\right] + PR_{D,estimated}\left[\frac{h_{OA}}{\frac{ROD_{desired}}{60}}\right] + PR_{cruise,estimated}[15 * 60] \quad (3.15)$$

$$E_{battpack,estimated} = PR_{TO,estimated}\left[\frac{h_{OA}}{\frac{ROC_{desired}}{60}}\right] + PR_{cruise,estimated}\left[End_{required} - \frac{h_{OA}}{\frac{ROC_{desired}}{60}} - \frac{h_{OA}}{\frac{ROD_{desired}}{60}}\right] + PR_{D,estimated}\left[\frac{h_{OA}}{\frac{ROD_{desired}}{60}}\right] + PR_{cruise,estimated}[15 * 60] \quad (3.16)$$

In this case study, the author decided to use the endurance as the performance requirement for the flight mission, for this reason, equation 3.16 will be used in place of equation 3.15 for the calculation of the battery pack total energy.

With this, the battery pack specifications can finally be defined, in particular the total battery pack mass, the total capacity and the total applicable voltage. With the battery cell energy to weight ratio, and the total battery pack energy, the total battery pack mass can be calculated by the following equation:

$$m_{battpack,estimated} = \frac{E_{battpack,estimated}}{E/m_{batt} * 3600} \quad (3.17)$$

Then the battery pack voltage value is defined as the maximum acceptable voltage applied to the EM and, with this, the total capacity of the battery pack can be estimated.

$$C_{battpack,estimated} = \frac{E_{battpack,estimated}}{U_{battpack,estimate} * 3600} \quad (3.18)$$

Finishing these steps, the code initiates a final verification for phase one, where the code will verify if the total combined mass of the airplane does not exceed the maximum take-off mass and if any earlier established constraint fails to be respected.

$$m_{empty,estimated} = m_{airframe} + m_{motor} \quad (3.19)$$

$$payload_{estimated} = m_{to} - m_{empty,estimated} - m_{battpack,estimated} \quad (3.20)$$

If the obtained estimated payload is lesser than the minimum acceptable payload defined in the beginning, the validation fails and the code sends out a warning to the user and asks for new battery and EM inputs to re-initiate the estimation process. If the obtained estimated payload is bigger than the minimum acceptable payload defined in the beginning then the current inputs are validated and the code moves on to its second phase.

3.4.4 Propeller Selection Function

The second phase of this code initiates with the selection of the properties of an undefined propeller, after this a simplified version of the Glauert Blade Element Theory [53] is applied and the code starts performing several iterative processes of calculations and validations, in order to verify if the propeller and the EM chosen, converge. If they do not converge, a warning is given to the user and, the code returns to the start of phase two and requests a new set of properties for the propeller, to restart the whole process again, until a match is obtained.

The Glauert Blade Element Theory is a relatively simple, yet effective method for predicting the performance of a propeller. The method consists in dividing the propeller blade, into several independent, equally distant sections along its length. In each section, a balance of forces is applied comprising of lift and drag resultant from thrust and torque produced by the section in 2D, as well as a balance of axial and angular momentums. This permits the formulation of a set of non-linear equations that can be iteratively solved for each blade section.

With the thrust and torque of each blade section calculated, an overall prediction of the propeller's performance can be obtained by simply summing them. Still some caution is advised as the simplification of this theory does not take into account secondary effects such as 3D flow velocities induced on the propeller by the shed tip vortex, radial components of flow induced by angular acceleration due to the rotation of the propeller, tip loss factor effects developed by Prandtl and finally the chord distribution along the blade's length is considered constant, which will ultimately lead to an over prediction in thrust and in contrast an underprediction in torque, compared with tested propeller results, producing an increase in theoretical efficiency of 5% to 10% over measured performance.

So, to start, the user is asked to introduce the desirable propeller properties, the propeller diameter, the fixed pitch, the blade chord, the number of blades and propeller speeds at take-off and cruise conditions. The blade is then divided into a discrete number of sections, in this case the author decided that the code would separate the blade into 10 equal sections. Figure 3.3 shows a visual representation of this process.

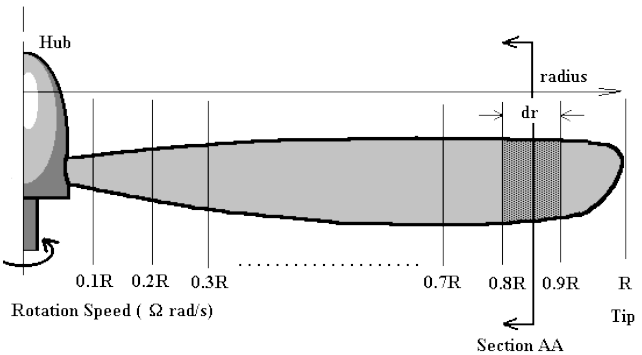

Figure 3.3: Blade division into subsections, taken from [54].

With this, if the assumption that for each section there are only axial and angular velocity components and that the induced flow resultant from other sections is negligible is made, each section's flow can be analyzed independently simplifying the process. In figure 3.4 all the components related to the flow applied to the blade section (Section AA from figure 3.3) are shown.

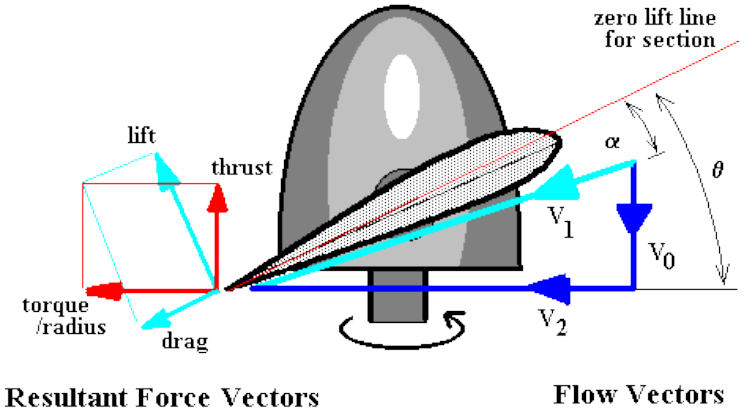

Figure 3.4: Blade flow components, taken from [54].

In order to be able to calculate the total thrust and torque produced from the propeller, the code uses a set of iterative processes along the radius of the blade. Then this process is iterated for every speed established in the speed range, in this case study it was defined from 1 m/s to 120 m/s with a step of 0.01 m/s.

Every blade section will be set at a given geometric fixed pitch angle "θ", which can be obtained from equation 3.21, with "r" referring to the local blade radius.

$$\theta = \tan^{-1}\left[\frac{p}{2\pi r}\right] \quad (3.21)$$

This will result in a flow angle of attack "α" on the blade section derived from the local flow velocity vector "V_1" as can be seen from figure 3.4.

$$\alpha = \theta - \phi \quad (3.22)$$

To get the flow angle of attack, the difference in angle between thrust and lift directions needs to be defined "Φ", which results from:

$$\phi = \tan^{-1}\left[\frac{V_0}{V_2}\right] \quad (3.23)$$

There is a major complexity when applying this theory to calculate the magnitude of the two flow components "V_0" and "V_2". The axial flow velocity vector "V_0" is roughly equal to the

airplane's forward velocity "V_{inf}" but is increased by the propeller's own induced axial flow into a slipstream. On the other hand, the angular flow velocity vector "V_2" is roughly equal to the blade's section angular speed "ωr", but is reduced slightly due to the swirling nature of the flow induced by the propeller. In equation 3.24 "N" is defined as the propeller's speed in rot/s.

$$\omega = 2\pi N \quad (3.24)$$

To determine the axial flow velocity and angular flow velocity vectors accurately, both axial and angular momentum balances need to be applied in order to predict the induced flow effects on a given blade element, for this the blade momentum theory is also applied in conjunction with the blade element theory. Figure 3.5 shows that the induced flow components can be defined as factors that increase the axial flow velocity vector and decrease the angular flow velocity vector.

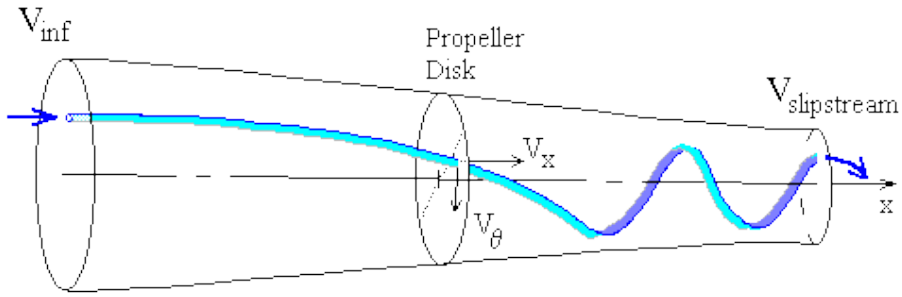

Figure 3.5: Side view of a typical stream tube of flow passing through a blade section, taken from [54].

From this, the inflow factors can be defined as, "a_1" axial inflow factor and, "a_2" angular inflow factor. Only after comprehending this, can the axial and angular flow velocity vectors be defined through the following equations:

$$V_0 = V_{inf}[1 + a_1] \quad (3.25)$$

$$V_2 = \omega r[1 - a_2] \quad (3.26)$$

With both flow vectors calculated, the blade section local flow velocity vector can be determined through the Pythagorean Theorem as follows.

$$V_1 = \sqrt{{V_0}^2 + {V_2}^2} \quad (3.25)$$

The only missing variables needed to calculate the blade's section thrust and torque, at this point, are the lift and drag components normal and parallel to the propeller disk, respectively. These can be acquired through the same method used with the airplane's wing airfoil. So, again with the use of the external program called XFLR5, a common airfoil is chosen as reference, in

this case study the NACA 0012 was used, and with this, 2 equations are formulated. The lift coefficient takes the form of a linear equation and the drag coefficient takes the form of a quadratic equation as follows, accordingly:

$$C_l = m\alpha + b \quad (3.26)$$

$$C_d = aC_l{}^2 + bC_l + c \quad (3.27)$$

From equation 3.26 and 3.27, it needs to be noted that the variables “m”, “b”, “a” and “c” are simply representation of constant values that are calculated from analyzing the graphs obtained by the XFLR5 program.

With all the required variables calculated, the blade’s elemental thrust and torque values can be found through the following equations:

$$\Delta T = \frac{1}{2}\rho V_1{}^2 Bc[C_l \cos\phi - C_d \sin\phi]dr \quad (3.28)$$

$$\Delta Q = \frac{1}{2}\rho V_1{}^2 Bcr[C_d \cos\phi + C_l \sin\phi]dr \quad (3.29)$$

Now, in order to define a good estimation of the axial and angular inflow factors, the governing principle of conservation of flow momentum must be applied for both axial and angular directions. From figure 3.6, for the axial direction, the change in flow momentum along a stream-tube starting upstream, passing through the propeller at section AA and then moving off into the slipstream, must equal the thrust produced by the blade’s section.

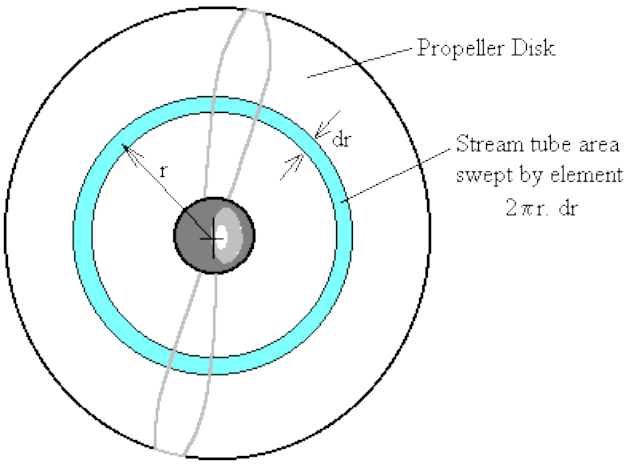

Figure 3.6: Front view of a typical streamtube of flow passing through a blade section, taken from [54].

To remove the unsteady effects due to the propeller’s rotation, the stream-tube used covers the complete are of the propeller disk sweep out by the blade section and all variables are

assumed as average values. By applying Bernoulli's equation and conservation of momentum for the three separate components of the tube, from freestream to the blade section, from the rear of the disk to slipstream far downstream and balancing pressure and area versus thrust, it can be demonstrated that the axial velocity at the disk will be the average of the free stream and slipstream velocities and, thus:

$$\Delta t = 4\pi r \rho {V_{inf}}^2 [1 + a_1] a_1 dr \quad (3.30)$$

For the angular momentum, by considering conservation of angular momentum in conjunction with the axial velocity change, it can be shown that the angular velocity in the slipstream will be twice the value at the propeller disk and, thus:

$$\Delta q = 4\pi r^3 \rho V_{inf} [1 + a_1] \omega a_2 dr \quad (3.31)$$

Finally, by defining a starting value for the axial and angular inflow factors and, through an iterative process with equations 3.32 and 3.33, a more precise value of the axial flow velocity vector and angular flow velocity vector can be estimated.

$$a_{1,new} = \frac{\frac{1}{2}\rho {V_1}^2 Bc[cl \cos\phi - cd \sin\phi]dr}{4\pi r \rho {V_{inf}}^2 [1+a_1]dr} \quad (3.32)$$

$$a_{2,new} = \frac{\frac{1}{2}\rho {V_1}^2 Bcr[cd \cos\phi + cl \sin\phi]dr}{4\pi r^3 \rho V_{inf} [1+a_1]\omega dr} \quad (3.33)$$

After "$a_{1,new}$" and "$a_{2,new}$" have converged within a specific tolerance, through equations 3.28 and 3.29, the values of thrust and torque produced by the blade's section can be found. To get the total propeller produced thrust and torque at a specific air speed, it is only needed to sum all of the blade's sections obtained thrust and torque results.

$$T = \sum \Delta T \quad (3.34)$$

$$Q = \sum \Delta Q \quad (3.35)$$

The next set of processes and equations are applied for the range of airspeed established, in this case study, as was mentioned before, ranging from 1 m/s to 120 m/s. It is also important to emphasize that these iterative processes are realized for 2 distinct conditions, one focused in studying the performance during climbing phase of flight and, the other focused in the overall performance of the airplane in the cruise segment.

After the finalization of the propeller selection phase, the constraints need to be established in order to verify if the propeller chosen properties yield feasible results. These constraints are represented as the thrust and power required to fly. They act as the minimum thrust and power required in order to fly for every airspeed, if the propeller cannot produce more thrust or power at any speed, the propeller's chosen properties are not sufficient and need to be readjusted. But, before the thrust and power required can be established, the lift and drag forces applied on the airplane as well as their respective coefficients need to be considered through the following equations.

$$C_L = \frac{MTOW}{\frac{1}{2}\rho {V_{inf}}^2 S} \quad (3.36)$$

$$C_D = C_{D,0} + K{C_L}^2 \quad (3.37)$$

$$L = \frac{1}{2}\rho {V_{inf}}^2 S C_L \quad (3.38)$$

$$D = \frac{1}{2}\rho {V_{inf}}^2 S C_D \quad (3.39)$$

$$E = \frac{L}{D} \quad (3.40)$$

After having defined the resultant drag and lift forces, the thrust required can be calculated and consequently the power required as well. Note that the available power is calculated the same way as the required power, the difference is, that the available power is obtained from the thrust produced by the propellers times the airspeed.

$$TR = \frac{W}{E} \quad (3.41)$$

$$PR = TRV_{inf} \quad (3.42)$$

With this, both "required and available" powers can be compared through the speed range. There is an infinite number of possible combinations for the results and, is up to the user, by trial and error and systematic iteration, to find the combinations that best fit the case in study. This means taking into account, propeller efficiency, excess of available power, interval of possible flight speeds, among others.

The code only guarantees that, if the selected propeller is not capable of providing at least one point where the available power is equal or greater than the required power, a warning will be given to the user that the current selected propeller properties are not sufficient for a good combination of results and that the user should readjust the properties, in order to restart the analysis.

If the validation succeeds the code moves on to the calculation of other performance variables, in order to acquire sufficient data to create more accurate and precise values of the total energy necessary to accomplish the flight mission established, so that the real mass of the total battery pack is calculated. This requires the division of the process into the three segments of the flight, which are the take-off/climbing, cruise and descending flight segments. The code will analyze each flight segment and through several equations, deliver the most crucial information about each of them.

The code calculates the propeller's coefficients, which then, allows for the calculation of the propeller's efficiency. Should the propeller's max efficiency prove to be too low, the user should consider trying a new propeller with different properties. Efficiency is the most important aspect regarding propellers, as it dictates how much the EM needs to supply the shaft to produce the propellers results, if it is too low the EM might not be capable of supplying the necessary mechanical power to feed the shaft and, make the current set of EM and propeller system not feasible. The higher it is the less energy will be consumed through the flight which will result directly in better performance results with the same total battery pack mass.

The following equations are representative of propeller's advance ratio "J", thrust coefficient "C_t", torque coefficient "C_q" and power coefficient "C_p".

$$J = \frac{V}{Nd} \quad (3.43)$$

$$C_{t,prop} = \frac{T_{prop}}{\rho N^2 d^4} \quad (3.44)$$

$$C_{q,prop} = \frac{Q_{prop}}{\rho N^2 d^5} \quad (3.45)$$

$$C_{p,prop} = \frac{Q_{prop}\omega}{\rho N^3 d^5} \quad (3.46)$$

With this, the propeller's efficiency can finally be calculated, as such:

$$\eta_{prop} = \frac{T_{prop}V}{Q_{prop}\omega} \quad (3.47)$$

The code also implements an equation that will help to determine the interval of airspeed at which the airplane can fly by calculating the difference between the available and required powers, at given airspeed. This will give the maximum and minimum cruise airspeed. The result is given as the absolute value, as this way the range of values can be sorted from lowest to

highest and, the two first values represent the two points where the available and required power lines intersect, giving then the two possible cruise speeds.

$$P_{excess} = \left| P_{prop} - PR \right| \quad (3.49)$$

At this point, there is a final constraint that needs to be implemented, which is the verification of the Mach number at the tip of the blade. If at any point, the Mach number at the tip exceeds the subsonic Mach number threshold "M_{Tip} >= 0.8", the user will need to readjust the propeller properties, as the theory used in this dissertation does not factor nor can predict the shock waves formed over the blade's sections which impact greatly the efficiency of the propeller and can also cause increased loads on the blade which can lead to the potential failure of the propeller.

$$M_{Tip} = \frac{\omega r_{Tip}}{V_{sound}} < 0.8 \quad (3.50)$$

After the cruise segment variables are calculated, the code calculates for both the take-off/climb and descent phase flight, the respective rates of climb and descent, as well as their respective angles, accordingly. Note that the rate of climb "ROC" and rate of decent "ROD" are expressed in meters per minute "m/min" in order to facilitate comparison between the results obtained and the previous values given.

$$ROC = \left[\frac{P_{prop} - PR}{MTOW}\right] 60 \quad (3.51)$$

$$\gamma_{ROC} = \sin^{-1}\left[\frac{\frac{ROC}{60}}{V_{inf}}\right] \quad (3.52)$$

$$\gamma_{ROD} = \tan^{-1}\left[\frac{1}{E}\right] \quad (3.53)$$

$$ROD = \left[V_{inf} \sin\left[\phi_{ROD} \frac{\pi}{180}\right]\right] 60 \quad (3.54)$$

Finally, the code also does an analysis on the parameters for the sustained turn flight and the maximum sustained turn for a better overall and complete representation of the airplane's turn performance.

The sustained turn rate is calculated with the airspeed range in the beginning and also the range of load factor given in the airplane's characteristics.

$$\dot{\psi} = \left[\frac{g}{V_{inf}} \sqrt{n^2 - 1}\right] \frac{180}{\pi} \quad (3.55)$$

The maximum sustained turn rate defines as the name suggests the maximum sustained turn rate at which the airplane can operate. Using equation 17.53 from [47] the airspeed can be calculated as a function of load factor to obtain the maximum sustained turn load factor.

$$V_{max,turn} = \sqrt{\frac{2nMTOW}{\rho_{OA}S\sqrt{Cd_0\pi eAR}}} \quad (3.56)$$

Then just as was done with the sustained turn rate, equation 3.54 Is used to define the maximum turn rate as a function of the load factor and airspeed.

$$\dot{\psi}_{max,turn} = \left[\frac{g}{V_{max,turn}}\sqrt{n^2-1}\right]\frac{180}{\pi} \quad (3.57)$$

The code is then tasked with finding the best values of the performance variables, stored in their own arrays. It will find the best rate of climb and its respective angle and airspeed, as well as the best rate of descent and its respective angle and airspeed as well, for both take-off and operating altitude with the propeller speed established by the user for the climbing segment. It will then calculate the take-off ground roll necessary and verify if the available power at that instant is higher than the required power. These calculations will be based on the equation 17.99 from reference [47].

$$K_T = \left[\left[\frac{T}{MTOW}\right] - \mu\right]_{V_{rot}} \quad (3.58)$$

$$K_A = \frac{\rho_{TO}}{2\left[{MTOW}/{S}\right]}\left[\mu C_L - C_{D,0} - K{C_L}^2\right] \quad (3.59)$$

$$S_{TO} = \left[\frac{1}{2gK_A}\right] ln\left[\frac{K_T+K_A{V_{rot}}^2}{K_T+K_A{V_{init}}^2}\right] \quad (3.60)$$

$$PR_{TO} = \frac{1.44V_{rot}MTOW^2}{g\rho_{TO}SC_{L,max}S_{TO}} \quad (3.61)$$

$$P_{TO} = \left[T_{prop}V\right]_{V_{rot}} \quad (3.62)$$

For the cruise segment variables, as was mentioned above, equation 3.49 will give the interval of excess power which relates directly with the interval of possible airspeeds. By sorting the array obtained from lowest to highest, the two first values will correspond to the airspeeds at which the available and required power lines intersect each other. Then the code needs to run a verification in order to find which point corresponds to the minimum and maximum cruising speeds. After obtaining the maximum cruise speed, speed at which the cruise segment will be

performed, the power usage at cruise can be calculated by use of equation 3.42. This concludes the *propeller_selection* function of the code.

3.4.5 Performance Function

Now with all the important variables stored from the previous section, a more elaborate and accurate estimation of the total combined energy needed for the flight mission can be described. The take-off segment is analyzed, by obtaining the total time needed to take-off from equation 3.63, neglecting acceleration along the runway.

$$t_{TO} = S_{TO} V_{rot} \quad (3.63)$$

Then, with the available power at take-off and time needed to take-off, in conjunction with the motor and propeller efficiencies, an estimation of the total energy needed for the take-off can be found, equation 3.64.

$$E_{TO} = \frac{1}{\eta_{motor}\eta_{prop}} [P_{TO} t_{TO}] \quad (3.64)$$

For the climbing segment, the process will differ from the one used for the early estimation, since at that time there is not much information about the availed power or speed or rate of climb through the climbing phase. So an average value was adopted to calculate the energy needed, but this method is not very precise, because during climbing, as the altitude of the airplane increases, if all properties of the propeller are maintained constant, the rate of climb will tend to diminish due to the air density decreasing. From [55] a good method for estimating time to climb can be developed, in the form of equation 3.65.

$$t_2 - t_1 = \frac{H}{ROC_0} ln \left[\frac{H-h_1}{H-h_2}\right] \quad (3.65)$$

where "H" represents the straight-line ceiling, and is calculated from:

$$H = \frac{h_{OA} ROC_{TO} - h_{TO} ROC_{OA}}{ROC_{TO} - ROC_{OA}} \quad (3.66)$$

and "ROC_0" represents the straight line sea-level rate of climb which can be defined by equation 3.67.

$$ROC_0 = \frac{h_{OA} ROC_{TO} - h_{TO} ROC_{OA}}{h_{OA} - h_{TO}} \quad (3.67)$$

This method allows for the determination of the total time to climb taking into consideration both take-off and operating altitude and their respective rates of climb, but it does not allow

for the calculation of the total energy needed for the climb, as the rate of climb changes at each time and consequently the power used.

In order to be able to calculate those variables, some considerations need to be taken. If the consideration that the airplane is always flying at the best rate of climb at each time frame is true, a straight line can be drawn directly from the point of best rate of climb at take-off altitude to the point of best rate of climb at operating altitude. By process of iteration through time, using equation 3.65 can yield the corresponding altitude at said time frame. If the altitude at time t is subtracted by the altitude at time t-1 the rate of climb at that time frame can be obtained and this value will be within said straight-line.

Now if the same concept of straight-line is applied to the power available curve, the point where the available power corresponding to the rate of climb at that time frame can be found enabling the calculation of the total energy needed to climb by integrating the power used over time.

$$E_{Climb} = \frac{1}{\eta_{motor}\eta_{prop}} \int_{ti}^{tf} P_{ROC} dt_{climb} \quad (3.68)$$

This method removes the need to iterate for every altitude from take-off to operating, which ultimately decreases the time necessary to run the code making this a very cost-efficient method.

The descending flight segment follows a similar process to the one used by the climbing segment. The difference here is that, since the gliding descent is being considered here, the power used at any instant will be the power consumed due to heat losses at the no load regime of the motor. Since P_{ROD} is already related to the electric power consumed by the motor at the no load regime, there is no need to take into consideration the motor and propeller efficiencies into equation 3.69.

$$E_{descent} = \int_{ti}^{tf} P_{ROD} dt_{descent} \quad (3.69)$$

As for the cruising segment, in order to get the total time of cruise, it's only needed to subtract the total time of both the climb and descent segments into the endurance requirement given by the user at the start. Then in order to obtain the total energy for the cruise segment, it is only needed to multiply the power used at cruise, which should be the same for all the segment, by the total cruising time. Equation 3.70 showcases this. Note that here, the motor and propeller efficiencies need to be taken into account again.

$$E_{cruise} = \frac{1}{\eta_{motor}\eta_{prop}} \int_{ti}^{tf} P_{cruise} dt_{cruise} \quad (3.70)$$

Finally, a loiter segment was added in order for the airplane to have a spare 15 minutes of energy in case it is needed due to unexpected events. This segment follows the same method used in the cruise segment, so the total energy for the loiter segment should be obtained by equation 3.70 changing the t_{cruise} for the t_{loiter}. The speed is the same used in the cruise segment.

Having found the total energy needed for each flight segment, it is only needed to sum them to yield the total energy needed for the whole flight mission. After this, using equations 3.17, 3.18, 3.19 and 3.20, the total battery pack mass can be obtained and the payload verification process can be initiated, if it does not respect the constraints given at the beginning, the user will be asked to use a propeller with new properties in order to reinitiate the *propeller_selection* function until a suitable match is found.

3.4.6 Data Processing and Mission Profile Functions

Once these constraints are respected, a solution has been found and the code will proceed to display the most important variables to the user and the corresponding graphs as well as a table showing the progress of the flight mission along its time frames.

Chapter 4

Results

Chapter 4 of this dissertation will present the results obtained from the developed code, as well as a discussion concerning them.

4.1 Results

The developed code focuses its analysis in the performance of the airplane using a newly defined EP system chosen by the author. The airplane's architecture was to remain the same for this analysis as it made more sense to the author, to do a side-by-side comparison between the two propulsive systems using the same architecture, although it has already been explained in the former chapters that electrically-propelled airplanes can benefit substantially from new architectures designs, from which ICE airplanes cannot. References [18-21] give an overview of what changes can be done and the gains associated with them.

The main focal points of the analysis will be weight changes relative to the removal of both the fuel storage system and ICE, and the integration of the batteries storage system and EM. Then other performance parameters will be presented regarding the electrically-propelled airplane's range and endurance among others. With the integration of the propeller design, the performance parameters regarding the propeller's efficiency, coefficients and power and thrust produced will be displayed, which will ultimately add-on to the performance of the electrically propelled airplane.

At the end, the developed code will also feature a mission profile table, which will display the evolution of range and altitude in function of time and, will also display other informative parameters at each instant, such as electric power and current consumed, airspeed, motor speed and the current flight segment.

As it was mentioned in Chapter 3, during the climb and descent segments, the airplane will be flying at the best rates of climb and descent at a constant motor speed. With this consideration, the graphs of rate of climb and descent will feature a straight line that links the best rate of climb and descent at both Initial and final altitude for each segment. This straight line will feature the variation of values of rate of climb and descent for each altitude at which the airplane stands for each instant. Also, only two propeller speeds were considered, one at 5760 rpm which represents the motor maximum speed, where it can produce the most power, that will be used for the take-off and climb segments of the flight and, one at 5000 rpm, that corresponds to the motor cruise speed, which the manufacturer of the EM EMRAX 208, displays the interval of mechanical power it can produce to the shaft. This was used as parameter to

define the properties of the propeller, in order to coincide with the interval of values, the EM offered at said regimes [52].

For the input values used in the code for the analysis, refer to tables 3.1, 3.2, 3.3 and 3.4. Following the structure of the code, the initial results of the estimation for sizing the battery system will be displayed (table 4.1). It is worth noting that these results are based on the performance values taken from the ICE configuration. This means the early estimation can differ slightly from the values obtained with the actual EM configuration, nonetheless these values should prove to be a useful reference for when designing the propeller for the EM configuration.

Table 4.1: Initial Battery System Sizing used for reference.

Initial Battery System Sizing		
$E_{battery}$	[J]	$7.94x10^7$
$m_{battery}$	[kg]	111.72
$U_{battery}$	[V]	320
$C_{battery}$	[Ah]	68.89
$I_{max,battery}$	[A]	344.47
$Payload_{availabe}$	[kg]	185.78

The initial estimation of the battery system sizing reveals that for a requirement of at least half an hour of bare minimum endurance, the available payload for the airplane using the ICE performance values as reference and, the chosen EM and battery cell used for sizing the battery system, meet the requirements established for a minimum acceptable payload of 165 kg. With the first verification process having yield acceptable results the code can continue to its second main process, that includes the selection of a propeller to use alongside the EM and, a more real estimate of the battery system sizing for the flight mission selected.

The propeller properties used for the study are introduced now, in table 4.2. Note that, as was mentioned in Chapter 3, the propeller was assumed as rigid, which means a constant chord distribution along the blade's length was considered.

Table 4.2: Chosen propeller properties.

Propeller Properties		
c	[m]	0.1
B	--	3
d	[m]	0.8
p	[m]	1.10
RPM_{climb}	[rev/min]	5760
RPM_{cruise}	[rev/min]	5000

With the propeller's properties established, the performance obtained through the combination of the EM, propeller and battery system can be displayed through the following graphs. The graphs will contain information regarding power available at cruise vs power required (figure 4.1), as well as, the thrust associated with each (figure 4.2). It will also display the propeller's thrust and power coefficients (figure 4.3), and the resulting efficiency vs the advance ratio of the propeller (figure 4.4). Finally, it will give an overview of the rates of climb for both altitudes used in the process of the code, the take-off and operating altitudes (figure 4.5), as well as the rates of descent (figure 4.6) and, rates of turn (figure 4.7) for the interval of loads defined by the airplane's structural limitations.

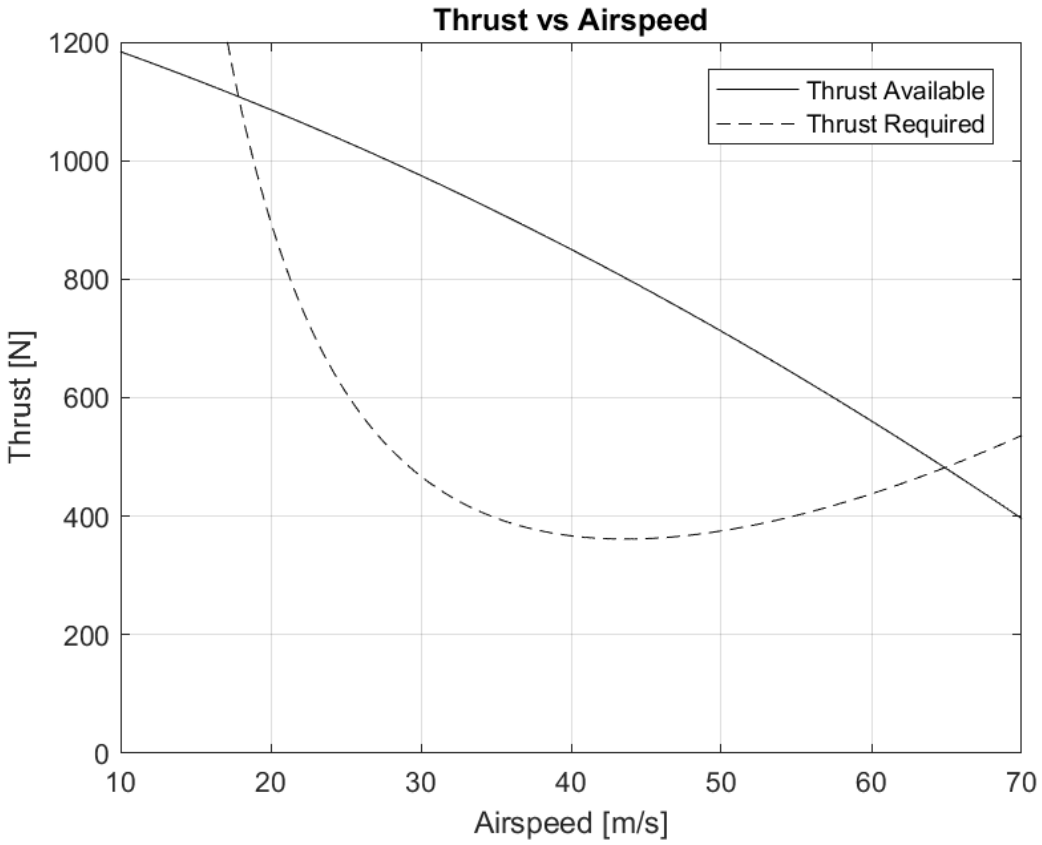

Figure 4.1: Thrust vs Airspeed graph.

Figure 4.1 displays the thrust distribution along the interval of airspeed defined. The full line distribution represents the thrust available obtained through the blade element and momentum theories applied in the code. The dashed line represents the minimum thrust required for each airspeed, obtained through equations 3.36 to 3.41 from Chapter 3.

Figure 4.2 displays the power distribution along the interval of airspeed defined. The full line distribution represents the power available obtained through the thrust calculated from the blade element and momentum theories applied in the code. The dashed line represents the minimum power required to be able to fly leveled at said airspeed, obtained through equations 3.36 to 3.42 from Chapter 3.

The interval where the available power is higher than the required power corresponds to an interval of excess power, which can be used to climb when needed. There are two intersection points, which are displayed in the figure, they represent the minimum and maximum cruising airspeeds for configuration in question.

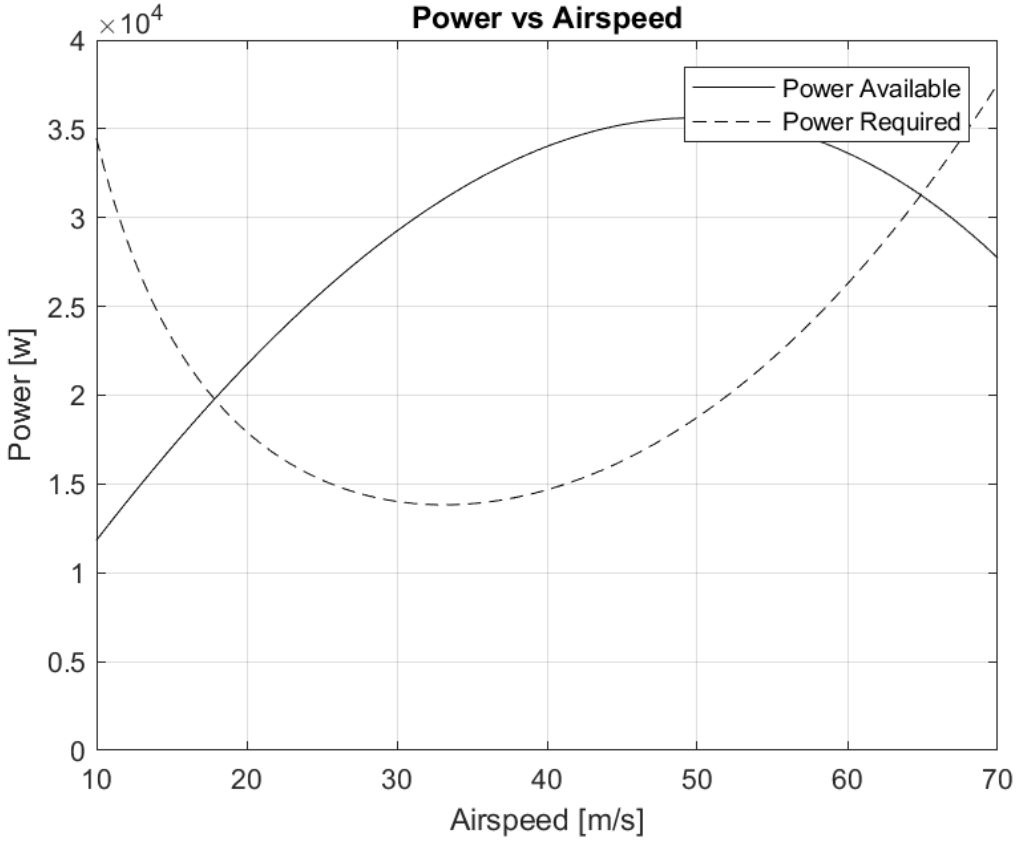

Figure 4.2: Power vs Airspeed graph.

Figure 4.3 represents the distribution of both thrust and power coefficients obtained through equations 3.44 and 3.46 from Chapter 3 along the propeller's advance ratio also calculated with equation 3.43 from the same Chapter.

Figure 4.4 displays the distribution of the propeller's efficiency along its advance ratio, calculated with equation 3.47 from Chapter 3. The propeller's power coefficient is displayed as well again in this graph, as it is usual to provide both in a same graph. It can be seen that the maximum propeller efficiency is a little bit higher than the normal maximum value, this was expected, due to the explanation given in Chapter 3 regarding the simplified method used for the blade element and momentum theories.

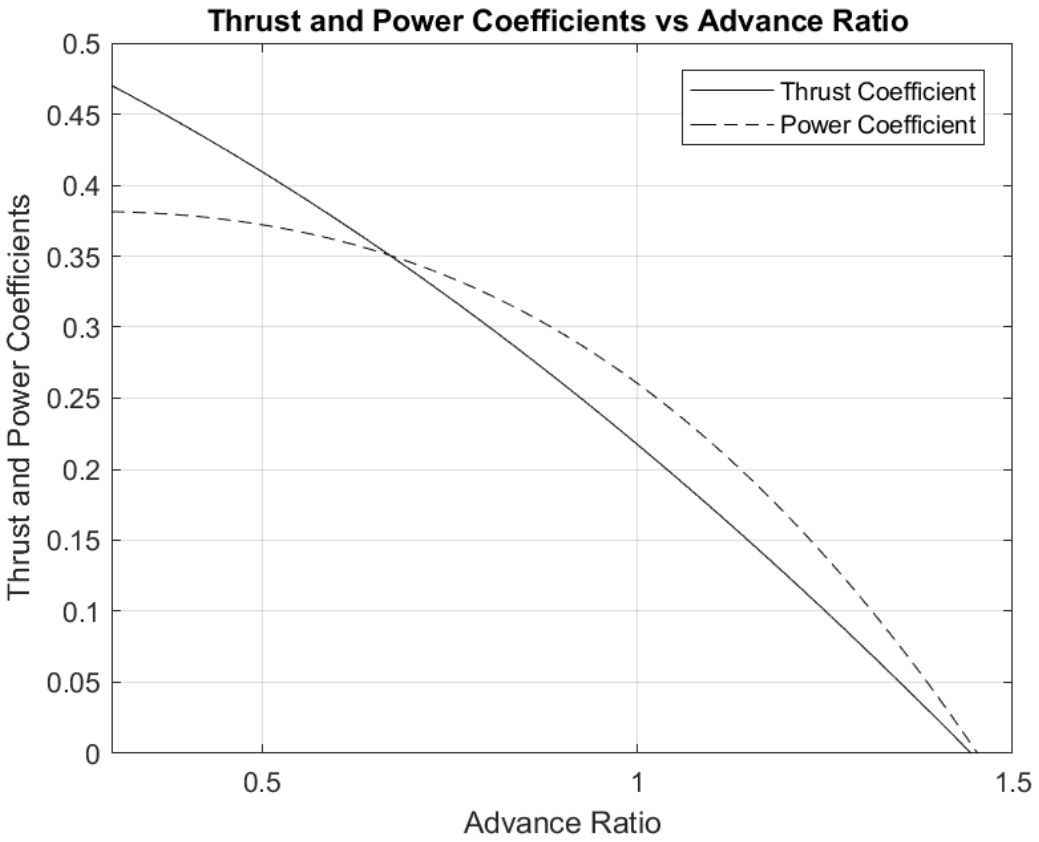

Figure 4.3: Thrust and Power Coefficients vs Advance Ratio graph.

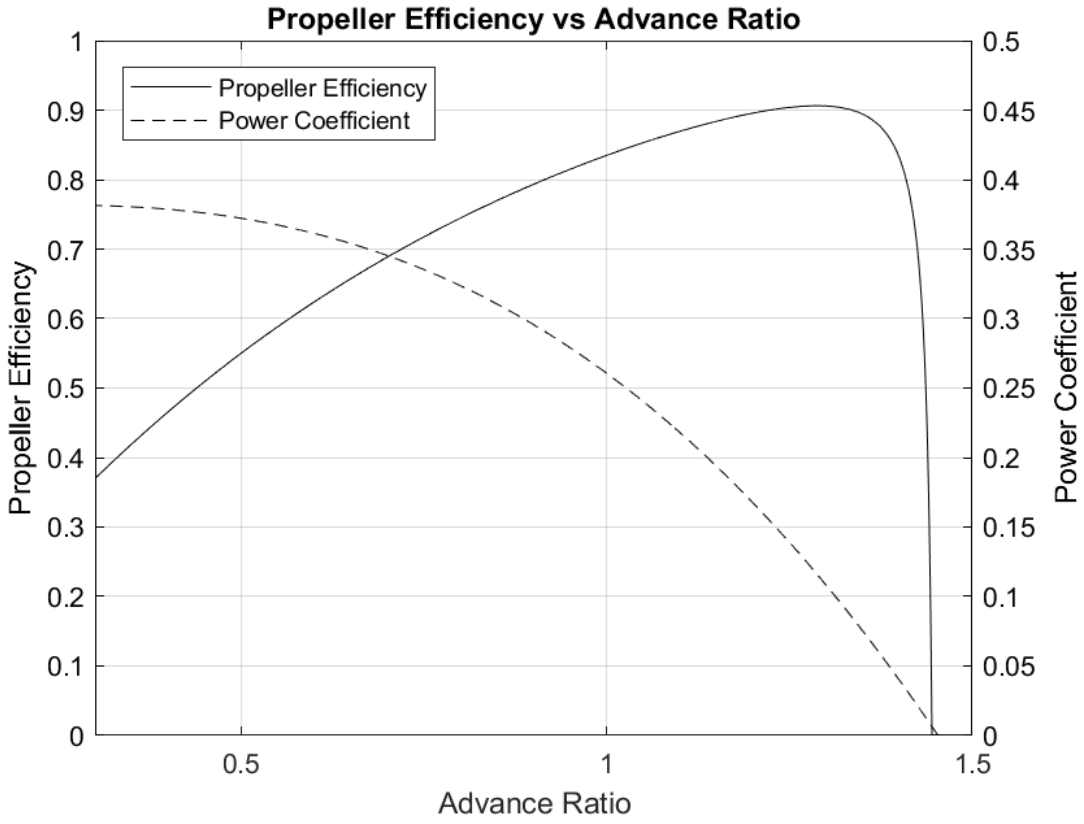

Figure 4.4: Porpeller's Efficiency and Power Coefficient vs Advance Ratio graph.

Figure 4.5 displays the rate of climb, due to the excess power available, the interval of airspeed where the available power is higher than the required power. Note that this excess power is not calculated from figure 4.2. These values are obtained the same way as figure 4.2 were, but here the power available is the one obtained from the propeller's take-off and climb regime defined in the code. Equations 3.51 and 3.52 from Chapter 3 show how to calculate these values.

The dashed-dot line connecting the two-maximum rate of climb points represents the evolution of the maximum rate of climb for each altitude starting from the take-off altitude to the operating altitude. Refer back to Chapter 3 for a more detailed explanation of the process used here.

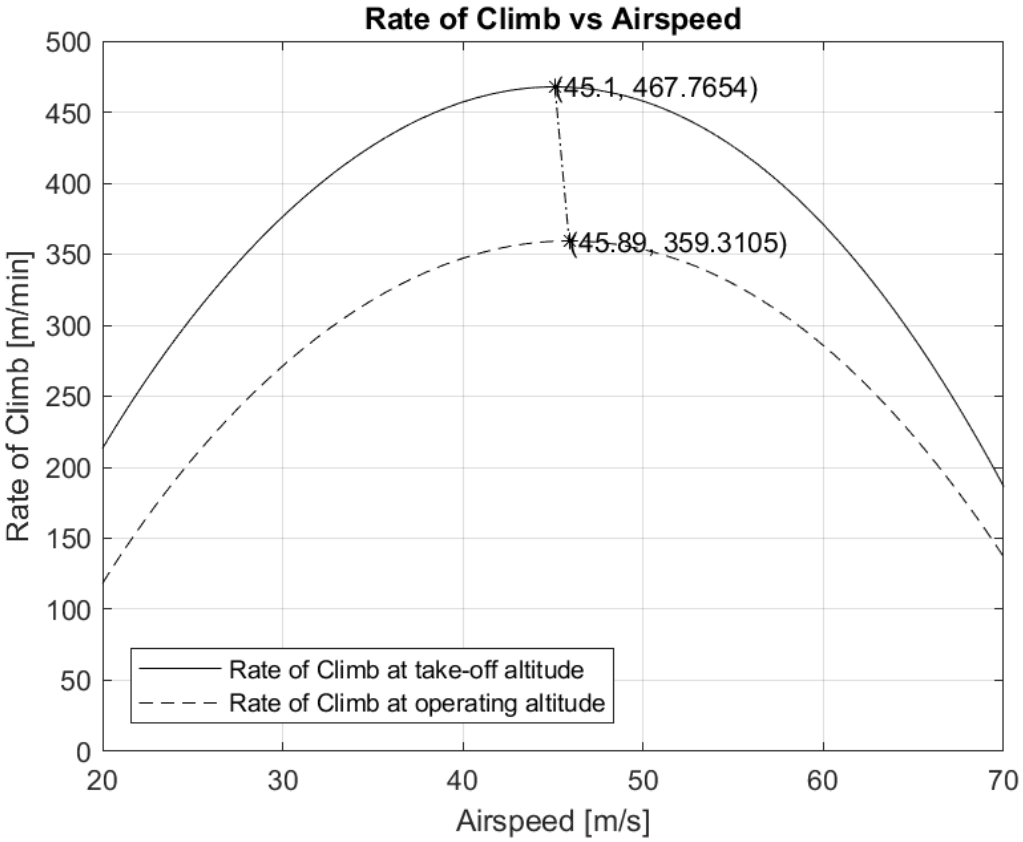

Figure 4.5: Rate of Climb vs Airspeed graph.

Figure 4.6, in contrast to figure 4.5, displays the rate of descent distribution along the airspeed interval. Since the gliding descent was considered here, the method to calculate the rates of descent differ from those used in the rates of climb. Equations 3.53 and 3.54 showcase this.

As was done with the rates of climb, the rates of descent graph also feature a dashed-dot line, which represents the evolution of the maximum rate of descent for each altitude starting from the operating altitude, into the landing altitude, which is assumed to be the same as the take-off altitude, using the same method used before.

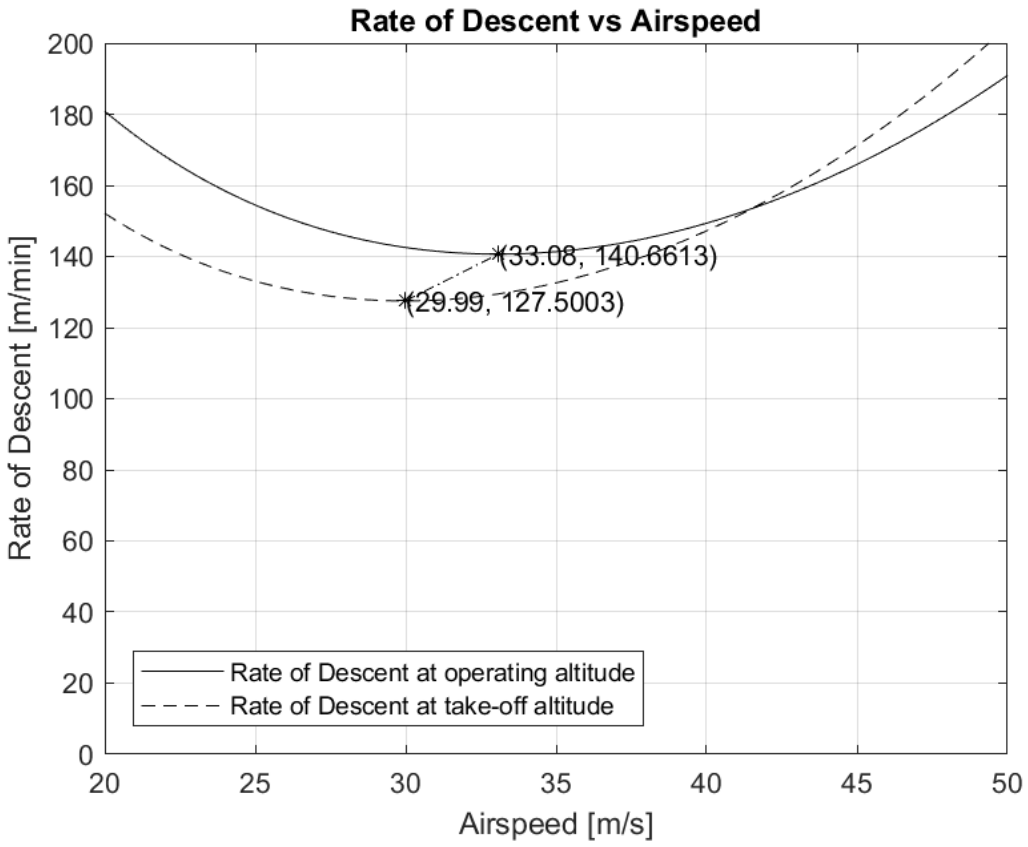

Figure 4.6: Rate of Descent vs Airspeed graph.

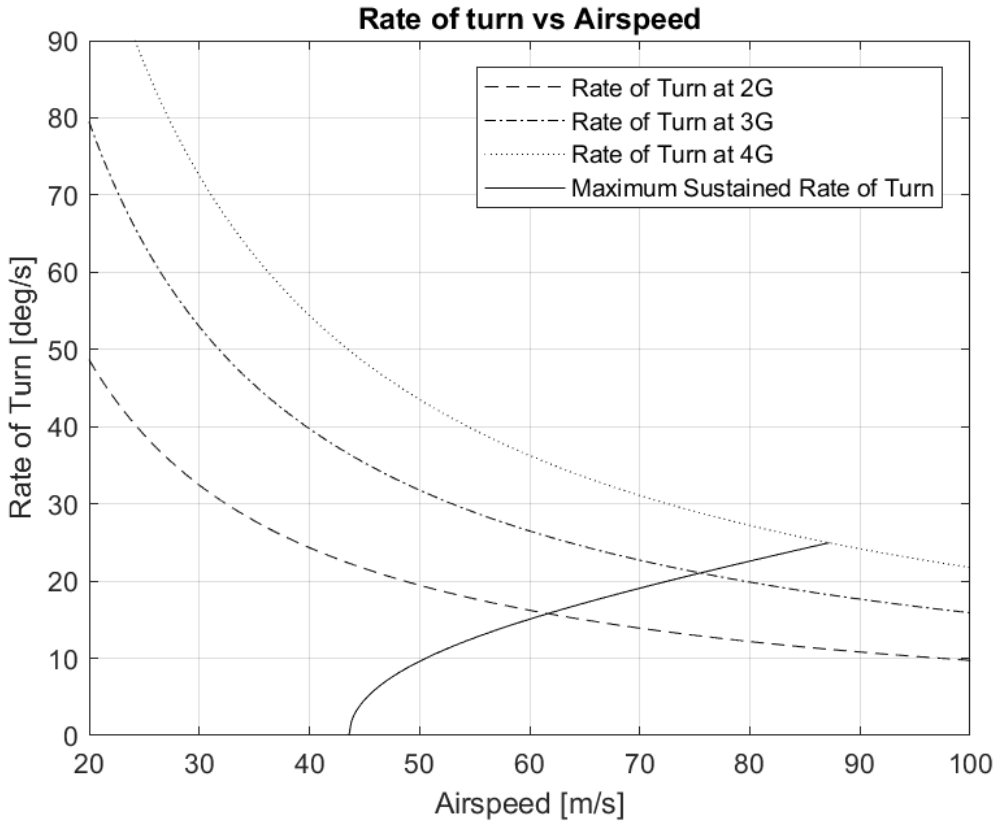

Figure 4.7: Rate of Turn vs Airspeed graph.

Figure 4.7 features the distribution of the rates of turn along the airspeeds for each possible load defined by the user, as well as the maximum sustained rate turn, which limits the form for each load, due to structural restraints. Refer to equations 3.55, 3.56 and 3.57 from Chapter 3 to see how they were calculated.

With the performance values obtained from the previous graphs, it is now possible to perform a final estimation of the actual battery system needed to perform the mission established by the user. Table 4.3 updates the values obtained from the initial estimation displayed in table 4.1 with the final estimation values.

Table 4.3: Final Battery System Sizing.

Final Battery System Sizing		
$E_{battery}$	[J]	$9.10x10^7$
$m_{battery}$	[kg]	128.07
$U_{battery}$	[V]	320
$C_{battery}$	[Ah]	78.98
$I_{max,battery}$	[A]	394.88
$Payload_{availabe}$	[kg]	169.43

With an increase in the battery system weight of about 16.4 kg, as a consequence of the increase in energy needed to accomplish the mission established by the user, with the new performance values, the final estimation of the available payload is 169.43 kg, which leaves about 4.43 kg of more payload than the bare minimum required to respect the constraint adopted.

This increase in payload available can be used to add more baggage, or to add an interval of possible masses for the passenger and pilot in question. Or if the user so desires, a new analysis can be done with a new endurance requirement bigger than the one used before and see when the new battery system mass calculated implicates, the available payload being smaller than the bare minimum required.

Following this, figure 4.8 and 4.9 display both ICE and EM configurations distribution of masses and Total Mass accordingly, in order to have a better understanding of the changes occurred with the airplane's mass. It can be observed that comparably, the difference in mass between the engine and motor is substantial, showcasing the aptitude of current EM to be lighter, more efficient and provide the same power as an ICE. The major issue, with the EM configuration is, while the ICE with a fuel tank filled with 85.2 kg of fuel is capable of realizing a flight endurance of 8.2 hours and, a range of 1411 km.

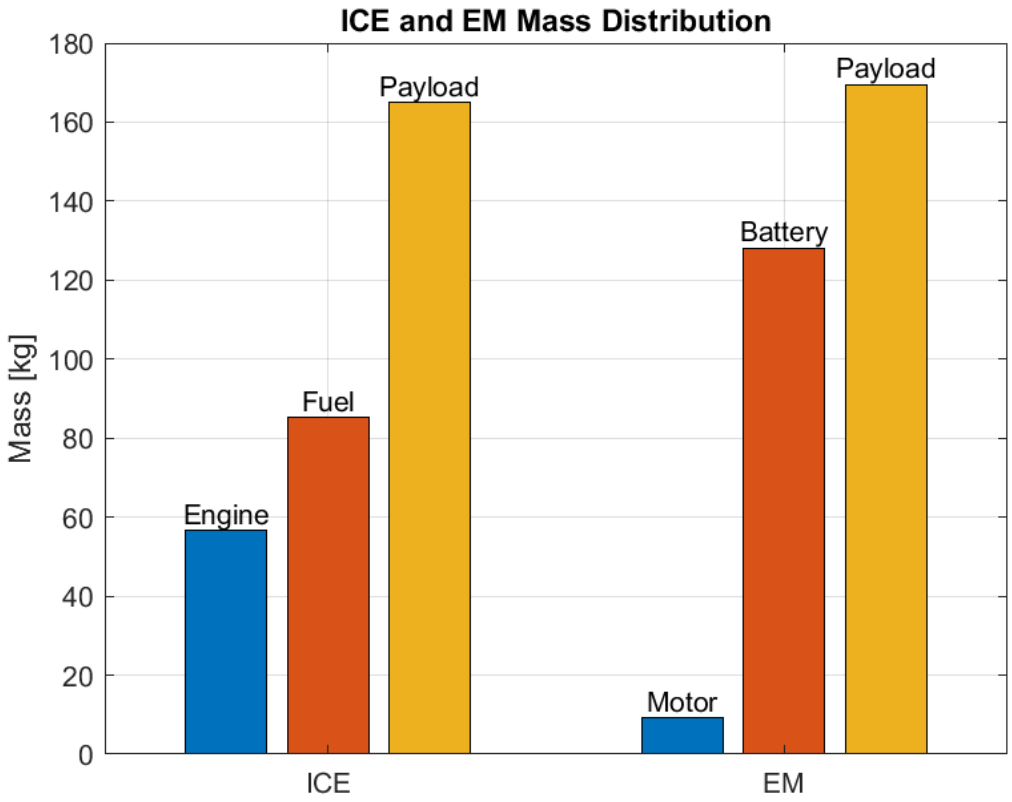

Figure 4.8: ICE and EM Mass Distribution.

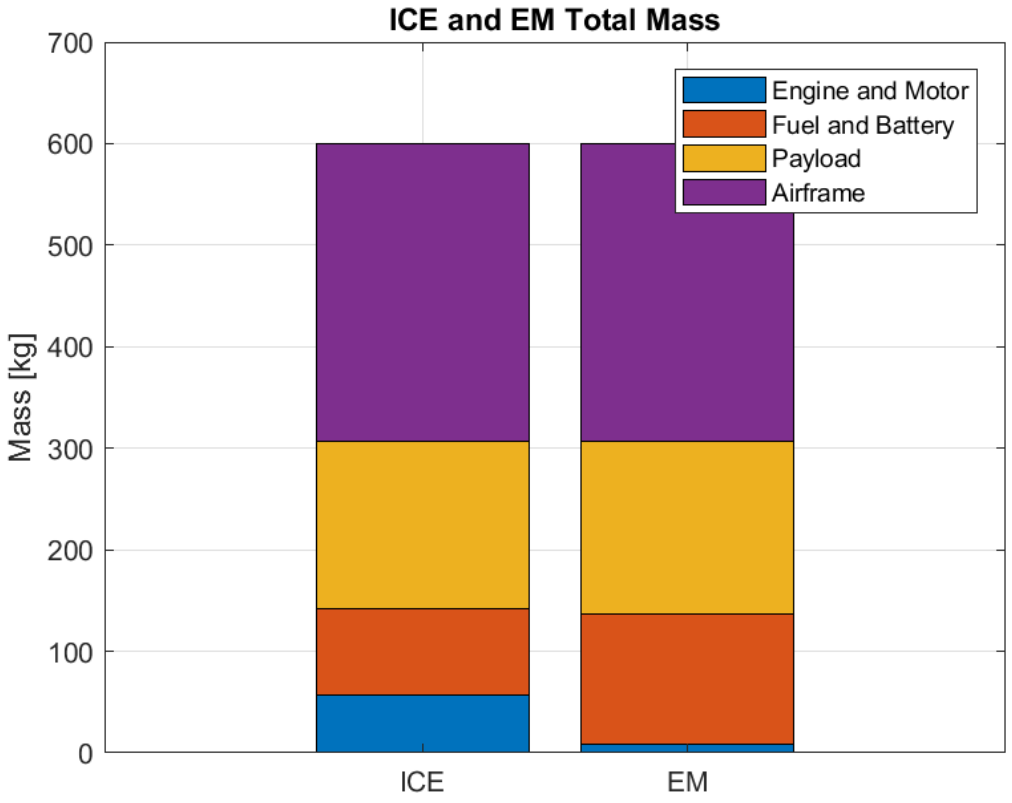

Figure 4.9: ICE and EM Total Mass.

The EM with a battery system of about 128.07 kg is only capable of flying half an hour of endurance and accomplish around 83 km, as can be seen in figure 4.10 which represents the possible mission profile, taking into account all of the performance values obtained with the algorithm.

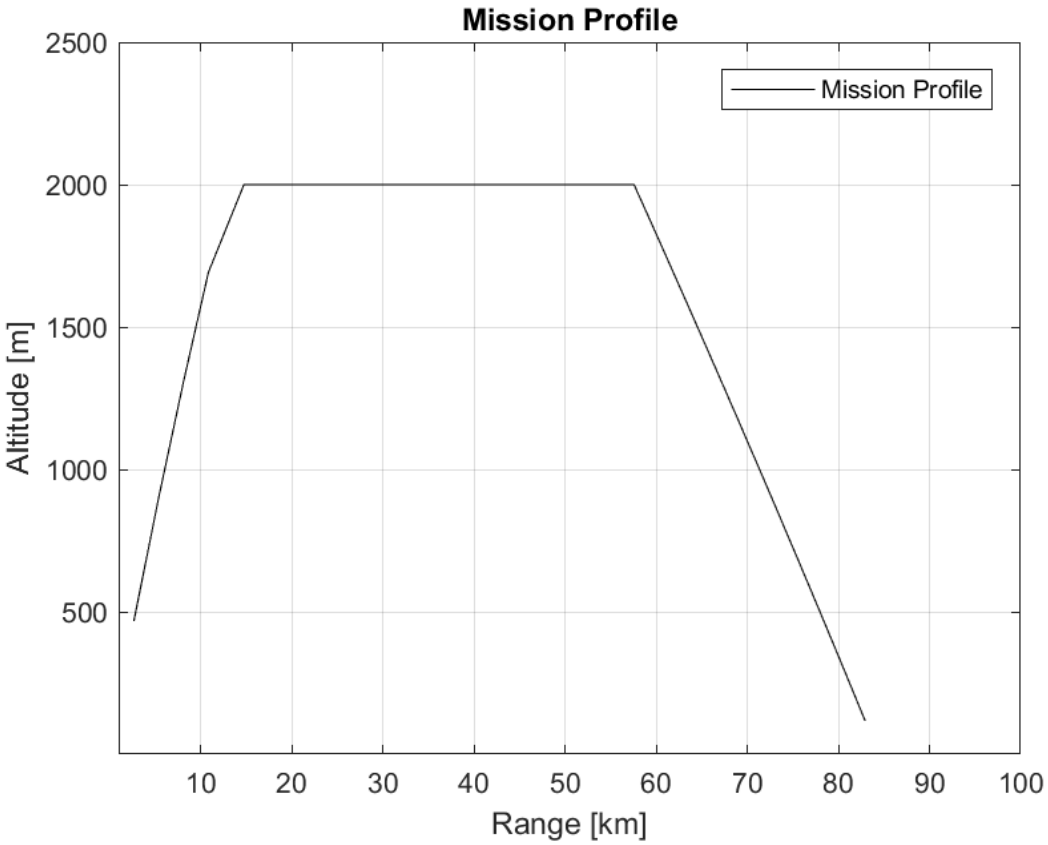

Figure 4.10: Mission Profile graph.

A table with the distribution of range and altitude through each time frame will be presented in appendix A, as well as the airspeed, power consumption, current used, motor regime and flight segment description. The table is also used to prove that the power consumed for the segments in question, is within the intervals establish by the EM manufacturer for each regime used [51].

Chapter 5

Conclusions and Future Work

Chapter 5 of this dissertation will discuss the conclusions taken from this work and some possible future work related to the subject.

5.1 Conclusions

The initial goal of this dissertation was accomplished. A code was developed and, as demonstrated, the capability of offering a good analysis for sizing a battery system for an airplane using its conventional architecture and ICE performance values as reference for comparison. The code is simple and effective and can produce results in a relative short amount of time. This can prove useful for inexperienced new designers, who may show an interest in researching and developing new EP platforms using GA airplanes as test beds.

An overview of current EP technology as well as a brief history of its development was done. A research on the current market trend and company goals regarding EP was done and proved to be very informative, as it showed that companies are slowly but steadily making efforts into making the all-electric airplane concept feasible in the near feature. Still, an overview of the barriers that EP needs to surpass was done and, it is clear that current battery technology to this day pose the biggest barrier for companies to progress in the development and research of new EP platforms. The next decades should prove to be instrumental for future developments in this department, as companies make strides to accomplish their objectives by the end of the next decade.

5.2 Future Work

Although the developed code accomplished its goal for this dissertation, many improvements can be made to it. Currently the code only focuses its attention in the propulsion field and even then, it features a simplified version of the blade element and momentum theories, which as was informed, can overestimate some values and underestimate of others. These should be furthered developed, in order to correct these minor errors. The use and implementation of the program JBLADE is advised.

The code currently bases itself on conventional airplane structural configurations, but as was referred through this work the concept of EP could benefit greatly from new ideas and concepts. It would be interesting to add the possibility to study this with the code. Using different set of structural configurations to study the different outcomes and report the trends associated with.

Finally, an optimization algorithm should be implemented in order to facilitate the process of iteration and validation, improving the time used by the algorithm and the user.

References

[1] Agency for Natural Resources and Energy, “Key World Energy statistics,” IEA Int. Energy Agency, 2017.

[2] European Environmental Agency (EEA), “Emissions of air pollutants from transport,” p. 11, 2017.

[3] R. J. Boucher, “History of Solar Flight”, 20th Joint Propulsion Conference, pp. 1–22, 1984.

[4] U. Muntwyler and A. Venzzini, “Electric flight history, state of the art and first applications,” EVS28 Int. Electr. Veh. Symp. Exhib., pp. 1–10, 2015.

[5] R. J. Boucher and A. F. Inc., “History of Solar Flight,” AIAA/SAE/ASME 20th Jt. Propuls. Conf., vol. c, July, pp. 1–22, 1984.

[6] B. Fehrm, “Airbus , Rolls-Royce and Siemens develops Hybrid-Electric demonstrator, Leeham News and Comment,” Leeham News Comment, vol. 2015. Figure 2, pp. 2–5, 2017.

[7] Joint Press Release, “Airbus, Rolls-Royce, and Siemens team up for electric future,” pp. 1–4, 2017.

[8] L. Umanand, “Hybrid Electric Propulsion,” Power, April, pp. 1–6, 2003.

[9] R. M. Hiserote, “Analysis of Hybrid-Electric Propulsion System Designs For Small Unmanned Aircraft Systems”, Air Force Institute of Technology, March, 2015.

[10] M. Armstrong, “Superconducting Turboelectric Distributed Aircraft Propulsion Rolls-Royce Products Today,” 2015.

[11] R. Dyson, “NASA Hybrid Electric Aircraft Propulsion,” NIEA Biomimicry Summit, Oct. 4, 2017.

[12] J. Felder, H. Kim, and G. Brown, “Turboelectric Distributed Propulsion Engine Cycle Analysis for Hybrid-Wing-Body Aircraft,” 47th AIAA Aerosp. Sci. Meet. Incl. New Horizons Forum Aerosp. Expo., pp. 1–25, 2009.

[13] C. Liu, “Turboelectric Distributed Propulsion System Modelling,” Diss. Cranf. Univ., December, 2013.

[14] H. Martin, “Electric Flight - Potential and Limitations,” AVT-209 Work. Lisbon, pp. 1–30, 2012.

[15] J. Fehrenbacher, D. L. Stanley, and J. Honchell, “Electric Motor & Power Source Selection for Small Aircraft Propulsion,”, 2011.

[16] S. Stückl, J. van Toor, and H. Lobentanzer, “VOLTAIR - The All Electric Propulsion Concept Platform – A Vision For Atmospheric Friendly Flight,” 28th Congr. Int. Counc. Aeronaut., Sci., pp. 1–11, 2012.

[17] “Boeing-Backed Electric Plane Could Fly in 2020s”, [online]. Retrieved March, 2018. https://www.popularmechanics.com/flight/news/a28540/boeing-backed-electric-plane-fly-2020s/

[18] A. M. Stoll, J. Bevirt, M. D. Moore, W. J. Fredericks, and N. K. Borer, “Drag Reduction Through Distributed Electric Propulsion,” 14th AIAA Aviat. Technol. Integr. Oper. Conf., June, pp. 16–20, 2014.

[19] A. S. Gohardani, G. Doulgeris, and R. Singh, “Challenges of future aircraft propulsion: A review of distributed propulsion technology and its potential application for the all electric commercial aircraft,” Prog. Aerosp. Sci., vol. 47, no. 5, pp. 369–391, 2011.

[20] A. S. Gohardani, “A synergistic glance at the prospects of distributed propulsion technology and the electric aircraft concept for future unmanned air vehicles and commercial/military aviation,” Prog. Aerosp. Sci., vol. 57, pp. 25–70, Feb. 2013.

[21] R. Kirner, L. Raffaelli, A. Rolt, P. Laskaridis, G. Doulgeris, and R. Singh, “An assessment of distributed propulsion: Part B - Advanced propulsion system architectures for blended wing body aircraft configurations,” Aerosp. Sci. Technol., vol. 50, pp. 212–219, 2016.

[22] “News on Electric Vertical Take-Off and Landing (eVTOL) concepts.”, Volocopter VC200 [online]. Retrieved April, 2018. http://evtol.news/aircraft/volocopter/

[23] “Ehang 184 passenger drone makes first public fligh in China.”, ABC NEWS, [online]. Retrieved May, 2018. http://www.abc.net.au/news/2018-02-07/first-passenger-drone-makes-maiden-public-flight-in-china/9405072

[24] J. Holden and N. Goel, “Fast-Forwarding to a Future of On-Demand Urban Air Transportation,” VertiFlite, pp. 1–98, 2016.

[25] “CityAirbus eVTOL urban air mobility program presses ahead”, Vertical Magazine, [online]. Retrieved May, 2018. https://www.verticalmag.com/news/cityairbus-evtol-urban-air-mobility-program-presses-ahead/

[26] “Airbus autonomous air taxi Vahana completes its first flight”, The Verge, [online] Retrieved April, 2018. https://www.theverge.com/2018/2/1/16961688/airbus-vahana-evtol-first-test-flight

[27] “Wright Electric unveils its commercial electric plane business”, Tech Crunch, [online]. Retrieved March, 2018. https://techcrunch.com/2017/03/21/wright-electric-planes/

[28] J. Gundlach, “Designing Unmanned Aircraft Systems: A Comprehensive Approach,” Aurora Flight Sci., Chapter 8, p. 320-384, 2011.

[29] “LITHIUM BATTERIES & LITHIUM BATTERY-POWERED DEVICES Aviation Cargo and Passenger Baggage Events Involving Smoke , Fire , Extreme Heat or Explosion Involving Lithium Batteries or Unknown Battery Types,” Fed. Aviat. Adm., no. Mci, pp. 1–32, 2016.

[30] N. Imanishi and O. Yamamoto, “Rechargeable lithium–air batteries: characteristics and prospects,” Mater. Today, vol. 17, no. 1, pp. 24–30, Jan. 2014.

[31] A. Kraytsberg and Y. Ein-Eli, “Review on Li–air batteries—Opportunities, limitations and perspective,” J. Power Sources, vol. 196, no. 3, pp. 886–893, Feb. 2011.

[32] K.-N. Jung, J. Kim, Y. Yamauchi, M.-S. Park, J.-W. Lee, and J. H. Kim, “Rechargeable lithium–air batteries: a perspective on the development of oxygen electrodes,” J. Mater. Chem. A, vol. 4, no. 37, pp. 14050–14068, 2016.

[33] M. Park, H. Sun, H. Lee, J. Lee, and J. Cho, “Lithium-air batteries: Survey on the current status and perspectives towards automotive applications from a Battery Industry Standpoint,” Adv. Energy Mater., vol. 2, no. 7, pp. 780–800, 2012.

[34] S. J. Visco, V. Y. Nimon, A. Petrov, K. Pridatko, N. Goncharenko, E. Nimon, L. De Jonghe, Y. M. Volfkovich, and D. A. Bograchev, “Aqueous and nonaqueous lithium-air batteries enabled by water-stable lithium metal electrodes,” J. Solid State Electrochem., vol. 18, no. 5, pp. 1443–1456, 2014.

[35] L. Qin, D. Zhai, W. Lv, W. Wei, W. Yu, Y. Lei, W. Yang, J. Huang, S. Yao, J. Cui, F. Kang, J.-K. Kim, and Q.-H. Yang, “Dense graphene monolithic oxygen cathodes for

ultrahigh volumetric energy densities," Energy Storage Mater., vol. 9, no. June, pp. 134–139, Oct. 2017.

[36] Z. Zhu, A. Kushima, Z. Yin, L. Qi, K. Amine, J. Lu, and J. Li, "Anion-redox nanolithia cathodes for Li-ion batteries," Nat. Energy, vol. 1, no. 8, pp. 1–7, 2016.

[37] C. Curry, "Lithium-ion Battery Costs and Market," Bloom. New Energy Financ., p. 14, 2017.

[38] G. E. Blomgren, "The Development and Future of Lithium Ion Batteries," J. Electrochem. Soc., vol. 164, no. 1, pp. A5019–A5025, 2017.

[39] Intertek, "The Future of Battery Technologies – Part II: Focus on Lithium-Ion Batteries," 2009.

[40] J. Wishart, "Fuel Cells vs Batteries In the Automotive Sector.", Intertek, Journal, 2014.

[41] "Solar plane makes history after completing round-the-world trip", The Guardian, [online]. Retrieved March, 2018. https://www.theguardian.com/environment/2016/jul/26/solar-impulse-plane-makes-history-completing-round-the-world-trip

[42] D. K. Hall, "Boundary Layer Ingestion Propulsion – Benefit , Challenges , and Opportunities Boundary Layer Ingestion (BLI) Reduces Wasted Energy," no. May, 2016.

[43] R. Del Rosario, G. Follen, R. Wahls, and N. Madavan, "Subsonic Fixed Wing Project," NASA Fundam. Aeronaut. Progr. - Tech. Conf. Clevel. 2011, pp. 1–28, 2011.

[44] A. Prievidza, "WT9 Dynamic LSA Speed S.", [online]. Retrieved October, 2017. https://www.aerospool.sk/downloads/bulletins/LSA/service_bulletins/MBWT9LSA_1A_2011_EN.pdf

[45] "Pilot' s Operating Handbook", [online], Retrieved October, 2017. http://www.liy.fi/images/FM_DLI_1.pdf

[46] "ENGINE TYPE 912 | 100 hp", [online]. Retrieved October, 2017. https://www.flyrotax.com/files/Bilder/Produkte%20Rotax/Datasheets/Produktdatenblatt_912_100hp_rev.BRP-Rotax_20160823.pdf

[47] D. P. Raymer, "Aircraft Design: A conceptual Approach," AIAA, 1992.

[48] PowerTech Systems, "Primary cells Lithium Thionyl Chloride (Li-$SOCl_2$)", [online]. Retrieved January, 2018.

https://www.powertechsystems.eu/home/products/primary-cells-lithium-thionyl-chloride-li-socl2/

[49] S. Sekalala, “Performance of A Three-Phase Permanent Magnet Motor Operating as a Synchronous Motor and a Brushless DC Motor”, 2006.

[50] R. Krishnan, “Permanent Magnet Synchronous and Brushless DC Motor Drives”, 2010.

[51] EMRAX, “User’s Manual for Advanced Axial Flux Synchronous Motors and Generators EMRAX 228 Technical Data Table (dynamometer test data)”, pp. 1–3.

[52] EMRAX, “Emrax 208 Technical data”, [online]. Retrived January, 2018. http://emrax.com/wp-content/uploads/2017/01/emrax_208_technical_data_4.5.pdf

[53] H. Glauert, “The elements of aerofoil and airscrew theory,” Journal of the Franklin Institute, vol. 236, no. 1. p. 102, 1943.

[54] Isidoro Martinez, “Propeller Performance”, [online]. Retrieved November, 2017. http://webserver.dmt.upm.es/~isidoro/bk3/c17/Propellers.pdf

[55] Aerospace and Ocean Engineering, “Climb performance,” [online]. Retrieved February, 2018. http://www.dept.aoe.vt.edu/~lutze/AOE3104/climb.pdf

Appendix A: Table of Results

Time [min]	Altitude [m]	Range [km]	Airplane Speed [m/s]	Motor RPM [rev/min]	Power Consumption [W]	Current Draw [A]	Flight Segment
1	467,77	2,67	45,10	5760	62750,49	255,33	Climbing Segment
2	898,38	5,38	45,37	5760	59039,14	240,23	Climbing Segment
3	1306,27	8,10	45,54	5760	56768,24	230,99	Climbing Segment
4	1692,63	10,86	45,69	5760	54617,20	222,24	Climbing Segment
5	2000,00	14,75	64,88	5000	31272,45	127,25	Cruising Segment
6	2000,00	18,64	64,88	5000	31272,45	127,25	Cruising Segment
7	2000,00	22,54	64,88	5000	31272,45	127,25	Cruising Segment
8	2000,00	26,43	64,88	5000	31272,45	127,25	Cruising Segment
9	2000,00	30,32	64,88	5000	31272,45	127,25	Cruising Segment
10	2000,00	34,21	64,88	5000	31272,45	127,25	Cruising Segment
11	2000,00	38,11	64,88	5000	31272,45	127,25	Cruising Segment
12	2000,00	42,00	64,88	5000	31272,45	127,25	Cruising Segment
13	2000,00	45,89	64,88	5000	31272,45	127,25	Cruising Segment
14	2000,00	49,78	64,88	5000	31272,45	127,25	Cruising Segment
15	2000,00	53,68	64,88	5000	31272,45	127,25	Cruising Segment
16	2000,00	57,57	64,88	5000	31272,45	127,25	Cruising Segment
17	1859,34	59,55	33,08	7040	2560,00	8,00	Descending Segment
18	1720,06	61,49	32,75	7040	2560,00	8,00	Descending Segment
19	1581,70	63,41	32,54	7040	2560,00	8,00	Descending Segment
20	1444,24	65,31	32,33	7040	2560,00	8,00	Descending Segment
21	1307,69	67,18	32,12	7040	2560,00	8,00	Descending Segment
22	1172,03	69,03	31,91	7040	2560,00	8,00	Descending Segment
23	1037,26	70,85	31,70	7040	2560,00	8,00	Descending Segment
24	903,38	72,65	31,49	7040	2560,00	8,00	Descending Segment
25	770,37	74,42	31,28	7040	2560,00	8,00	Descending Segment
26	638,23	76,17	31,08	7040	2560,00	8,00	Descending Segment
27	506,97	77,90	30,87	7040	2560,00	8,00	Descending Segment
28	376,56	79,60	30,67	7040	2560,00	8,00	Descending Segment
29	247,01	81,28	30,47	7040	2560,00	8,00	Descending Segment
30	118,31	82,94	30,27	7040	2560,00	8,00	Descending Segment

Appendix B: Source Code

```
function [] = Electric_Design_Code()
clc; close all;
disp('Electric Propulsion System Design Code');
disp('Micael Teixeira');
disp('Universidade da Beira Interior');
disp('Masters Degree');
disp(' ');
timestamp = clock;
disp(['Date:   ',date,'                                Time:   ',num2str(timestamp(4)),':',
num2str(timestamp(5))]);
disp(' ');

global g h_TO h_OA h T a p rho S b AR e K Cl_max Cd_0 Max_TO_W W Wing_ld Airframe_W
Min_Payload Max_pos_ld_fac Max_neg_ld_fac V_stall V_rot V_maneuv Des_V_cruise Terrain1
u1  Des_TO_dist  Des_ROC  Des_ROD  n_prop0  Perf_Req  Rng  End  Est_Payload  Est_Airplane_W
Est_Empty_W Est_Batt_W PR_TO P_TO Payload Airplane_W Empty_W Batt_W Engine_W Fuel_W

fprintf(['This program requests various inputs related to the characteristics of the
airplane, as well as the motor and battery models used, and returns through an algorithm
the results of different performance parameters, as well as the battery system needed
for the mission.\n']);
disp(' ');
g = 9.80665; disp(['Acceleration due to gravity [m/s^2]: ',num2str(g)]);
disp(' ');
disp('Select take-off and operating altitude for the calculations.');
%atmosisa function uses ISA database to return the values temperature, speed of sound,
pressure and air density at given altitude.
h_TO = input('Take-off altitude [m]: ');
h_OA = input('Operating Altitude [m]: ');
disp(' ');
h = [h_TO,h_OA,h_OA];
T = [1,size(h,2)];
a = [1,size(h,2)];
p = [1,size(h,2)];
rho = [1,size(h,2)];
for x = 1:size(h,2)
[T(x), a(x), p(x), rho(x)] = atmosisa(h(x));
end
disp([' Temperature at takeoff altitude [K]: ',num2str(T(1))]);
disp([' Speed of sound at takeoff altitude [m/s]: ',num2str(a(1))]);
disp([' Pressure at takeoff altitude [Pa]: ',num2str(p(1))]);
disp([' Air density at takeoff altitude [kg/m^3]: ',num2str(rho(1))]);
disp(' ');
disp([' Temperature at operating altitude [K]: ',num2str(T(2))]);
disp([' Speed of Sound at Operating Altitude [m/s]: ',num2str(a(2))]);
disp([' Pressure at operating altitude [Pa]: ',num2str(p(2))]);
disp([' Air density at operating altitude [kg/m^3]: ',num2str(rho(2))]);
disp(' ');
disp('Airplane aerodynamic characteristics.');
S = input(' Wing area [m^2]: ');
b = input(' Wing span [m]: ');
AR = (b^2)/S; disp([' Wing aspect ratio: ',num2str(AR)]);
e = input(' Oswald wing efficiency factor: ');
K = 1/(pi*e*AR); disp([' Drag-due-to-lift factor: ',num2str(K)]);
Cl_max = input(' Maximum lift coefficient: ');
Cd_0 = input(' Drag coefficient at zero lift: ');
```

```
disp(' ');
disp('Airplane weight characteristics.');
Max_TO_W = input(' Airplane maximum takeoff mass [kg]: ');
W = Max_TO_W * g; disp([' Airplane weight [N]: ',num2str(W)]);
Wing_ld = W/S; disp([' Wing loading [N/m^2]: ',num2str(Wing_ld)]);
Airframe_W = input(' Airplane airframe mass [kg]: ');
Min_Payload = input(' Minimum acceptable payload of airplane [kg]: ');
disp(' ');
disp('Airplane performance parameters.');
Max_pos_ld_fac = input(' Maximum positive load factor: ');
Max_neg_ld_fac = input(' Maximum negative load factor: ');
V_stall    =    sqrt(((2*W)/(rho(1)*S*Cl_max)));    disp(['    Stall    speed    [m/s]:
',num2str(V_stall)]);
V_rot = 1.2*V_stall; disp([' Rotation speed [m/s]: ',num2str(V_rot)]);
V_maneuv    =    sqrt(Max_pos_ld_fac)*V_stall;    disp(['    Maneuvering    speed    [m/s]:
',num2str(V_maneuv)]);
Des_V_cruise = input(' Desired cruise speed [m/s]: ');
disp('Select one of the following types of terrain for takeoff:');
disp(' 1: Asphalt');
disp(' 2: Concrete');
disp(' 3: Dirt');
disp(' 4: Low grass');
disp(' 5: High grass');
Terrain1 = input('Enter your type of terrain for takeoff selection here: ');
switch Terrain1
    case 1
         Terrain1 = 1;
         u1 = 0.020;
    case 2
         Terrain1 = 2;
         u1 = 0.030;
    case 3
         Terrain1 = 3;
         u1 = 0.050;
    case 4
         Terrain1 = 4;
         u1 = 0.050;
    case 5
         Terrain1 = 5;
         u1 = 0.100;
end
Des_TO_dist = input(' Desired takeoff ground roll [m]: ');
Des_ROC = input(' Desired rate of climb [m/min]: ');
Des_ROD = input(' Desired rate of descent [m/min]: ');
n_prop0 = input(' Propeller efficiency: ');
disp('Select one of the following mission parameters:');
disp(' 1: Range [km]');
disp(' 2: Endurance [h]');
Perf_Req = input('Enter your mission parameter selection here: ');
switch Perf_Req
    case 1
         Perf_Req = 1;
         Rng_1 = input(' Desired range requirement [km]: ');
         Rng = Rng_1*1000;
    case 2
         Perf_Req = 2;
         End_2 = input(' Desired endurance requirement [h]: ');
         End = End_2*3600;
end
disp(' ');
disp('Internal Combustion Engine mass values.');
```

```
Engine_W = input(' Engine mass [kg]: ');
Fuel_W = input(' Stored Fuel mass [kg]: ');
disp(' ');
Motor_Battery_Selection();
disp(' ');
Performance_Estimation();
if Est_Payload > Min_Payload
    Est_Airplane_W = Est_Empty_W + Est_Batt_W + Est_Payload; disp([' Total mass
     estimate of airplane [kg]: ',num2str(Est_Airplane_W)]);
    disp(' ');
    disp('Airplane mass estimate matches maximum takeoff mass.');
    disp('Mass verification passed.');
else
    while Est_Payload < Min_Payload
        Est_Airplane_W = Est_Empty_W + Est_Batt_W + Min_Payload; disp([' Total mass of
         airplane [kg]: ',num2str(Est_Airplane_W)]);
        disp(' ');
        disp('Airplane mass estimate surpasses maximum takeoff mass.');
        disp('Mass verification failed.');
        disp('Please select a new motor and battery model for estimation.');
        disp(' ');
        Motor_Battery_Selection();
        disp(' ');
        Performance_Estimation();
        if Est_Payload > Min_Payload
            Est_Airplane_W = Est_Empty_W + Est_Batt_W + Est_Payload; disp([' Total
            weight estimate of aircraft [kg]: ',num2str(Est_Airplane_W)]);
            disp(' ');
            disp('Airplane mass estimate matches maximum takeoff mass.');
            disp('Mass verification passed.');
        end
    end
end
disp(' ');
Propeller_Selection();
while PR_TO > P_TO
    disp('The motor plus propeller model selected cannot satisfy takeoff condition.')
    disp('Select a new propeller design for calculation.')
    Propeller_Selection();
end
Performance();
if Payload > Min_Payload
    Airplane_W = Empty_W + Batt_W + Payload; disp([' Total mass of airplane [kg]:
    ',num2str(Airplane_W)]);
    disp(' ');
    disp('Airplane mass matches maximum takeoff mass.');
    disp('Mass verification passed.');
else
    while Payload < Min_Payload
        Airplane_W = Empty_W + Batt_W + Min_Payload; disp([' Total mass of airplane
       [kg]: ',num2str(Airplane_W)]);
        disp(' ');
        disp('Airplane mass surpasses maximum takeoff mass.');
        disp('Mass verification failed.');
        disp('Select a new propeller design for calculation.');
        disp(' ');
        Propeller_Selection();
        while PR_TO > P_TO
            disp(' ');
            disp('The motor plus propeller model selected cannot satisfy takeoff
            condition.')
```

```
            disp('Select a new propeller design for calculation.')
            Propeller_Selection();
        end
        Performance();
        if Payload > Min_Payload
            Airplane_W = Empty_W + Batt_W + Payload; disp([' Total mass of airplane
            [kg]: ',num2str(Airplane_W)]);
            disp(' ');
            disp('Airplane mass matches maximum takeoff mass.');
            disp('Mass verification passed.');
        end
    end
end
disp(' ');
DataProcessing();
MissonProfile();
end

function [] = Motor_Battery_Selection()

global Batt_cap Batt_nv Batt_w Batt_SpecEGY Motor_maxV Motor_maxI Motor_I_nl Motor_maxQ
Motor_maxRPM_nl   Motor_maxRPM_fl   Motor_KV_nl   Motor_KV_fl   Motor_KV   Motor_KT
Motor_maxPower  Motor_W  Motor_PowerDEN  n_motor  Est_PR_TO  V_rot  W  g  rho  S  Cl_max
Des_TO_dist n_prop0


disp('Motor and battery model selection.');
disp('Battery cell model.');
Batt_cap = input(' Battery capacity [Ah]: ');
Batt_nv = input(' Battery nominal voltage [V]: ');
Batt_w = input(' Battery mass [kg]: ');
Batt_SpecEGY = (Batt_cap*Batt_nv)/Batt_w; disp([' Battery specific energy [Wh/kg]:
',num2str(Batt_SpecEGY)]);
disp(' ');
disp('Electric motor model.');
Motor_maxV = input(' Maximal motor voltage [V]: ');
Motor_maxI = input(' Maximal motor current [A]: ');
Motor_I_nl = input(' Motor no-load current [A]: ');
Motor_maxQ = input(' Maximal motor torque [Nm]: ');
Motor_maxRPM_nl = input(' Motor maximum no-load regime [1/min]: ');
Motor_maxRPM_fl = input(' Motor maximum full-load regime [1/min]: ');
Motor_KV_nl = Motor_maxRPM_nl/Motor_maxV; disp([' Specific idle speed of motor [RPM/V]:
',num2str(Motor_KV_nl)]);
Motor_KV_fl = Motor_maxRPM_fl/Motor_maxV; disp([' Specific full-load speed of motor
[RPM/V]: ',num2str(Motor_KV_fl)]);
Motor_KV = Motor_KV_fl:0.1:Motor_KV_nl; disp([' Specific load speed of motor [RPM/V]:
',num2str(Motor_KV_fl),'-',num2str(Motor_KV_nl)]);
Motor_KT = Motor_maxQ/Motor_maxI; disp([' Specific load torque of motor [Nm/A]:
',num2str(Motor_KT)]);
Motor_maxPower = input(' Peak motor power [W]: ');
Motor_W = input(' Motor mass [kg]: ');
Motor_PowerDEN = Motor_maxPower/Motor_W; disp([' Motor power density [W/Kg]:
',num2str(Motor_PowerDEN)]);
n_motor = input(' Motor efficiency: ');
Est_PR_TO = ((V_rot*1.44*W^2)/(g*rho(1)*S*Cl_max*Des_TO_dist))*(1/n_prop0);
if Est_PR_TO < (Motor_maxPower/n_motor)
   disp(['Power required at takeoff [W]: ',num2str(Est_PR_TO),' < Eletric motor peak
    power [W]: ',num2str(Motor_maxPower)]);
   disp('Motor model passed validation.');
else
    while Est_PR_TO > (Motor_maxPower/n_motor)
```

```
            disp(['Power required at takeoff [W]: ',num2str(Est_PR_TO),' > Eletric motor
             peak power [W]: ',num2str(Motor_maxPower)]);
            disp('Motor model failed validation.');
            disp('Please insert a new motor model for calculation.')
            Motor_maxV = input(' Maximal motor voltage [V]: ');
            Motor_maxI = input(' Maximal motor current [A]: ');
            Motor_I_nl = input(' Motor no-load current [A]: ');
            Motor_maxQ = input(' Maximal motor torque [Nm]: ');
            Motor_maxRPM_nl = input(' Motor maximum no-load regime [1/min]: ');
            Motor_maxRPM_fl = input(' Motor maximum full-load regime [1/min]: ');
            Motor_KV_nl  =  Motor_maxRPM_nl/Motor_maxV;  disp([' Specific  idle  speed  of
             motor [RPM/V]: ',num2str(Motor_KV_nl)]);
            Motor_KV_fl = Motor_maxRPM_fl/Motor_maxV; disp([' Specific full-load speed
             of motor [RPM/V]: ',num2str(Motor_KV_fl)]);
            Motor_KV = Motor_KV_fl:0.1:Motor_KV_nl; disp([' Specific load speed of motor
             [RPM/V]: ',num2str(Motor_KV_fl),'-',num2str(Motor_KV_nl)]);
            Motor_KT  =  Motor_maxQ/Motor_maxI;  disp(['  Specific  load  torque  of  motor
             [Nm/A]: ',num2str(Motor_KT)]);
            Motor_maxPower = input(' Peak motor power [W]: ');
            Motor_W = input(' Motor mass [kg]: ');
            Motor_PowerDEN = Motor_maxPower/Motor_W; disp([' Motor power density [W/Kg]:
            ',num2str(Motor_PowerDEN)]);
            n_motor = input(' Motor efficiency: ');
            disp(' ');
            if Est_PR_TO < (Motor_maxPower/n_motor)
               disp(['Power  required  at  takeoff  [W]:  ',num2str(Est_PR_TO),'  <  Eletric
               motor peak power [W]: ',num2str(Motor_maxPower)]);
               disp('Motor model passed validation.');
            end
    end
end
end

function [] = Performance_Estimation()

global Est_PR_Cruise n_prop0 n_motor rho Des_V_cruise S Cd_0 W K Est_PR_D Motor_I_nl
Motor_maxRPM_nl Motor_KV_nl Perf_Req Est_Batt_EGY Est_PR_TO h_OA Des_ROC Rng Des_ROD
End  Est_Batt_W  Batt_SpecEGY  Est_Batt_NV  Motor_maxV  Est_Batt_CAP  Est_Batt_IMAX
Est_Empty_W Airframe_W Motor_W Est_Payload Max_TO_W

disp('Initial estimate of battery system needed for flight mission.');
Est_PR_Cruise                                                                    =
(1/(n_prop0*n_motor))*(0.5*rho(end)*Des_V_cruise^3*S*Cd_0+(W/S)*((K*W)/(0.5*rho(end)*
Des_V_cruise)));
Est_PR_D = Motor_I_nl*(Motor_maxRPM_nl/Motor_KV_nl);
if Perf_Req == 1
    Est_Batt_EGY  =  Est_PR_TO*(h_OA/(Des_ROC/60))+Est_PR_Cruise*((Rng/Des_V_cruise)-
    (h_OA/(Des_ROC/60))-
    (h_OA/(Des_ROD/60)))+Est_PR_D*(h_OA/(Des_ROD/60))+Est_PR_Cruise*(15*60);  disp(['
    Estimate  of  battery  energy  needed  to  accomplish  flight  mission  [J]:
    ',num2str(Est_Batt_EGY)]);
elseif Perf_Req == 2
    Est_Batt_EGY          =          Est_PR_TO*(h_OA/(Des_ROC/60))+Est_PR_Cruise*(End-
    (h_OA/(Des_ROC/60))-
    (h_OA/(Des_ROD/60)))+Est_PR_D*(h_OA/(Des_ROD/60))+Est_PR_Cruise*(15*60);  disp(['
    Estimate  of  battery  energy  needed  to  accomplish  flight  mission  [J]:
    ',num2str(Est_Batt_EGY)]);
end
Est_Batt_W = Est_Batt_EGY/(Batt_SpecEGY*3600); disp([' Estimate of battery system mass
[kg]: ',num2str(Est_Batt_W)]);
```

```
Est_Batt_NV  =    Motor_maxV;  disp([' Estimate of battery system voltage [V]: ',num2str(Est_Batt_NV)]);
Est_Batt_CAP = (Est_Batt_EGY/Est_Batt_NV)/3600; disp([' Estimate of battery system capacity [Ah]: ',num2str(Est_Batt_CAP)]);
Est_Batt_IMAX = 5 * Est_Batt_CAP; disp([' Estimate of battery system maximum current draw [A]: ',num2str(Est_Batt_IMAX)]);
disp(' ');
disp('Aircraft total weight estimate verification.');
Est_Empty_W = Airframe_W + Motor_W; disp([' Estimate of empty mass of airplane [kg]: ',num2str(Est_Empty_W)]);
Est_Payload = Max_TO_W - Est_Batt_W - Est_Empty_W; disp([' Estimate of avaiable payload of airplane [kg]: ',num2str(Est_Payload)]);
end

function [] = Propeller_Selection()

global c B p d r rt rh Prop_RPM_TO n_TO Prop_RPM_OA n_OA rstep R V Load1 Max_pos_ld_fac Load2 Cl h Cd L D E TR PR Thrust Torque Power_prop ct cq cp J n_prop Power_shaft ROC ROD phi_C phi_D Turn vel Turn_max P n omega W rho S Cd_0 K n_prop0 thrust torque theta a1 b1 V0 V2 phi alpha cl cd V1 DTDr DQDr DtDr DqDr a2 b2 anew bnew g e AR M1 N1 Best_ROC Best_ROC_V Best_ROC_phi P_ROC M2 N2 Best_ROD Best_ROD_V Best_ROD_phi P_ROD Motor_I_nl Motor_maxRPM_nl Motor_KV_nl V_rot_rounded V_rot N3 Kt_TO u1 Ka_TO TO_Dist PR_TO Cl_max P_TO  Value  index  V_cruise1  V_cruise2  V_cruiseMAX  V_cruiseMIN  V_stall  V_cruise V_cruise_rounded N4 P_cruise N5 V_cruise1_rounded P_cruise1

disp('Please insert your propeller design parameters.')
c = input(' Blade chord: ');
B = input(' Number of blades: ');
d = input(' Propeller diameter [m]: ');
p = input(' Propeller pitch [m]: ');
r = d/2.0; %propeller radious
rt = r; %tip radious
rh = 0.100*r; %hub radious
Prop_RPM_TO = input(' Propeller regime at takeoff and climbing [1/min]: ');
n_TO = Prop_RPM_TO/60.0; %propeller regime in rot/s at takeoff altitude
Prop_RPM_OA = input(' Propeller regime at cruising [1/min]: ');
n_OA = Prop_RPM_OA/60.0; %propeller regime in rot/s at operating altitude
rstep = (rt-rh)/10; %division of propeller blade into 10 seperate sections, each with the same lenght as the other.
R = rh:rstep:rt;

V = 1:0.01:120; %vector with values of velocity ranging from 1 to 120 [m/s] with a step of 0.01.

Load1 = 1:1:Max_pos_ld_fac; %vector with values of load ranging from 1 to maximum positive load with a step of 1 for calculation of leveled turn rates.
Load2 = 1:0.01:Max_pos_ld_fac; %vector with values of load ranging from 1 to maximum positive load with a step of 0.01 for calculating the maximum sustained leveled turn rate.

%in order for matlab to run the code more efficiently, the size of the vectors and matrixes that will be calculated, is established first.
Cl = [size(h,2),size(V,2)];
Cd = [size(h,2),size(V,2)];
L = [size(h,2),size(V,2)];
D = [size(h,2),size(V,2)];
E = [size(h,2),size(V,2)];
TR = [size(h,2),size(V,2)];
PR = [size(h,2),size(V,2)];
Thrust = [size(h,2),size(V,2)];
Torque = [size(h,2),size(V,2)];
```

```
Power_prop = [size(h,2),size(V,2)];
ct = [size(h,2),size(V,2)];
cq = [size(h,2),size(V,2)];
cp = [size(h,2),size(V,2)];
J = [1,size(V,2)];
n_prop = [size(h,2),size(V,2)];
Power_shaft = [size(h,2),size(V,2)];
ROC = [size(h,2),size(V,2)];
ROD = [size(h,2),size(V,2)];
phi_C = [size(h,2),size(V,2)];
phi_D = [size(h,2),size(V,2)];
Turn = [size(Load1,2),size(V,2)];
vel = [size(h,2),size(Load2,2)];
Turn_max = [size(h,2),size(Load2,2)];
P = [size(h,2),size(V,2)];

for i = 1:size(h,2) %this for cycle calculates all variables for the established
altitudes.
for j = 1:size(V,2) %this for cycle calculates all variables for the estipulated
velocity interval for each altitude.
    n(i) = n_TO;
    omega(i) = n_TO*2.0*pi;
    if i == size(h,2)
        n(i) = n_OA;
        omega(i) = n_OA*2.0*pi;
    end
    % Lift Coefficient
    Cl(i,j) = W/((1/2)*rho(i)*V(j)^2*S);
    % Drag Coefficient
    Cd(i,j) = Cd_0+K*Cl(i,j)^2;
    % Lift Force
    L(i,j) = (1/2)*rho(i)*V(j)^2*S*Cl(i,j);
    % Drag Force
    D(i,j) = (1/2)*rho(i)*V(j)^2*S*Cd(i,j);
    % Lift to Drag Ratio
    E(i,j) = L(i,j)/D(i,j);
    % Thrust Required
    TR(i,j) = W/(Cl(i,j)/Cd(i,j));
    % Power Required
    PR(i,j) = TR(i,j)*V(j);
    thrust = 0; %for each iteration of the velocity it is guaranteed that thrust
     variable will initiate at 0 value.
    torque = 0; %for each iteration of the velocity it is guaranteed that torque
     variable will initiate at 0 value.
    %the next for cycle is based on the Glauert Blade Element Theory.

    for k = 1:size(R,2) %this for cycle calculates the thrust and torque values for
     each section of the blade and sums them at the end of each iteration, for each
     velocity.
        theta = atand(p/(2*pi*R(k))); %geometric pitch angle at each blade section.
        a1 = 0; %axial inflow factor
        b1 = 0; %angular inflow factor
        finished = 0;
        sum = 1;
        while finished == 0
              V0 = V(j)*(1+a1); %axial flow at propeller disk.
              V2 = omega(i)*R(k)*(1-b1); %angular flow velocity vector.
              phi = atan2d(V0,V2); %difference in angle between thrust and lift
              directions.
              alpha = theta-phi; % angle of incidence at each blade section.
              cl = 0.1058*alpha+0.0001;
```

```
            cd = 0.0099*cl^2-8*10^-6*cl+0.0042;
            V1 = sqrt(V0^2+V2^2); %blade section local flow velocity vector.
            DTDr   =   0.5*rho(i)*V1^2*B*c*(cl*cosd(phi)-cd*sind(phi));   %elemental
            thrust of blade section.
            DQDr = 0.5*rho(i)*V1^2*B*c*R(k)*(cd*cosd(phi)+cl*sind(phi)); %elemental
            torque of blade section.
            DtDr = 4.0*pi*R(k)*rho(i)*V(j)^2*(1+a1); %change in momentum flow rate
            along a stream-tube.
            DqDr  =  4.0*pi*R(k)^3*rho(i)*V(j)*(1+a1)*omega(i);  %change  in  angular
            momentum rate for flow times radius along a stream-tube.
            a2 = DTDr/DtDr; %calculated axial inflow factor.
            b2 = DQDr/DqDr; %calculated angular inflow factor.
            anew = (1/2)*(a1+a2); %new axial inflow factor.
            bnew = (1/2)*(b1+b2); %new angular inflow factor.
            %if difference between new and previous axial inflow factor and angular
            inflow factor is less than 1.0e-5 finnish this while cycle.
            if (abs(anew-a1)<1.0e-5)
                if (abs(bnew-b1)<1.0e-5)
                    finished = 1;
                end
            end
            %as long as this while cycle iterates, at each iteration the axial inflow
            factor and angular inflow factor become the new calculated values.
            a1 = anew;
            b1 = bnew;
            %if the axial inflow factor and angular inflow factor don't converge, at
            the 1000th iteration, the while cycle stops.
            sum = sum+1;
            if (sum > 1000)
                finished = 1;
            end
        end
        %the thrust and torque calculated at each section are summed and stored into
        these variables which will give the total thrust and torque values at each
        velocity.
        thrust = thrust+DTDr*rstep;
        torque = torque+DQDr*rstep;
    end
    % Propeller Thurst
    Thrust(i,j) = thrust;
    % Propeller Torque
    Torque(i,j) = torque;
    % Propeller Power
    Power_prop(i,j) = Thrust(i,j)*V(j);
    Vsound = 340.27;
    while Power_prop(i,j) >= PR(i,j)
          if (omega(i)*rt)/Vsound > 0.8
              disp('The mach number at the tip of the blade is higher than the subsonic
              mach number threshold')
              Propeller_Selection()
          else
              break
          end
     end
    % Advance Ratio
    J(j) = V(j)/(n(i)*d);
    % Propeller Thrust Coefficient
    ct(i,j) = Thrust(i,j)/(rho(i)*n(i)^2*d^4);
    % Propeller Torque Coefficient
    cq(i,j) = Torque(i,j)/(rho(i)*n(i)^2*d^5);
    % Propeller Power Coefficient
```

```
    cp(i,j) = (omega(i)*Torque(i,j))/(rho(i)*n(i)^3*d^5);
    if (ct(i,j)<0 || cq(i,j)<0)
        % Propeller Efficiency
        n_prop(i,j) = 0;
    else
        % Propeller Efficiency
        n_prop(i,j) = (Thrust(i,j)*V(j))/(Torque(i,j)*omega(i));
    end
    % Rate of Climb
    ROC(i,j) = (((Power_prop(i,j)-PR(i,j)))/W)*60;
    phi_C(i,j) = asind(((ROC(i,j))/60)/(V(j)));
    % Rate of Descent
    phi_D(i,j) = atand(1/E(i,j));
    ROD(i,j) = (V(j)*sin(phi_D(i,j)*(pi/180)))*60;
    % Sustained Turn Rate
    for z = 1:size(Load1,2)
        Turn(z,j) = (g*sqrt((Load1(z)^2-1))/(V(j)))*(180/pi);
    end
    % Maximum Sustained Turn Rate
    for y = 1:size(Load2,2)
        vel(i,y) = sqrt((Load2(y)*W*2)/(rho(i)*S*sqrt(Cd_0*pi*e*AR)));
        Turn_max(i,y) = (g*sqrt((Load2(y)^2-1))/(vel(i,y)))*(180/pi);
    end
    % Leveled Flight
    P(i,j)= abs(Power_prop(i,j)-PR(i,j)); %this will serve to find the minimum and
     maximum cruise speed of the airplane.
end
end

% Best Rate of Climb
M1 = [1,size(h,2)];
N1 = [1,size(h,2)];
Best_ROC = [1,size(h,2)];
Best_ROC_V = [1,size(h,2)];
Best_ROC_phi = [1,size(h,2)];
P_ROC = [1,size(h,2)];
for i = 1:size(h,2)
[M1(i),N1(i)] = max(ROC(i,:)); %M1 gives the max rate of climb value of row 1 and N1
gives the index of the corresponding column.
Best_ROC(i) = M1(i); %best rate of climb.
Best_ROC_V(i) = V(N1(i)); %best rate of climb velocity.
Best_ROC_phi(i) = phi_C(i,N1(i)); %best rate of climb angle.
P_ROC(i) = Thrust(i,N1(i))*V(N1(i));
end

% Best Rate of Descent
M2 = [1,size(h,2)];
N2 = [1,size(h,2)];
Best_ROD = [1,size(h,2)];
Best_ROD_V = [1,size(h,2)];
Best_ROD_phi = [1,size(h,2)];
for i = 1:size(h,2)
[M2(i),N2(i)] = min(ROD(i,2000:size(V,2))); %M2 gives the min rate of descent value of
row 2 and N2 gives the index of the corresponding column in the established interval.
Best_ROD(i) = M2(i); %best rate of descent.
Best_ROD_V(i) = V(N2(i)+2000); %best rate of descent velocity.
Best_ROD_phi(i) = phi_D(i,N2(i)+2000); %best rate of descent angle.
%since the interval starts at 2000 N2 will start counting from there, so in order to
get the correct index number for the minimum rate of descent velocity and angle, 2000
must be added to N2.
end
```

```
P_ROD = Motor_I_nl*(Motor_maxRPM_nl/Motor_KV_nl); %power consumed while gliding.

% Takeoff Ground roll
V_rot_rounded = round(V_rot,2); %rotational speed is defined as the speed at which the
airplane takes-off, and here it's value is rounded with 2 decimals in order to find
the corresponding index number from the velocity vector.
N3 = find(V(:)==V_rot_rounded); %index number where rotation speed is equal to
velocity.
Kt_TO = (Thrust(1,N3)/W)-u1;%thrust terms
Ka_TO = (rho(1)/(2*(W/S)))*(u1*Cl(1,N3)-Cd_0-K*Cl(1,N3).^2); %aerodynamic terms.
TO_Dist = (1/(2*g*Ka_TO))*log((Kt_TO+Ka_TO*V(N3)^2)/(Kt_TO+Ka_TO*V(1)^2)); %takeoff
distance.
PR_TO = ((V(N3)*1.44*W^2)/(g*rho(1)*S*Cl_max*TO_Dist)); %required power to takeoff.
P_TO = (Thrust(1,N3)*V(N3)); %avaiable power to takeoff.

% Leveled Flight
[Value,index] = sort(P(end,:)); %sorts the vector from lowest value to highest value,
all values are positive since abs was used above, so the 2 first values will correpond
to the 2 cruise speeds.
V_cruise1 = V(index(1)); %stores the 1st value of velocity into this variable.
V_cruise2 = V(index(2)); %stores the 2nd value of velocity into this variable.
if V_cruise1 > V_cruise2 %if the 1st velocity is higher than the second, it means that
the 1st velocity correnponds to the maximum cruise speed and the second to the minimum
cruise speed, if not the inverse can be said.
    V_cruiseMAX = V_cruise1;
    V_cruiseMIN = V_cruise2;
else
    V_cruiseMAX = V_cruise2;
    V_cruiseMIN = V_cruise1;
end
if V_cruiseMIN < V_stall %if the minimum cruise speed is lower than the stall speed,
the minimum cruise speed becomes the stall speed.
    V_cruiseMIN = V_stall;
end
V_cruise1 = V_cruiseMIN;
V_cruise = V_cruiseMAX;
V_cruise1_rounded = round(V_cruise1,2);
V_cruise_rounded = round(V_cruise,2);
N4 = find(V(:)==V_cruise_rounded); %N4 corresponds to the index number where the cruise
speed is equal to velocity.
N5 = find(V(:)==V_cruise1_rounded);
P_cruise1 = (Thrust(end,N5)*V_cruise1);
P_cruise = (Thrust(end,N4)*V_cruise); %avaiable power at cruise speed.

disp(' ');
end

function [] = Performance()

global Perf_Req t_TO TO_Dist V N3 t_climb h_OA Best_ROC Best_ROD Rng V_cruise t_loiter
Batt_EGY n_prop0 n_motor P_TO P_ROC P_ROD P_cruise End Batt_W Batt_SpecEGY Batt_NV
Motor_maxV Batt_CAP Batt_IMAX Empty_W Airframe_W Motor_W Payload Max_TO_W h_TO
h_dot_climb h_climb h_dot_descent h_descent t_descent H_climb H_descent h_descent1
t_cruise h_cruise h_loiter climb_slope Best_ROC_V b_climb climb_step v_climb
climb_power_slope b_climb_power p_climb Energy_climb Energy_TO Energy_descent
climb_angle p_cruise Energy_cruise Energy_loiter descent_slope Best_ROD_V b_descent
descent_step v_descent descent_angle

disp('Battery system needed for flight mission. ');
if Perf_Req == 1
    % take-off segment
```

```
t_TO = (TO_Dist/(V(N3)*60));
Energy_TO = (1/(n_prop0*n_motor))*(P_TO*(t_TO*60));
% climbing segment
t_climb(1) = 1;
H_climb  =  ((h_TO*Best_ROC(2))-(h_OA*Best_ROC(1)))/(Best_ROC(2)-Best_ROC(1));  % straight line ceiling
h_dot_climb = ((h_OA*Best_ROC(1))-(h_TO*Best_ROC(2)))/(h_OA-h_TO); % straight line sea-level rate of climb
h_climb(1) = Best_ROC(1);

climb_slope = (Best_ROC(2)-Best_ROC(1))/(Best_ROC_V(2)-Best_ROC_V(1));
b_climb = Best_ROC(2)-climb_slope*Best_ROC_V(2);
climb_step(1) = Best_ROC(1);
v_climb(1) = Best_ROC_V(1);
climb_angle(1) = asind(((climb_step(1))/60)/(v_climb(1)));

climb_power_slope = (P_ROC(2)-P_ROC(1))/(Best_ROC_V(2)-Best_ROC_V(1));
b_climb_power = P_ROC(2)-climb_power_slope*Best_ROC_V(2);
p_climb(1) = climb_power_slope*v_climb(1)+b_climb_power;
Energy_climb(1) = (1/(n_prop0*n_motor))*(p_climb(1)*(t_climb(1)*60));

for i = 2:1:(Rng/V_cruise)/60
    t_climb(i) = i;
    h_climb(i)          =          H_climb          -          (H_climb-h_climb(i-1))/(exp((h_dot_climb/H_climb)*(t_climb(i)-t_climb(i-1))));
    climb_step(i) = h_climb(i)-h_climb(i-1);
    v_climb(i) = (climb_step(i)-b_climb)/climb_slope;
    climb_angle(i) = asind(((climb_step(i))/60)/(v_climb(i)));
    p_climb(i) = climb_power_slope*v_climb(i)+b_climb_power;
    Energy_climb(i)     =     (1/(n_prop0*n_motor))*(p_climb(i)*((t_climb(i)*60)-(t_climb(i-1)*60)));
    if h_climb(i) > h_OA
        t_climb(end) = [];
        h_climb(end) = [];
        break
    end
end
% descending segment
t_descent(1) = 1;
H_descent  =  ((h_TO*Best_ROD(1))-(h_OA*Best_ROD(2)))/(Best_ROD(1)-Best_ROD(2));  % straight line ceiling
h_dot_descent  =  ((h_OA*Best_ROD(2))-(h_TO*Best_ROD(1)))/(h_OA-h_TO);  % straight line sea-level rate of descent
h_descent1(1) = Best_ROD(2);
h_descent(1) = h_OA - h_descent1(1);

descent_slope = (Best_ROD(2)-Best_ROD(1))/(Best_ROD_V(2)-Best_ROD_V(1));
b_descent = Best_ROD(2)-descent_slope*Best_ROD_V(2);
descent_step(1) = Best_ROD(2);
v_descent(1) = Best_ROC_V(2);
descent_angle(1) = asind(((descent_step(1))/60)/(v_descent(1)));

Energy_descent(1) = P_ROD*(t_descent(1)*60);
for j = 2:1:(Rng/V_cruise)/60
    t_descent(j) = j;
    h_descent1(j)       =       H_descent       -       (H_descent-h_descent1(j-1))/(exp((h_dot_descent/H_descent)*(t_descent(j)-t_descent(j-1))));
    h_descent(j) = h_OA - h_descent1(j);
    descent_step(j) = h_descent(j-1)-h_descent(j);
    v_descent(j) = (descent_step(j)-b_descent)/descent_slope;
    descent_angle(j) = asind(((descent_step(j))/60)/(v_descent(j)));
```

```
        Energy_descent(j) = P_ROD*((t_descent(j)*60)-(t_descent(j-1)*60));
        if h_descent(j) < h_TO
            t_descent(end) = [];
            h_descent(end) = [];
            break
        end
    end
    % cruise segment
    for k = 1:1:((Rng/V_cruise)/60)-t_TO(end)-t_climb(end)-t_descent(end)
        t_cruise(k) = k;
        h_cruise(k) = h_OA;
        p_cruise(k) = P_cruise;
        Energy_cruise(k) = (1/(n_prop0*n_motor))*(p_cruise(k)*(t_cruise(1)*60));
    end
    % loiter segment
    t_loiter = 15;
    h_loiter = h_OA;
    Energy_loiter = (1/(n_prop0*n_motor))*(P_cruise*(t_loiter*60));

elseif Perf_Req == 2
    % take-off segment
    t_TO = (TO_Dist/(V(N3)*60));
    Energy_TO = (1/(n_prop0*n_motor))*(P_TO*(t_TO*60));
    % climbing segment
    t_climb(1) = 1;
    H_climb  =  ((h_TO*Best_ROC(2))-(h_OA*Best_ROC(1)))/(Best_ROC(2)-Best_ROC(1));  %
     straight line ceiling
    h_dot_climb = ((h_OA*Best_ROC(1))-(h_TO*Best_ROC(2)))/(h_OA-h_TO); % straight line
     sea-level rate of climb
    h_climb(1) = Best_ROC(1);

    climb_slope = (Best_ROC(2)-Best_ROC(1))/(Best_ROC_V(2)-Best_ROC_V(1));
    b_climb = Best_ROC(2)-climb_slope*Best_ROC_V(2);
    climb_step(1) = Best_ROC(1);
    v_climb(1) = Best_ROC_V(1);
    climb_angle(1) = asind(((climb_step(1))/60)/(v_climb(1)));

    climb_power_slope = (P_ROC(2)-P_ROC(1))/(Best_ROC_V(2)-Best_ROC_V(1));
    b_climb_power = P_ROC(2)-climb_power_slope*Best_ROC_V(2);
    p_climb(1) = climb_power_slope*v_climb(1)+b_climb_power;
    Energy_climb(1) = (1/(n_prop0*n_motor))*(p_climb(1)*(t_climb(1)*60));

    for i = 2:1:End
        t_climb(i) = i;
        h_climb(i)          =          H_climb          -          (H_climb-h_climb(i-
        1))/(exp((h_dot_climb/H_climb)*(t_climb(i)-t_climb(i-1))));
        climb_step(i) = h_climb(i)-h_climb(i-1);
        v_climb(i) = (climb_step(i)-b_climb)/climb_slope;
        climb_angle(i) = asind(((climb_step(i))/60)/(v_climb(i)));
        p_climb(i) = climb_power_slope*v_climb(i)+b_climb_power;
        Energy_climb(i)     =     (1/(n_prop0*n_motor))*(p_climb(i)*((t_climb(i)*60)-
         (t_climb(i-1)*60)));
        if h_climb(i) > h_OA
            t_climb(end) = [];
            h_climb(end) = [];
            break
        end
    end
    % descending segment
    t_descent(1) = 1;
```

```
    H_descent = ((h_TO*Best_ROD(1))-(h_OA*Best_ROD(2)))/(Best_ROD(1)-Best_ROD(2)); % straight line ceiling
    h_dot_descent = ((h_OA*Best_ROD(2))-(h_TO*Best_ROD(1)))/(h_OA-h_TO); % straight line sea-level rate of descent
    h_descent1(1) = Best_ROD(2);
    h_descent(1) = h_OA - h_descent1(1);

    descent_slope = (Best_ROD(2)-Best_ROD(1))/(Best_ROD_V(2)-Best_ROD_V(1));
    b_descent = Best_ROD(2)-descent_slope*Best_ROD_V(2);
    descent_step(1) = Best_ROD(2);
    v_descent(1) = Best_ROD_V(2);
    descent_angle(1) = asind(((descent_step(1))/60)/(v_descent(1)));

    Energy_descent(1) = P_ROD*(t_descent(1)*60);
    for j = 2:1:End
        t_descent(j) = j;
        h_descent1(j) = H_descent - (H_descent-h_descent1(j-1))/(exp((h_dot_descent/H_descent)*(t_descent(j)-t_descent(j-1))));
        h_descent(j) = h_OA - h_descent1(j);
        descent_step(j) = h_descent(j-1)-h_descent(j);
        v_descent(j) = (descent_step(j)-b_descent)/descent_slope;
        descent_angle(j) = asind(((descent_step(j))/60)/(v_descent(j)));
        Energy_descent(j) = P_ROD*((t_descent(j)*60)-(t_descent(j-1)*60));
        if h_descent(j) < h_TO
            t_descent(end) = [];
            h_descent(end) = [];
            break
        end
    end
    % cruise segment
    for k = 1:1:(End/60)-t_climb(end)-t_descent(end)
        t_cruise(k) = k;
        h_cruise(k) = h_OA;
        p_cruise(k) = P_cruise;
        Energy_cruise(k) = (1/(n_prop0*n_motor))*(p_cruise(k)*(t_cruise(1)*60));
    end
    % loiter segment
    t_loiter = 15;
    h_loiter = h_OA;
    Energy_loiter = (1/(n_prop0*n_motor))*(P_cruise*(t_loiter*60));
end

Batt_EGY = Energy_TO+sum(Energy_climb)+sum(Energy_descent)+sum(Energy_cruise)+Energy_loiter ;
disp([' Battery energy needed to accomplish flight mission [J]: ',num2str(Batt_EGY)]);
Batt_W = Batt_EGY/(Batt_SpecEGY*3600); disp([' Battery system mass [kg]: ',num2str(Batt_W)]);
Batt_NV = Motor_maxV; disp([' Battery system voltage [V]: ',num2str(Batt_NV)]);
Batt_CAP = (Batt_EGY/Batt_NV)/3600; disp([' Battery system capacity [Ah]: ',num2str(Batt_CAP)]);
Batt_IMAX = 5 * Batt_CAP; disp([' Battery system maximum current draw [A]: ',num2str(Batt_IMAX)]);
disp(' ');
disp('Aircraft total weight verification.');
Empty_W = Airframe_W + Motor_W; disp([' Empty mass of airplane [kg]: ',num2str(Empty_W)]);
Payload = Max_TO_W - Batt_W - Empty_W; disp([' Avaiable payload of airplane [kg]: ',num2str(Payload)]);
end

function [] = DataProcessing()
```

```
global V Thrust TR Power_prop PR J ct cp n_prop ROC ROD Turn vel Turn_max Best_ROC_V
Best_ROC Best_ROD_V Best_ROD V_cruise P_cruise V_cruise1 P_cruise1 Engine_W Fuel_W
Min_Payload Motor_W Batt_W Payload y str labels hT Airframe_W y1

figure(1)
plot(V,Thrust(end,:),'k-',V,TR(end,:),'k--')
axis([20 80 0 1200])
title('Thrust vs Airspeed')
xlabel('Airspeed [m/s]')
ylabel('Thrust [N]')
legend('Thrust Available','Thrust Required')
set(gcf,'color','w')
grid on
print('figure1','-dpng')

figure(2)
plot(V,Power_prop(end,:),'k-',V,PR(end,:),'k--
',V_cruise,P_cruise,'k*',V_cruise1,P_cruise1,'k*')
axis([20 70 0 40000])
title('Power vs Airspeed')
xlabel('Airspeed [m/s]')
ylabel('Power [w]')
legend('Power Available','Power Required')
text(V_cruise,P_cruise,['(', num2str(V_cruise), ', ', num2str(P_cruise), ')'])
text(V_cruise1,P_cruise1,['(', num2str(V_cruise1), ', ', num2str(P_cruise1), ')'])
set(gcf,'color','w')
grid on
print('figure2','-dpng')

figure(3)
plot(J,ct(end,:),'k-',J,cp(end,:),'k--')
axis([0.30 1.4 0 0.5])
title('Thrust and Power Coefficients vs Advance Ratio ')
xlabel('Advance Ratio')
ylabel('Thrust and Power Coefficients')
legend('Thrust Coefficient','Power Coefficient')
set(gcf,'color','w')
grid on
print('figure3','-dpng')

figure(4)
plt = gca;
yyaxis left
plot(J,n_prop(end,:),'k-');
axis([0.30 1.4 0 1])
title('Propeller Efficiency vs Advance Ratio')
xlabel('Advance Ratio')
ylabel('Propeller Efficiency')
plt.YAxis(1).Color = 'k';
yyaxis right
plot(J,cp(end,:),'k--');
axis([0.30 1.4 0 0.5])
ylabel('Power Coefficient')
plt.YAxis(2).Color = 'k';
legend({'Propeller Efficiency','Power Coefficient'},'location','northwest')
set(gcf,'color','w')
grid on
print('figure4','-dpng')

figure(5)
```

```
plot(V,ROC(1,:),'k-',V,ROC(2,:),'k--
',Best_ROC_V(1),Best_ROC(1),'k*',Best_ROC_V(2),Best_ROC(2),'k*',[Best_ROC_V(1),Best_R
OC_V(2)],[Best_ROC(1),Best_ROC(2)],'k-.')
title('Rate of Climb vs Airspeed')
axis([20 70 0 600])
xlabel('Airspeed [m/s]')
ylabel('Rate of Climb [m/min]')
legend({'Rate of Climb at take-off altitude','Rate of Climb at operating
altitude'},'location','southwest')
text(Best_ROC_V(1),Best_ROC(1),['(',       num2str(Best_ROC_V(1)),       ',       ',
num2str(Best_ROC(1)), ')'])
text(Best_ROC_V(2),Best_ROC(2),['(',       num2str(Best_ROC_V(2)),       ',       ',
num2str(Best_ROC(2)), ')'])
set(gcf,'color','w')
grid on
print('figure5','-dpng')

figure(6)
plot(V,ROD(2,:),'k-',V,ROD(1,:),'k--
',Best_ROD_V(1),Best_ROD(1),'k*',Best_ROD_V(2),Best_ROD(2),'k*',[Best_ROD_V(1),Best_R
OD_V(2)],[Best_ROD(1),Best_ROD(2)],'k-.')
title('Rate of Descent vs Airspeed')
axis([20 60 0 250])
xlabel('Airspeed [m/s]')
ylabel('Rate of Descent [m/min]')
legend({'Rate of Descent at operating altitude','Rate of Descent at take-off
altitude'},'location','southwest')
text(Best_ROD_V(2),Best_ROD(2),['(',       num2str(Best_ROD_V(2)),       ',       ',
num2str(Best_ROD(2)), ')'])
text(Best_ROD_V(1),Best_ROD(1),['(',       num2str(Best_ROD_V(1)),       ',       ',
num2str(Best_ROD(1)), ')'])
set(gcf,'color','w')
grid on
print('figure6','-dpng')

figure(7)
plot(V,Turn(2,:),'k--',V,Turn(3,:),'k-
.',V,Turn(4,:),'k:',vel(end,:),Turn_max(end,:),'k-')
title('Rate of turn vs Airspeed')
axis([20 100 0 90])
xlabel('Airspeed [m/s]')
ylabel('Rate of Turn [deg/s]')
legend('Rate of Turn at 2G','Rate of Turn at 3G','Rate of Turn at 4G','Maximum Sustained
Rate of Turn')
set(gcf,'color','w')
grid on
print('figure7','-dpng')

figure(8)
y = [Engine_W Fuel_W Min_Payload; Motor_W Batt_W Payload];
str = {'ICE';'EM'};
labels = {'Engine', 'Fuel', 'Payload';'Motor', 'Battery', 'Payload'};
hB = bar(y);
hAx = gca;
hAx.XTickLabel = str;
hT = [];
for i = 1:length(hB)
    hT                                                                    =
[hT,text(hB(i).XData+hB(i).XOffset,hB(i).YData,labels(:,i),'VerticalAlignment','botto
m','horizontalalign','center')];
end
```

```
title('ICE and EM Mass Distribution')
ylabel('Mass [kg]')
set(gcf,'color','w')
grid on
print('figure8','-dpng')

figure(9)
y1 = [Engine_W Fuel_W Min_Payload Airframe_W; Motor_W Batt_W Payload Airframe_W];
str = {'ICE';'EM'};
bar(y1,'stacked');
hAx = gca;
hAx.XTickLabel = str;
title('ICE and EM Total Mass')
ylabel('Mass [kg]')
set(gcf,'color','w')
grid on
print('figure9','-dpng')
end

function [] = MissonProfile()

global Time1 t_climb Time2 t_cruise Time3 t_descent h1 h2 h3 v1 v2 v3 Range1 Range2
Range3 rpm1 rpm2 rpm3 power1 power2 power3 current1 current2 current3 F1 F2 F3 h_climb
v_climb climb_angle Motor_maxRPM_fl p_climb n_prop0 n_motor Motor_maxV h_OA V_cruise
h_descent  v_descent  descent_angle  Motor_maxRPM_nl  Prop_RPM_OA  P_cruise  P_ROD
Motor_I_nl time h range v rpm power current F Table

Time1 = [1,size(t_climb,2)];
Time2 = [1,size(t_cruise,2)];
Time3 = [1,size(t_descent,2)];
h1 = [1,size(t_climb,2)];
h2 = [1,size(t_cruise,2)];
h3 = [1,size(t_descent,2)];
v1 = [1,size(t_climb,2)];
v2 = [1,size(t_cruise,2)];
v3 = [1,size(t_descent,2)];
Range1 = [1,size(t_climb,2)];
Range2 = [1,size(t_cruise,2)];
Range3 = [1,size(t_descent,2)];
rpm1 = [1,size(t_climb,2)];
rpm2 = [1,size(t_cruise,2)];
rpm3 = [1,size(t_descent,2)];
power1 = [1,size(t_climb,2)];
power2 = [1,size(t_cruise,2)];
power3 = [1,size(t_descent,2)];
current1 = [1,size(t_climb,2)];
current2 = [1,size(t_cruise,2)];
current3 = [1,size(t_descent,2)];
F1 = {1,size(t_climb,2)};
F2 = {1,size(t_cruise,2)};
F3 = {1,size(t_descent,2)};

for i = 1:1:size(t_climb,2) %climbing segment flight.
    Time1(i) = t_climb(i); %time at each minute.
    h1(i) = h_climb(i); %altitude at each minute.
    v1(i) = v_climb(i); %speed at each minute.
    Range1(i) = ((v_climb(i)*60)*cosd(climb_angle(i))*i)/1000; %range at each minute.
    rpm1(i) = Motor_maxRPM_fl; %motor regime at each minute.
    power1(i) = p_climb(i); %power consumed at each minute.
    current1(i) = (p_climb(i)/n_prop0)/(n_motor*Motor_maxV); %current draw at each
     minute.
```

```
    F1{i} = 'Climbing Segment'; %flight segment information.
end
for j = 1:size(t_cruise,2) %cruise segment flight.
    Time2(j) = Time1(end)+j; %time at each minute.
    h2(j) = h_OA; %altitude at each minute.
    v2(j) = V_cruise; %speed at each minute.
    Range2(j) = Range1(end)+((V_cruise*60)*j)/1000; %range at each minute.
    rpm2(j) = Prop_RPM_OA; %motor regime at each minute.
    power2(j) = P_cruise; %power consumed at each minute.
    current2(j) = (P_cruise/n_prop0)/(n_motor*Motor_maxV); %current draw at each
     minute.
    F2{j} = 'Cruising Segment'; %flight segment information.
end
for k = 1:size(t_descent,2) %descending segment flight.
    Time3(k) = Time2(end)+k; %time at each minute.
    h3(k) = h_descent(k); %altitude at each minute.
    v3(k) = v_descent(k); %speed at each minute.
    Range3(k) = Range2(end)+((v_descent(k)*60)*cosd(descent_angle(k))*k)/1000; %range
     at each minute.
    rpm3(k) = Motor_maxRPM_nl; %motor regime at each minute.
    power3(k) = P_ROD; %power consumed at each minute.
    current3(k) = Motor_I_nl; %current draw at each minute.
    F3{k} = 'Descending Segment'; %flight segment information.
end
time = [Time1,Time2,Time3]';
h = [h1,h2,h3]';
range = [Range1,Range2,Range3]';
v = [v1,v2,v3]';
rpm = [rpm1,rpm2,rpm3]';
power = [power1,power2,power3]';
current = [current1,current2,current3]';
F = [F1,F2,F3]';

Table = table(time,h,range,v,rpm,power,current,F);
Table.Properties.VariableNames = {'Time' 'Altitude' 'Range' 'AircraftSpeed' 'MotorRPM'
'PowerConsuption' 'CurrentDraw' 'FlightSegment'};
Table.Properties.VariableUnits = {'min' 'm' 'km' 'm/s' '1/m' 'W' 'A' ''};
writetable(Table,'Table.xlsx','Sheet',1);
disp(Table);

figure(10)
plot(range,h,'k-')
title('Mission Profile')
axis([1 420 1 5000])
xlabel('Range [km]')
ylabel('Altitude [m]')
legend('Mission Profile')
set(gcf,'color','w')
grid on
print('figure10','-dpng')
end
```